UNIVERSIDAD DE GUANAJUATO

DIVISIÓN DE CIENCIAS NATURALES Y EXACTAS

CAMPUS GUANAJUATO

POSGRADO EN QUÍMICA

SYNTHESIS, CHARACTERIZATION AND EVALUATION OF HYDROXYAPATITE DOPED WITH ZINC FOR SEVERAL APPLICATIONS

TESIS

Para obtener el Grado de

MAESTRO EN CIENCIAS QUÍMICAS

Presenta:

Tania Guadalupe Peñaflor Galindo

Guanajuato, Gto. Diciembre 2015

CONTENTS

Chapter 1. General Introduction

Chapter 2.   Wet Chemical Synthesis of Zinc-substituted Hydroxyapatite Nanocrystals

Chapter 3.   Fabrication of Nanocrystalline Zinc-substituted Hydroxyapatite Films on Biomedical Polymers and Their Fibroblast Compatibility and Antibacterial Properties

Chapter 4. Summary and Future Perspectives

INDEX OF TABLES

Chapter 1. General Introduction

Chapter 2. Wet Chemical Synthesis of Zinc-substituted Hydroxyapatite Nanocrystals

Chapter 3. Fabrication of Nanocrystalline Zinc-substituted Hydroxyapatite Films on Biomedical Polymers and Their Fibroblast Compatibility and Antibacterial Properties

LIST OF FIGURES

Chapter 1. General Introduction

Chapter 2. Wet Chemical Synthesis of Zinc-substituted Hydroxyapatite Nanocrystals

Chapter 3. Fabrication of Nanocrystalline Zinc-substituted Hydroxyapatite Films on Biomedical Polymers and Their Fibroblast Compatibility and Antibacterial Properties

A quien corresponda:

Por medio de la presente nos responsabilizamos de la autenticidad y originalidad del presente trabajo de investigación.

"SYNTHESIS, CHARACTERIZATION AND EVALUATION OF HYDROXYAPATITE DOPED WITH ZINC FOR SEVERAL APPLICATIONS"

Realizado por la Q.F.B. Tania Guadalupe Peñaflor Galindo en el laboratorio de Diseño experimental en la División de Ciencias Naturales y Exactas del Campus Guanajuato de la Universidad de Guanajuato.

_____

Director de Tesis

Dr. Merced Martínez Rosales

_____

Tesista

Q.F.B. Tania Guadalupe Peñaflor Galindo

Miembros del Comité del Jurado del Examen Recepcional para obtener el grado de Maestro en Ciencias Químicas, presenta Q.F.B. Tania Guadalupe Peñaflor Galindo con el trabajo que lleva por título

"SYNTHESIS, CHARACTERIZATION AND EVALUATION OF HYDROXYAPATITE DOPED WITH ZINC FOR SEVERAL APPLICATIONS"

Presidente

Dr. Jorge Armando Cervantes Jáuregui

Secretario

Dra. Rosalba Fuentes Ramírez

Vocal

Dr. Ramón Antonio Zárraga Núñez

Suplente

Dr. Gustavo Cruz Jiménez

ACKNOWLEDGMENTS

Tania Guadalupe Peñaflor Galindo

December 2015

ABSTRACT

Low bio-affinity of medical catheters often causes bacterial infection through the permeation interspaces between catheters and skin tissues. Thus, the surface modification of the biomedical polymer (e.g., silicone resin) used as catheters is desired for improving the biocompatible and antibacterial properties. As the modification materials, hydroxyapatite ($Ca_{10}(PO_4)_3(OH)_2$) (HAp), which is crystallographically and chemically similar to the components of human's hard tissues, is a good candidate. Importantly, naturally-formed HAp is not absolutely pure and has some impurities of ions (Zn^{2+}, Mg^{2+}, K^+, etc.), which provides biocompatibility as well as antibacterial properties. Thus, the substituted ions not only alter the space group of crystal structure, thermal stability and mechanical properties of HAp but also play an important role in the biological behaviors. In this study, the synthesis of zinc-substituted HAp (Zn:HAp) nanocrystals and subsequent formation of the nanocrystalline film on the biomedical polymer without using chemical reagents for investigating their biocompatibility as well as antibacterial properties ("*Chapter 1*"). In "*Chapter 2*", Zn:HAp nanocrystals were synthesized by a wet chemical method. In the method, the initial (Ca+Zn)/P ratio of 1.67 and 2.00 were adjusted from the reagents ($CaCl_2$, $ZnCl_2$, and K_2HPO_4) to resultantly form the stoichiometric and carbonate HAp nanocrystals, respectively. The initial $ZnCl_2$ was changed as the dopant concentration of Zn/(Ca+Zn) = 0.0, 2.5, 5.0 and 10 mol%. The zinc-substitution significantly suppressed the crystal growth to obtain the optimized crystalline nano-sizes for the modification. In "*Chapter 3*", an electrophoretic deposition at the optimized voltage of 100 V was used for the surface modification of biomedical polymers. As a result, the nanocrystalline Zn:HAp film formation on the surfaces was successfully achieved. Furthermore, the fibroblast compatibility as well as antibacterial activity was confirmed on the film surfaces. In particular, the films made from the Zn:HAp nanocrystals with (Ca+Zn)/P =2.00 and Zn/(Ca+Zn) =5 mol% is the best possibility for the surface modification. In "*Chapter 4*", the nanocrystalline Zn:HAp films were summarized to provide good biocompatibility as well as antibacterial properties on biomedical polymer surfaces, suggesting useful catheter surface modification technique.

Tania Guadalupe Penaflor Galindo

December 2015

Chapter 1

General Introduction

1.1 Percutaneous Devices

1.1.1 Current State and Issues

Percutaneous devices have been serving with a variety of different purposes in clinical applications and biomedical research [1]. These devices usually are a non-biological material, which penetrates into and through the skin. For that reason, they can provide a connection between the interior and exterior of the body.

The percutaneous devices applications are shown in **Table 1.1** which has been grouped as blood and body cavity access devices, then concludes for power or signal transmission and internal prosthetic devices.

The interfacial failure modes identified are marsupialization, permigration, avulsion, infection, alone or in combination. Single or multiple etiological factors may be responsible for these failure modes. These factors can be surgically created skin defects around the penetrating foreign implant, epidermal healing characteristics that prevent the formation of a suitable seal at the implant-skin interface and mechanical forces that may disrupt dermal attempts to seal the interface [1]. Eventually, the interface becomes infected necessitating removal of the device. The most widely used is the "silicone rubber catheter".

In medicine, a catheter (from the Greek καθετήρ) is a device shaped and elongated narrow tube that can be introduced into a tissue or vein. Catheters allow the injection of nutrients, drugs, fluid drainage or access other medical instruments.

The catheters are usually inserted into a body cavity, a pipe, or a blood vessel. These devices can be thin tubes, called soft, flexible catheters or catheters thicker and inflexible called hard catheters. A catheter can be left in the body, whether temporarily or permanently (see **Figure 1.1**).

Table 1.1 Possible applications of the percutaneous devices.

Percutaneous device	Applications
Blood access devices	a) Continuous infusions or blood sampling. b) External circulation. c) Intravascular pacemaker. d) Dialysis.
Tissue access devices	a) Windows for optical tissue studies. b) Probes for monitoring tissue parameters including O_2, CO_2, pH, temperatures, biopotentials, and enzymes.
Body cavities access devices	a) Prosthetic urethra. b) Peritoneal dialysis. c) Middle ear ventilating tubes.
Power and signal conduits	a) Pneumatic, hydraulic or electrical power for activation of internal artificial organs. b) Electrical signals for stimulation or control of natural or artificial organs. c) Recording of electrical potentials from internal natural or artificial organs.
Internal/ external prosthetic devices	a) Urethral. b) Corneal implant. c) Artificial limb. d) Snap button for fixation of external prosthetic devices e) Dental implants

A difference in ancient times, when the inflexible metal was used for catheters, the modern technology employs a range of polymers such as silicone rubber, latex, and polyurethane elastomers for the tubes. Of these, because it does not react with body fluids, silicon is the most used material. The first modern catheter was built by David S. Sheridan, who invented it in the 40s; and at the beginning of the 90s, Walsh and a famous Scottish urologist named Norman Gibbon created the standard catheter, which is currently used in hospitals, called catheter Gibbon-Walsh. The catheters are generally inserted percutaneously, and often some complications arise after the catheter is placed; these complications can be caused by several factors. The Catheter-related common complications could be exit/tunnel infection, external cuff extrusion, pericatheter leak, inflammation, catheter obstruction, infusion or pressure pain [1].
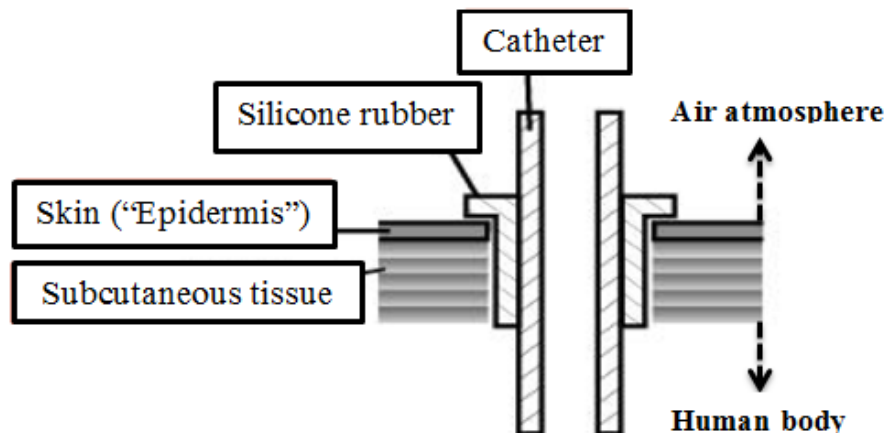
Figure 1.1 Scheme of the silicone catheter as the percutaneous device at the human body.

1.1.2 Skin Down-growth and Bacterial Infection

Health Care-Associated Infections (HCAI-CDC in 2008) are a major public health, increasing patient mortality, use of medical supplies, hospital stay and costs [2, 3]. Globally, WHO (World Health Organization) reported that in Europe, the HCAI caused 16 million additional hospital days and 37,000 deaths. Additionally, others 110,000 deaths with an estimated cost of 7 billion of € annually in the US are responsible for about 99,000 deaths in 2002, and an estimated cost of 6.5 billion dollars in 2004 are related to them. Large studies carried out by WHO in USA and Europe, showed that HCAI incidence density ranged from 13.0 to 20.3 episodes per 1000 patient-days and pooled cumulative incidence was 17.0 episodes per 1000 patient-days in adult high-risk patients in industrialized countries. Based on a report from the USA NNIS system, high frequency of infection is associated with the use of invasive devices, particularly in central lines, urinary catheters, and ventilators [4]. Of these HCAI, catheter-related infections are the most common diseases. An analysis of 173 Intensive Care Unit (ICUs) in 25 countries in Latin America, Asia, Africa and Europe, reported an excess mortality of 18.5% for Catheter-Related Urinary Tract Infection (CRUTI) and 23.6% for Catheter-Related Blood Stream Infection (CRBSI). Among adult ICU patients in high-income countries, pooled cumulative incidence densities of catheter-related BSI (CR-BSI), urinary catheter-related UTI (CR-UTI), were 3.5 (95% CI 2.8-4.1) per 1000 CI-days, 4.1 (95% CI 3.7-4.6) per 1000 urinary catheter-days, respectively these results are summarized in **Table 1.2** [4].

Table 1.2. Pooled cumulative incidence density of health care-associated infection (HCAI) and device-associated infection in adult ICU patients in high-, middle- and low-income countries. (CR-BSI=Catheter-Related Blood Stream Infection; CR-UTI=Catheter-Related Urinary Tract Infection, NHSN=National Healthcare Safety Network, KISS=Krankenhaus Infections Surveillance System; INICC=International Nosocomial Infection Control Consortium), which is reprinted and modified based on the report "the burden of endemic health care-associated infection worldwide 2011" [4].

Surveillance networks/reviews, study period, country	HCAI/ 1000 patient-days (95% CI)	Patient days	CR-BSI/ 1000 central line days (95% CI)	Catheter-days	CR-UTI/ 1000 urinary catheter days (95% CI)	Urinary catheter-days
NHSN, 2006–2008, USA	/	/	2.1	699 300	3.4	547 824
KISS, 2004-2009, Germany	/	/	1.3	4 002 108	2.0	4 757 133
Systematic review, high-income countries 1995-2010	17.0 (14.2-19,8)	32,537,324	3.5 (2.8-4.1)	5 339 322	4.1 (3.7-4.6)	13 614 567
INICC, 2003–2008, 25 developing countries	/	/	7.4	362 882	6.1	403 545
Systematic review, low- and middle-income countries (1995-2010)	42.7 (34.8-50.5)	193 139	12.2 (10.5-13.9)	891 220	8.8 (7.4-10.3)	970 710

In catheterized patients, bacteria can adhere rapidly to the surface on indwelling devices in a process known as bacteria docking after the interlocking, creating an extracellular stronger polymeric matrix, which adheres to the catheter surface, where bacteria colonize in a process known as biofilm [5−7]. This biofilm is very resistant to the antibacterial treatment, resulting in catheter-related infections and in many cases, in death [8].

Catheter-related infection: It is the significant microbial growth (greater than 15 colony forming units (CFU)) in a culture of a catheter segment [9−10]. Usually, these infections start at the end of the catheter that penetrates the skin and then extraluminal extend along the catheter surface, or appear in the catheter lumen and extending intraluminal into the bloodstream. Only in very rare cases these infections are initiated by hematogenous seeding in the intravascular portion of the catheter; and even in more rare cases, the infection may appear by the solution infused through the catheter.

Showed in a descending frequency, the most common microorganisms that cause these infections are [11]:

- Staphylococcus aureus
- Enterobacteriaceae
- Pseudomonas spp
- Enterococci
- Escherichia coli
- Candida spp
- Coagulase-negative staphylococci
- Acinetobacter spp.

Because the silicon is not a biocompatible material, it cannot bind with the body tissues, creating space (passway) between the skin and the percutaneous device. Using this passway, the bacteria can easily permeate the body (Skin Downgrowth), and it can cause bacterial infection (see **Figure 1.2**).
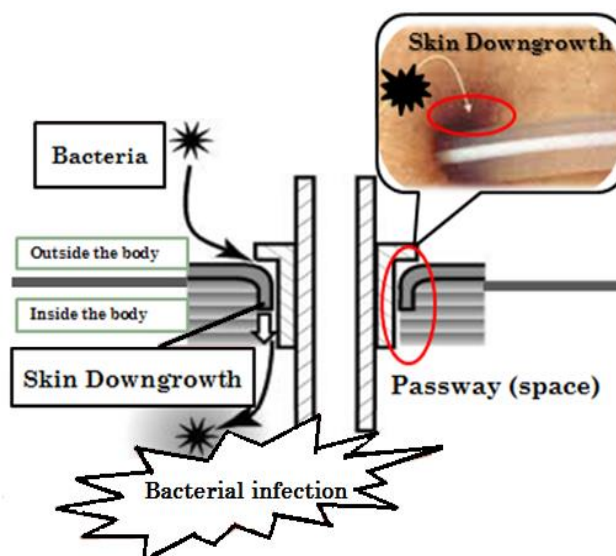
Figure 1.2 Scheme of the skin down growth mechanism, which often causes bacterial infection.

In order to prevent bacterial infection, the surface coating technique by biocompatible materials on a silicone rubber is required (see **Figure 1.3**).
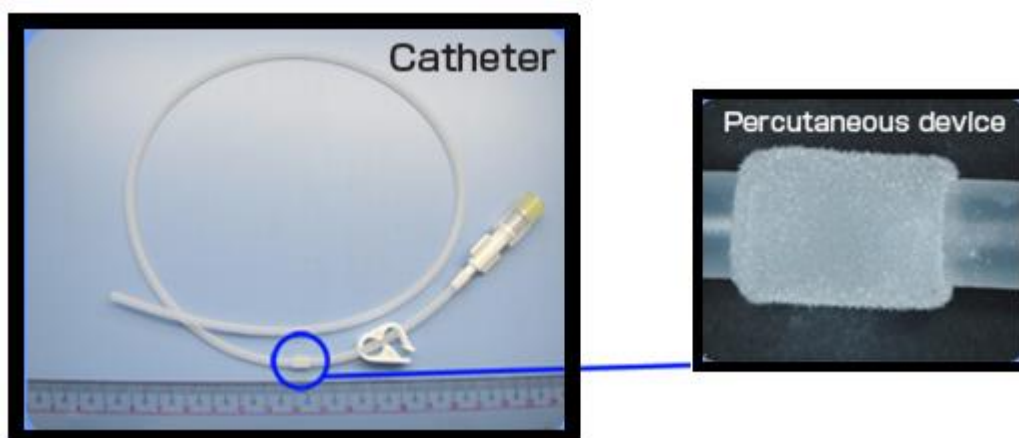
Figure 1.3. The cuff of the catheter made of silicone rubber. The cuff is the part of the catheter that is in direct contact with the skin for that is the part that has to be covered with a biocompatible material, which is reprinted and modified based on the report by the report [12].

Some of the most common biomaterials are explained in **Table 1.3**. There are multiple definitions for biomaterial; however, the accepted definition is the one mentioned in the Second Consensus Conference on definitions in Biomaterials, held in the UK in 1992 [13]:

A biomaterial is "designed to interact with biological systems to evaluate, treat, augment or replace any tissue, organ or body function media". According to this definition, a biomaterial can be a part of any device or instrument, appliance, implant, etc., that helps in the prevention, diagnosis or treatment of disease. It is also very important that the biomaterial used in the repair of a body part complies with all the features and functions required by the replaced organ or tissue, and it do not result in toxic reactions which may result in rejection of the body.

The biomaterial is a natural or synthetic substance engineered to interact with biological systems. To meet the needs of the biomedical community, every material composition, from metals and ceramics to glasses and polymers must be researched.

Table 1.3. Representative applications of the biomaterials prepared from ceramics, polymers, and metals.

Cardiovascular implants	Intended use
	(values of heart, vascular grafts, pacemakers, stents, etc.)
Plastic and reconstructive implants	▪ Breast augmentation or reconstruction ▪ Maxilofacial reconstruction ▪ Penile implant.
Orthopedic prostheses	▪ Knee join ▪ Hip join ▪ Fracture fixation
Opthalmic systems	▪ Contact lenses ▪ Intraocular lenses
Neural implants	▪ Cochlear implant ▪ Dialyzers ▪ Plasmapheresis
Divices for controlled drug delivery	▪ Coating for tablets or capsule ▪ Transdermal systems ▪ Microcapsules ▪ Implants
General surgery	▪ Sutures ▪ Staples ▪ Adhesives ▪ Blood substitutes
Diagnosis	Fiber optics for endoscopy

There are several ways to classify biomaterials. One of them is based on the body response in this case, is cataloged in the previous reports [13−15]:

▪ **Bioactive Materials**: The materials can produce a chemical response during its contact with physiological solutions, creating an interfacial link between the material and surrounding tissues. Depending on the compound, it may also have osteoconductive properties. However, it do not possess good mechanical properties. This classification consists of the hydroxyapatite ($Ca_{10}(PO_4)_6(OH)_2$) (HAp), and glass-ceramics.

- **Bioinert Materials**: The materials are properly accepted by the body because they do not provide a biological response. Additionally, they possess good mechanical properties; and they are resistant to the physiological condition of the body. These materials are mainly affected by corrosion in the link between the material and the tissue. However, this corrosion is usually poor. Examples of these materials are alumina, zirconia, Ti, and Cr-Co alloys.

- **Biodegradable or Bioabsorbable Materials**: The materials are characterized by its gradual degradation into the body to become part of the tissue where it is implemented. Calcium phosphates, such as α- and β- or tetracalcium phosphates, tricalcium phosphates and calcium sulfate are examples of these bioabsorbable materials.

The most common classification of the biomaterials is based on their structure. The advantages and disadvantages of using these materials are shown in **Table 1.4**. This classification consists in:

- **Metals and Alloys**: These minerals are inorganic compounds containing one or more metallic elements that may or not contain other non-metals. The most used elements are titanium, chromium, nickel, aluminum, etc. The most important alloys are those of titanium, stainless steel, chrome-cobalt-zinc and aluminum, which are primarily used to replace joints such as the hip or knee, bone plates, screws, nails and to the development of surgical material. Because these metal implants do not present bioactive behavior, they do not form a chemical bond with the inorganic component of bone. These materials deteriorate after a certain time, making its replacement is necessary.

- **Polymers**: This is the majority group of biomaterials, and it has a variety of structures, high effectiveness, and diversity of properties. Because their mechanical properties are inferior compared to other materials, like metals or composites, generally, these materials are blended with additives, in order to improve its mechanical properties. The most common polymers used in medical applications are polymethylmethacrylate (PMMA), polyethylene, polyvinyl chloride (PVC), polietilentereftalato (PET), polycaprolactone (PCL), polylactic

acid (PLA), polyglycolic acid (PGA), acid (lactic-co-glycolic acid). Disadvantage: Incompatibility of the generated wear particles with the agency.

- **Ceramics (Bioceramics)**: These biomaterials are polycrystalline and inorganic compounds, linked by ionic and covalent bonds, generally treated at elevated temperatures. Most of these biomaterials are characterized by their refractory nature, exhibit high resistance to compression, great stability and not chemical activity. However, these biomaterials are susceptible to fracture. One classification consists in bioinert bioceramics (such as alumina and zirconia), resorbable (such as tricalcium phosphate) bioactive (HAp, bioactive glasses, glass ceramics) or porous bone filling for (HAp coated metals). Ceramics is biocompatible thanks to the similarity of their chemical structure with the native bone. Additionally, a great contact between these materials and the bone is observed. The however process represents a difficulty, especially in a porous form, since it is not flexible as the bone, being very rigid and brittle. Bioceramics have been used for the repair, reconstruction, and replacement of diseased or damaged parts of the body since the 1960s.

- **Composites**: There are mixtures of constituents which retain their chemical identity and together form a one integral structure. These materials are composed of a matrix, which is generally the most abundant component and filler or reinforcement, which enhances the mechanical properties of the matrix. Polyethylene-HAp is an example.

Table 1.4 Advantages and disadvantages of the biomaterials when used in the body.

Biomaterials	Advantages	Disadvantages	Example use
Polymers (e.g., nylon, silicon, polyester, etc.)	Resilient, Easy to fabricate, elasticity	Not strong, Deforms with time, compressive and shear strengths casualties.	Blood vessels, sutures, ear, nose, Soft tissues
Metals (e.g., Ti and its alloys, Co-Cr alloys, stainless steels)	Strong tough, ductile, High transverse strength and tension, High	May corrode, dense, difficult to make, cytotoxicity of ions can occur	Join replacement, bone plates and screws, dental root implant, pacer, and suture

	wear resistance.	Co, Cr, Mo.		
Ceramics (e.g., aluminum Oxide, calcium phosphates, including hydroxyapatite carbon)	biocompatible Inert strong in compression	Brittle, resilient, Inelasticity.	Not	Dental coating, Orthopedic implants, Femoral head of hip
Composites (e.g., carbon, carbon wire or fiber reinforced, bone cement)	Compression strong	Difficult to make		Joint implants, Heart valves

1.1.3 Problems in Conventional Material Preparation and Surface Coatings

The main problem found in percutaneous devices is originated by the lack of a true bioactive behavior of these materials, factor that allows the bacteria to enter. Due to this, there is a growing interest in the use of HAp for coating percutaneous devices.

The coating has to transform a non-bioactive in a bioactive surface. Also has to protect the substrate from chemical attack by separating it from the surrounding tissue, for avoiding adverse reactions and for doing biocompatible compound. The physical integrity of the biomaterial-tissue interface and mechanical stability depend primarily on two factors: effectiveness of the mechanism of biomaterial osseointegration; and the biological response of the immune system. Surface functionalization provides a way to transform a bio-inert material into a biomimetic, or even bioactive material by coupling of protein layers to the surface, or coating the surface with self-assembling peptide scaffolds to lend bioactivity and/or cell attachment 3-D matrix.

Even though the binding properties of the skin and the percutaneous device are improved using surface coating technique on silicon with biocompatible materials, the conventional surface coating technique has many problems that can not completely prevent bacterial infection. These problems are the following [16]:

1) The biomaterial can provide biocompatibility, but it has not antibacterial activity. Because of the biocompatibility of the coating material, the bacteria can easily adhere on the material surfaces and can cause bacterial infection.

2) Generally, micro-size particles are used, and the problem is that bacteria are smaller than those particles, so the bacteria can permeate through the interspace among the microparticles (see **Figure 1.4**).

3) The problem with the use of this aminosilane coupling agents is that these agents present cyto- and bio- toxicity. Because they can damage the cells of the human body, is preferable to not use them (see **Figure 1.4**).

Silane coupling agents are used in a wide range of applications because of their unique ability to bond polymers with dissimilar materials such as inorganic oxides-i.e., silica and alumina [16−19]. The bond thus formed has good initial strength. The siliceous matter or metal may be in the form of fibers, particulate fillers, or massive structures. Almost every type of organic polymer is compatible with silane coupling agents, ranging from thermoset resins through elastomers to thermoplastic resins. The silane may be applied to the substrate as a pretreatment or, in many systems, is added to the resin, where it migrates to the substrate during normal mixing and application procedures. The application of silane coupling agents to promote bonding has led to improved physical properties of composite materials such as filled and reinforced resins, filled elastomers, caulks for adhesion of metal and glass, resin-coated, painted metal and coating surface of the catheter. Furuzono and collaborators synthesized a composite of HAp microparticles covalently coupled to a silicone elastomer [16]. The layer of HAp is formed by covalently linking amino groups of modified HAp particles and a silicone substrate grafted with a polymer containing carboxyl groups. With this surface modification, the bioactivity to the surface of an elastic implant is obtained without impairing substrate elasticity.

Coronas can generate audible and radio-frequency noise, particularly in the nearby of electric power transmission lines. They also represent a power loss, and their action on atmospheric particulates, along with associated ozone and NOx production, can also be disadvantageous to human health where power lines run through built-up areas.

Figure 1.4 (a) SEM image of the hydroxyapatite microparticles, and (b) scheme of the fixation of the microparticles on a silicone rubber surface using aminosilane coupling agents, indicating the problems of both "micrometer-sizes" and "silane coupling reagent usage" in the conventional surface coating, which is reprinted and modified based on the report [16].

1.1.4 Assignments for both Biocompatibility and Antibacterial Activity

Biocompatibility is related to the behavior of biomaterials in various contexts. For this reason, there are many definitions about biocompatibility. Two of the IUPAC definitions are more according to this topic are:

1. Biocompatibility: Ability to be in contact with a living system without producing an adverse effect.

2. Biocompatibility (biomedical therapy): Ability of a material to perform with an appropriate host response in a specific application. The biomaterial performs its desired function with respect to medical therapy, without eliciting any undesirable local or systemic effects in the recipient or beneficiary of that therapy, but generating the most appropriate beneficial cellular or tissue response in that specific situation, and optimizing the clinically relevant performance of that therapy.

The host response to both tissue engineering and drug delivery devices depends on the chemical, physical, and biological properties of the biomaterials. On the other hand, the antibacterial activity is a compound or substance that has the ability of kills or slows the growth of bacteria. The determination of the antibacterial activity of surfaces is described in the following norms: ISO 22196 and the Japanese norm JIS Z2801 published in 2000, and published again in 2007 as the internationally valid norm ISO 22196. Therefore, ISO 22196 and JIS Z 2801 are identical [15]. The definition of the ISO 22196:2007(E) for antibacterial activity is: difference in the logarithm of the viable cell count found on an antibacterial-treated product and an untreated product after inoculation with and incubation of bacteria [15].

With the increasing concern over microbial infections, in particular, hospital-acquired infections (many of them are catheter-related infections; being the bacterial adhesions on implant surfaces the initial crucial step in infection), there is growing demand for effective and safe antimicrobial agents. Additionally, if the material also has biocompatibility, the medical devices will be highly favored. Materials with biocompatibility and antibacterial activity have been used in several biomedical products, including wound or burn dressings, catheters, and bone cement.

The conventional studies of biomaterials that exhibit biocompatibility as well as antibacterial activity are polymer nanocomposites incorporating Ag and Cu nanoparticles. These materials had been regarded as particularly useful for applications in various fields including biomedical equipment and devices, water treatment, and food processing. Among these materials that exhibit both properties:

- **Silver nanoparticles (AgNPs):** The antibacterial effect of AgNPs is proposed to arise from the release of silver ions or alternatively from oxidation. It is known that the silver ions that cause damages to bacterial DNA, proteins, and enzymes, for that reason can directly inhibit bacteria growth. Especially, induction of the reactive oxygen species (ROS) is the mechanism responsible for the antibacterial effect of AgNPs and AgNP-mediated cytotoxicity in different cells.

- **Ag-doped HAp/poly(3-hydroxybutyrateco-3-hydroxyvalerate (PHBV) composites:** Silver (Ag) is a well-known antibacterial agent used in various biomedical applications such as antibacterial bandages, silver coated catheters or

implant materials. The incorporation of silver into HAp provides osteoconduction ability as well as bactericidal effect.

Silver has been widely investigated regarding with its antimicrobial activity due to its superior effectiveness and strong cytotoxicity towards a broad range of microorganisms, such as bacteria and fungi. In low concentrations, Ag ions are shown to be nontoxic to eukaryotic cells, but high concentrations of silver can cause cytotoxicity.

- **Nanocomposites of copper with cellulose**: Copper is a natural and an essential oligomer component in plants and animals tissues, where it participates in a number of important roles. It has been reported that Cu nanoparticles (Cu-NPs) have bactericidal effects comparable to Ag nanoparticles in single strains of *E. coli* and *B. subtilis*. However, high concentration the copper is toxic. Cu-NPs were found to cause multiple toxic effects such as generation of reactive oxygen species, lipid peroxidation, protein oxidation and DNA degradation in *E. coli* cells. Certain limits exist; the human body has mechanisms available for protection against copper toxicity at the cellular, tissue, and organ levels because the Cu can cause damage to the liver and kidneys and even death.

- **Ag- and/or Cu- and/or Zn- doped HAp**: Synthesized composed metal ion (Ag; Cu;Zn) doped HAp by wet method but did not clearly demonstrate any antimicrobial effect with the Cu(II) and Zn (II) sample. Synthetized composed zinc-doped HAp with the antimicrobial effect, but the use of nitrate salts as a starting reagent may cause the incorporation of NO_3^- into the HAp and affect its structure.

Silver, zinc or/and copper on a calcium phosphate, zeolite or silica substrate can be listed as inorganic antimicrobial materials. The heavy metal ions give the biocidal action [19–21]. Among them, synthetic HAp, one of the calcium phosphate, is the most promising material because of its biocompatibility, good action exchange rate with metals and high affinity for the pathogenic microorganism.

To obtain a material with both biocompatibility and antibacterial activity, it is necessary to drop a biomaterial with metal to provide the antimicrobial property. The most used materials were mentioned above: metals like copper and silver, also zinc can be used. Copper and zinc ions in small quantities are essential for various metabolic processes in

most of the living organisms, while, in higher amounts, they are potentially toxic. However, zinc also has a stimulatory effect on bone formation *in vitro* and *in vivo*.

1.2 Hydroxyapatite

1.2.1 Synthetic Methods

HAp is a ceramic, and its chemical formula is $Ca_{10}(PO_4)_6(OH)_2$. This compound is interesting for catalysis, fertilizers industry, pharmaceutical products, protein chromatography applications; water treatment processes, preparation of biocompatible materials. This is because it is the main inorganic component in calcified hard tissues of vertebrates (e.g., bone and teeth).

The biological HAp is found mainly in animals or in fish teeth and bones where the amounts are small. It is also formed pathologically as a result of functional irregularities resulting in cartilage arthritis, the formation of renal, bladder, salivary, brain, urethral and bile stones, atheromatic plaque, gallstone, tonsillolith and calcification of transplanted cardiac valves.

The tooth surface is composed of *c*-lattice planes of HAp crystals due to the preferred orientation. **Table 1.5** shows the amounts of water, inorganic and organic substances in the bone and tooth and **Table 1.6** presents the contents of elements in inorganic substances. These contents are little different by species, age and treatment after extraction [22−24].

Table 1.5 Representative contents (wt%) in inorganic and organic components and water in human bone and tooth.

	Bone (wt %)	Tooth	
		Dentine (wt %)	Enamel (wt %)
Inorganic	55	70	96
Organic	30	17	2
Wáter	15	13	2

Table 1.6 Representative contents (wt%) of Ca, P, and the other substituted elements in the inorganic components of human bone and tooth.

	Bone (wt %)	Tooth	
		Dentine (wt %)	Enamel (wt %)
Ca	34	35	37
P	15	16	17
Mg	0.5	1	0.4
Na	0.8	0.4	0.60
K	0.2	0.1	0.2
C	1.6	1.1	0.8
Cl	0.2	Trace	0.3
F	0.08	0.03	0.01
Zn	1−10	2.25	1.75
Residual	47.62	46.37	43.69

Synthetic HAp has occurred since the last century by various methods. The study of their properties and characteristics is a complex problem because many factors, such as temperature, pressure, pH, etc., influence in the transformation of this compound. The commercial HAp used in clinical and research applications is a solid in granular form, having a porosity of one hundred microns, suitable to cause bone growth in direct application as a bone substitute. The control of the porosity of synthetic HAp would result in better adhesion to the tissue where it was implemented.

Many routes have been developed for obtaining this material using hydrolysis, hydrothermal, wet methods, etc., giving different characteristics to the material depending on the technique used. The wet method is the most widely used method, and it is characterized by its simplicity and low cost. The methods for preparing HAp are shown in the previous report as follows [22]:

a) Wet chemical method: Using a solution reaction (from solution to solid). It is available for mass production of small crystalline or noncrystalline HAp powder. Typically, there are 2 kinds of the process in this method: one involving a neutral reaction of acid and

alkaline solution, and the other involves the reaction of calcium salts and phosphates salts. The typically chemical formulas for these processes are:

i. $10Ca(OH)_2 + 6H_3PO_4 \rightarrow Ca_{10}(PO_4)_6(OH)_2 + 18H_2O$

ii. $10Ca(NO_3)_26(NH_4)_2HPO_4 + 2H_2O \rightarrow Ca_{10}(PO_4)_6(OH)_2 + 12NH_4NO_3 + 8HNO_3$

The calcium source may be administered as aqueous solutions of $CaCl_2$, $Ca(NO_3)_2$, $CaCO_3$, $Ca(CH_3COO)_2$ or $CaSO_4.2H_2O$. As phosphate sources, can be used aqueous solutions of $(NH_4)_2HPO_4$, $NH_4H_2PO_4$, K_2HPO_4, KH_2PO_4, Na_2HPO_4 or $NaH2PO4$. The pH is controlled during synthesis by a flow of NH_3 gaseous or by adding aqueous solutions of NH_4OH, NaOH or KOH. Depending on the concentration of reactants and temperature, there will be substantial variation in the molar Ca/P ratio and crystallinity of HAp obtained. The process is by slow addition of the reactants to avoid drastic changes in the reaction conditions. A source is slowly added over the other previously placed in the reactor.

CO_2 in atmospheric air is absorbed by the alkaline aqueous solutions as CO_3^{2-} ion and eventually incorporated to HAp, replacing PO_4^{3-} ions or OH^- ions of HAp reticle. When the synthesis is performed in the presence of sodium or potassium ions, these ions partially substitute the Ca^{2+} ions into the product

b) Dry method: Using solid state reaction at high temperature in a mixture of calcium and phosphate compounds such that the Ca/P ratio of the mixture corresponds a theoretical value of 1.67 (from solid to solid), is convenient to prepare a well-crystallized HAp. For example, when brushite and calcium carbonate are used as a start material for preparation of HAp, the following continuous reactions occurs:

$$6CaHPO_42H_2O + 4CaCO_3 \xrightarrow{>900°C} Ca_{10}(PO_4)_6(OH)_2 + 4CO_2 + 14H_2O$$
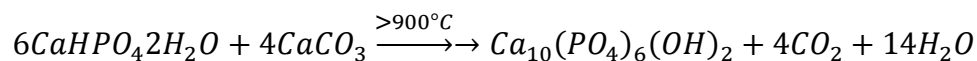
The HAp synthesized by this method is very fine; the crystallinity is excellent and has low solubility.

c) Hydrothermal method: Using hydrothermal reaction (from solution to solid). Used for obtaining large, perfect single crystals of HAp. Peroff and associates (1956) succeeded in growing HAp crystal to 0.3mm under hydrothermal conditions of 300°C and about 85 kg/cm^2 [22].

d) Alkoxide method: Using hydrolysis reaction (from solution to solid) to prepare an HAp film. One example is using calcium nitrate 4-hydrate and trimethyl phosphate as

starting materials and then dissolved it in ethanol or formamide as solvents. After the solvent had vaporized, the mixture was heated at 500−1000°C to produce well-crystallized HAp. The formula is represented as:

$$Ca(NO_3)_2 4H_2O + (CH_3O)_3PO \rightarrow Ca_{10}(PO_4)_6(OH)_2$$
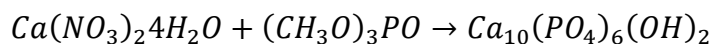
e) Flux method: Using fused salt reaction (from the melt to solid). Used for preparing big single crystals. Pure HAp is not prepared using this method but apatite single crystals like fluorapatite, chlorapatite and boronapatite have been synthesized by this method using CaF_2, $CaCl_{2,}$ and B_2O_3 flux.

1.2.2 Structures and Properties

HAp is a crystalline isomorphic biomaterial, classified as a ceramic. This material has a molecular weight of 1004.64 g/mol, a theoretical density of 3.156 g/cm^3 and a molar ratio of Ca/P of 1.67 related to its stoichiometry [22, 25−26]. The bioactivity of calcium phosphates is related to the crystal structure, the porosity and its rate of dissolution in the body, the latter in turn is affected by the molar Ca/P ratio. Calcium phosphates with highest Ca/P are precipitated in alkaline solution, and those with lower Ca/P ratios are precipitated in acid solution. Generally HAp is produced in neutral or alkaline solution. The crystalline structure of HAp (see **Figure 1.5**) is characterized by a hexagonal system with space group P6$_3$/m, although it may have a slight variation in cell sizes associated with the presence of impurities such as magnesium (replacing part of calcium), carbonates (replacing some phosphate) and fluorine (replacing some hydroxyl). In this condition, a very low solubility is presented, and as biomaterial structure, solubility ensures high chemical exchange activity in the extracellular medium. The lattice constants of hexagonal HAp are *a*=9.423Å and *c*=6.875Å. The hexagonal HAp has mirror planes at z = ¼, ¾, and the hydroxyl arrangement shows two-fold disorder [22, 27].

There are two crystallographically independent Calcium atoms in the unit cell (see **Figure 1.5**). The Ca(2) atom is surrounded by six oxygen atoms belonging to phosphate (PO$_4$) groups and the hydroxyl (OH) group, whereas the Ca(1) atom is nearly octahedrally surrounded by six oxygen atoms. The Ca(2) triangles stack along the *c*-axis, rotating mutually 60° from each other. In the HAp structure, the OH group is not located at the

center but shifted above or below the center of the triangle. The phosphorus atom is surrounded by four oxygen atoms and forms a tetrahedron. The PO_4 tetrahedron is almost regular with only slight distortion. Ca(2) is exposed on the crystal surface, thus playing a large role in the physical properties of HA, such as surface charge, and in interactions with organic compounds [22, 25−28].

OH channel
Ca(I) site
Ca(II) site
a
b   c
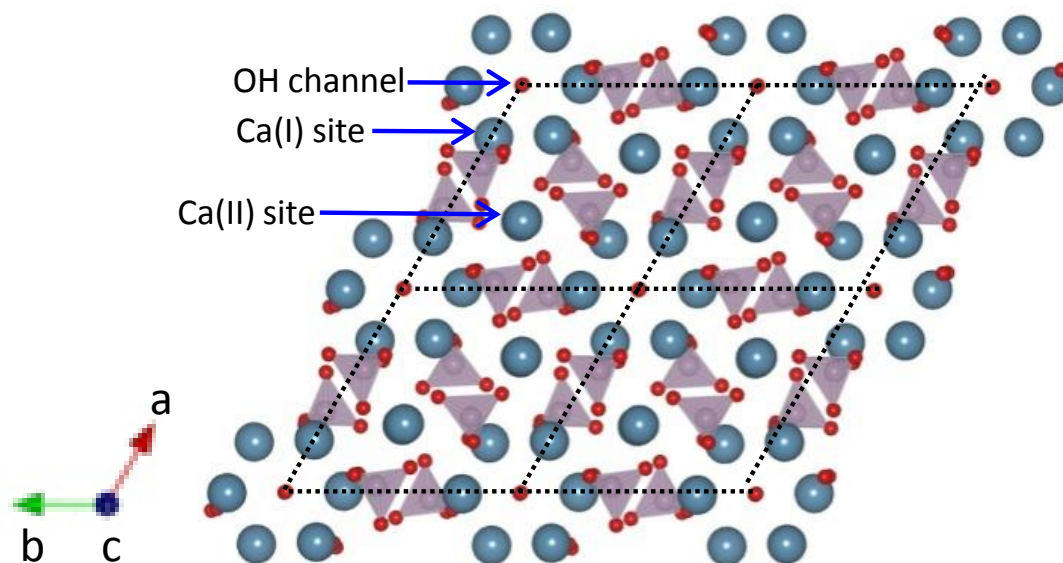
Figure 1.5 Crystal structure of HAp seen in the top view along *c*-axis, and the top view of $2 \times 2 \times 1$ cell, centered on hexagonal *c*-axis channel**.**

The HAp is highly biocompatible and presents bioactive properties. The crystal structure, morphology, thermal stability and mechanical properties play an important role in the biological responses of bone cells. HAp physicochemically bonds to the bone and promotes bone formation necessary for implant osseointegration. This property is needed to minimize damage to the surrounding tissues and to increase the implant efficiency. However, even that HAp can form a direct bond with neighboring bones, for its application as biomaterial, it should also consider other important factors such as strength, hardness, porosity, dissolution, adhesion, etc., besides physical and chemical aspects; and it should not ignore the intent to use, as the environment where they will place has specific characteristics, considering it is not the same use as filler, as a support or as a substitute.

HAp has several attractive, useful properties in the medical field; the main characteristics are: it has a very slow resorption, and it allows a better new bone, it is osteoconductive, biocompatible, resorbable (10−30%), osteofilic, undergoes a process of

osseointegration, and it has a highly porous structure; these porous structure allows a better neovascularization of the formed bone. The problem with this material in monolithic form is its unsatisfactory mechanical properties so that it is undesirable to use in weight bearing parts. This problem could be solved by the reinforcement using a material with good mechanical properties.

1.2.3 Heteroelement-substituted Hydroxyapatite

HAp is a member of the "apatite" that is a general term for crystalline mineral with a general composition of $M_{10}(ZO_4)_6X_2$ [22, 26−28]. The name was taken from the greek word "apate" (απαταω) that means deceit. Many elements could occupy the M, Z and X sites like:

M=Ca, Mg, Sr, Ba, Mn, Fe, Zn, Cd, Pb, Na, K, Al, etc.

Z=P, V, As, S, Si, Ge, CO_3, etc.

X=F, Cl, OH, O, Br, CO_3, etc.

If the X is fluorine, it is given the name fluorapatite. It is the main source of phosphorus, used as the standard mineral for hardness level 5 on the Mohs scale, making it an invaluable source of rock-forming minerals. When the X is OH⁻, i.e. $Ca_{10}(PO_4)_6(OH)_2$, it is given the name HAp.

HAp is one of many types of calcium phosphate, but there are several others in this class. The main compounds of calcium phosphate are listed in **Table 1.7**. The simplest way to arrange these compounds into order is by the calcium-phosphorus composition ratio, Ca/P ratio (number of moles of Ca divided by the number of moles of P existing in the compound). The most stable phase of calcium phosphate ceramics depends significantly on the temperature and the presence of water, either during processing or in the use environment. At physiological pH (7.2−7.6), HAp is more stable. MCPM, DCP, DCPD, and TeCP are used as the ingredients of calcium phosphate cement [29].

A biological apatite is a non-stoichiometric form of HA, characterized by Ca^{2+} deficiency but containing trace elements such as cations (Mg^{2+}, Mn^{2+}, Zn^{2+}, Na^{2+}, Sr^{2+}) or anions (HPO_4^{2-} or CO_3). Reports confirm that this substitution by cations can lead advantageous effects on biomaterial properties, such as the degree of structural order (i.e. crystallinity, lattice parameters), solubility in chemical solvents, and surface change

dissolution rate under simulated physiological conditions. The most common advantageous effect is obtained with the CO_3^{2-} ion, which constitutes 5-8% of apatite in bone, by weight. The CO_3^{2-} ion can replace both OH^- and PO_4^{3-} within the HAp structure, termed A-type and B-type replacement, respectively. B-type replacement is common in bones, and it is an essential factor in altering the melting point of the biological apatite. Increases in positive charge with the replacement of PO_4^{3-} by CO_3^{2-} are balanced out either by the loss of Ca^{2+} sites or by the introduction of Na^+ ions; the name for this type of apatite is calcium-deficient HAp (CDHA) is greater for biological interest than stoichiometric because the mineral portion of bone is primarily CDHA partially substituted with carbonate. This has shown that CDHA plays an important role in the formation and bone turnover [22, 30].

Table 1.7 Classification of calcium phosphate compounds depending on the chemical formula and Ca/P ratio.

Name	Abbreviation	Formula	Ca/P
Tetracalcium phosphate	TeCP	$Ca_4O(PO_4)_2$	2.0
Hydroxyapatite	HAp	$Ca_{10}(PO_4)_6(OH)_2$	1.67
Amorphous calcium phosphate	ACP	$Ca_{10-x}H_{2x}(PO_4)_6(OH)_2$	
Hydroxyapatite calcium deficient	CDHA	$Ca_9(HPO_4)(PO_4)_5(OH)_2$	1.5
Tricalcium phosphate (α,β,γ)	TCP	$Ca_3(PO_4)_2$	1.5
Octacalcium phosphate	OCP	$Ca_8H_2(PO_4)_6.5H2O$	1.33
Dicalcium phosphate dihydrate (Brushite)	DCPD	$CaHPO_4.2H_2O$	1.0
Dicalcium phosphate (Monetite)	DCP	$CaHPO_4$	1.0
Calcium pyrophosphate (α,β,γ)	CPP	$Ca_2P_2O_7$	1.0
Calcium pyrophosphate dihydrate	CPPD	$Ca_2P_2O_7.\ 2H_2O$	1.0
Heptacalcium phosphate (Trömelite)	HCP	$Ca_7(P_5O_{16})_2$	0.7

Tricalcium dihydrogen phosphate	TDHP	$Ca_4H_2P_6O_{20}$	0.67
Monocalcium phosphate monohydrate	MCPM	$Ca(H_2PO_4)_2.H_2O$	0.5
Calcium metaphosphate (α,β,γ)	CMP	$Ca(PO_3)_2$	0.5

1.2.4 Zinc-substituted Hydroxyapatite

Zinc is a nutritionally essential trace element needed for catalytic, structural, and regulatory functions in the body. Numerous aspects of cellular metabolism are zinc-dependent. Zinc plays important roles in growth and development, the immune response, neurological functions, and reproduction. On the cellular level, the function of zinc can be divided into three categories: (a) catalytic, (b) structural, and (c) regulatory [31].

(a) **Catalytic role**: Over 300 different enzymes depend on zinc for their ability to catalyze vital chemical reactions. The six classes of enzymes (oxidoreductases, transferases, hydrolases, ligases, isomerases and ligases), require zinc in the structural role

(b) **Structural role**: Zinc plays an important role in the structure of proteins and cell membranes. A finger-like structure, known as a zinc finger motif, stabilizes the structure of a number of proteins.

(c) **Regulatory role**: Zinc-finger proteins have been found to regulate gene expression by acting as transcription factors (binding to DNA and influencing the transcription of specific genes). Zinc also plays a role in cell signaling and has been found to influence hormone release and nerve impulse transmission. Zinc has been found to play a role in apoptosis (gene-directed cell death), a critical cellular regulatory process with implications for growth and development, as well as a number of chronic diseases.

Therefore, zinc is involved in a range of biochemical processes related to human metabolism, so physiological and metabolic functions are altered when the deficiency

occurs. Zinc is present in all organs, tissues, fluids and secretions from the human body. Approximately 83% of zinc in the body is muscle and bone, and 95% of this is located intracellularly.

In low concentrations, zinc is very helpful in healing wounds, reducing the duration and severity of colds. Additionally, it has antimicrobial properties that help relieve the symptoms of gastroenteritis, and it is used in toothpaste to prevent bad breath and shampoo to stop dandruff. However, high concentrations of zinc can be toxic.

The U.S. recommended dietary allowance (RDA) for adult men and women is 11 mg/day and 8 mg/day of zinc, respectively (see **Table 1.8**) [31]. Zinc enters the body through the digestive tract when people eat food or drink water containing it. It can also enter the lungs when zinc dust or fumes from zinc smelters or operations soldier in work areas inhaled. The most important route of exposure near waste sites appears to be through the contaminated water with zinc. Normally, zinc leaves the body via the urine and feces.

Table 1.8 Recommended dietary allowance (RDA) for zinc in a specific age and gender group, which is reported by U.S. government agency, which is reprinted and modified based on the report by Dietary Reference Intakes (DRI reports) [32].

The Recommended Dietary Allowance (RDA) for Zinc

Life Stage	Age	Males (mg/day)	Females (mg/day)
Infants	0−6 months	2 (AI)	2 (AI)
Infants	7−12 months	3	3
Children	1−3 years	3	3
Children	4−8 years	5	5
Children	9−13 years	8	8
Adolescents	14−18 years	11	9
Adults	19 years and older	11	8
Pregnancy	18 years and younger	−	12
Pregnancy	19 years and older	−	11

Breast-feeding	18 years and younger	–	13
Breast−feeding	19 years and older	–	12

The levels of zinc that produce health effects are generally much higher than those recommended dietary allowance. If large doses of zinc are ingested (10 to 15 times higher than recommended), even for a short time, stomach and digestive problems may occur. High quantities of zinc can also interfere with the body's immune system and the body's ability to absorb and use other essential minerals like copper and iron. Isolated outbreaks of acute zinc toxicity have occurred as a result of the consumption of food or beverages contaminated with zinc released from galvanized containers. Signs of acute zinc toxicity are abdominal pain, diarrhea, nausea, and vomiting. Single doses of 225 to 450 mg of zinc usually induce vomiting. Milder gastrointestinal distress has been reported at doses of 50 to 150 mg/day of supplemental zinc. The major consequence of long-term consumption of excessive zinc (60 mg/day) is a copper deficiency. In order to prevent copper deficiency, the U.S. Food and Nutrition Board set the tolerable upper intake level (UL) for adults (UL) for adults at 40 mg/day, including dietary and supplemental zinc (see **Table 1.9**).

Table 1.9 Human Tolerable Upper Intake level (UL) for Zinc reported from the U.S. Food and Nutrition agency, which is reprinted and modified based on the report by Dietary Reference Intakes (DRI reports) [32].

Tolerable Upper Intake Level (UL) for Zinc	
Age Group	**UL (mg/day)**
Infants 0−6 months	4
Infants 7−12 months	5
Children 1−3 years	7
Children 4−8 years	12
Children 9−13 years	23
Adolescents 14−18 years	34
Adults 19 years and older	40

There are three mechanisms for the antimicrobial activity of zinc ions. In the first one, zinc ion bind to protein deactivate them (see **Figure 1.6**). In the second mechanism, zinc ions can interact with the microbial membrane, which causes structural change and permeability. In the last one, metal ions interact with microbial nucleic acids, preventing microbial replication [33].

Covalent bonds like disulfide (-SS-) are important in the tertiary structure of many proteins. The biological activity of a protein depends mainly on the specific primary structure which is held together by such links. When a protein is heated or treated with any of a variety of chemicals, like metals, the tertiary structure is lost. Espiralazas peptide chains are unfolded to give a random configuration accompanied by a loss of biological activity of the protein. This change is called "denaturation" and results in the precipitation of the protein. Heavy metals precipitate proteins are creating links (cross-linkages) between the free amino groups and the free carboxyl groups, or can also be linked to sulfur breaking the disulfide bonds of the proteins.

Figure 1.6 shows protein precipitation caused by toxicity of metals, like zinc, in which the metal is bound to sulfur by breaking protein disulfide bonds, thereby generating the loss of tertiary structure and thus its biological activity.
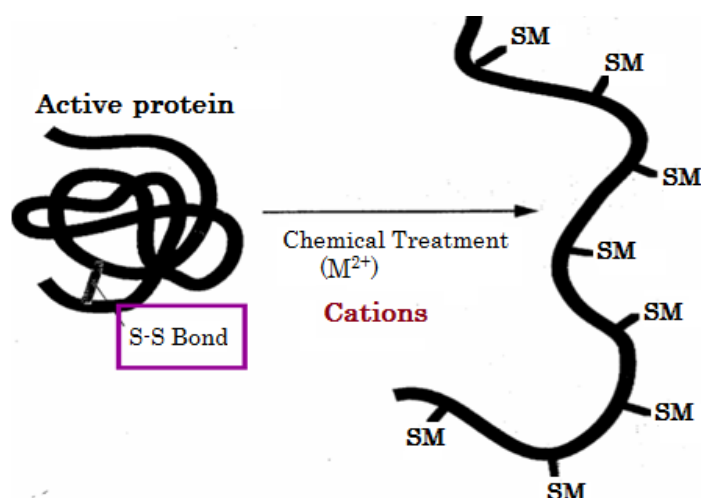
Figure 1.6 Scheme of metal toxicity mechanism of protein precipitation by metal ion reaction.

Hexagonal HAp structure enables some ionic substitutions according to charge type, charge size and ionic radii. These substitutions change structural, mechanical and biological properties of HAp. Zinc ion has +2 changes for that reason could be incorporated into the HAp structure by replacement with Ca^{2+} ion. The incorporation of Zn^{2+} decreased the grain sizes and increased the solubility of pure or carbonated HAp.

The interest for doping HAp with Zn is because biological tissue, like bone and enamel of human teeth, are composed of HAp containing zinc. Zinc incorporation into implants promotes bone formation around the implant and decreases the inflammatory response and also results in osteoclastic inhibition [34−36]. This element has an important role in the activity of much as 200 enzymes, and its uptake and release are strongly mediated by the bone reservoir in the body. Additionally the zinc has antibacterial and antifungal effects against *Escherichia coli, Staphylococcus aureus* and the pathogen yeast *Candida albicans* [33].

1.3 Fixation Technique of Nanocrystals without Chemical Reagents

Bioactive coatings increase the strength of the bone-implant interface, improve the biocompatibility of materials and offer high strength to the physiological conditions of the body, abrasion resistance and high fracture resistance.

The different approaches to functionalization of biomaterials exist. Different techniques vary in terms of coating thickness, substrate adhesion, density and consequently the phases present in the coating. Shown in **Table 1.10** summarizes the advantages and disadvantages of some HAp coating techniques [37].

HAp powders can be applied to the metal substrates by plasma sprayed, magnetron sputtering, electrophoretic deposition, enameling techniques and other methods.

Table 1.10 Advantages and disadvantages of the HAp coating techniques on solid substrates.

Technique	Thickness	Advantages	Disadvantages
Electron Beam Sputtering (EBS) Ion Sputtering (IS)	0.5-3 μm	▪ Coatings with uniform thickness. ▪ Dense coatings.	▪ Long times. ▪ Amorphous Coatings
Laser ablation	0.05-5 μm	▪ Dense and Porous coatings. ▪ Crystalline coatings.	Developing Technique
Dynamic Mixed Methods	0.05−1.3 μm	High adhesion between the coating and the substrate.	▪ Developing Technique. ▪ Expensive. ▪ Amorphous Coatings.
Dip Coating	0.05−0.5mm	▪ Cheap. ▪ Fast. ▪ Coating different geometries.	▪ High-temperature sintering. ▪ HAp decomposition.
Sol-Gel Method	< 1 μm	▪ Coating different geometries. ▪ Low temperatures. ▪ Relatively inexpensive because the coatings are thin.	▪ High-temperature sintering. ▪ HAp decomposition.
Electrophoretic Deposition	0.1−2 mm	▪ Nonuse of silane coupling agent ▪ Coatings with uniform thickness. ▪ Fast deposition rate. ▪ Coating different geometries.	▪ Coatings with cracks. ▪ High-temperature sintering. ▪ HAp decomposition
Biomimetic Coatings	< 30 μm	▪ Low temperatures. ▪ Similar to the formation of bone apatites. ▪ Coating different geometries. ▪ Possible incorporation	▪ Long times. ▪ FCS control solution (pH) and continuous regeneration.

27

		of bone forming components.	
Hot Isostatic Pressing (HIP)	0.2−20 mm	Dense coatings	▪ No coating different geometries. ▪ Elevated temperatures. ▪ Mismatch in thermal expansion. ▪ Differences in elastic properties. ▪ Expensive.
Thermal Spray Plasma Spray	50 µm−2mm	▪ Coating different geometries. ▪ Relatively inexpensive.	▪ Elevated temperatures. ▪ HAp decomposition.

According to the characteristics of these covering techniques, two of them will be studied electrophoretic deposition and plasma processing because an aminosilane coupling agent is not required, and its realization is easy.

a) **Electrophoretic Deposition:**

The interest in the use of electrophoretic deposition for biomedical applications is increasing because there are several advantages in the use of this technique like:

- Deposition without using chemical reagents.
- Simplicity
- Low cost
- Possibility of deposition of stoichiometric, high purity material to a degree not easily to achievable by other processing techniques with control of the film thickness
- Uniformity and deposition rate, possibility of forming coatings in bodies with complex shape,
- The electric field provides a higher deposition rate in defect region, resulting in better packing and uniformity of the deposit.

In the general principles, two simultaneous processes lead to the formation of solid films: the movement of the charged particles under the applied electric field and the

deposition of those particles onto the electrode. Electrophoretic deposition is a powerful method for the production of both thin and thick films.

Figure 1.7 represents a simplified plating cell. DC source, usually a rectifier or motor generator, supplies current flow in one direction through the external portion of the circuit when a potential difference is imposed across the system. The current flow is that of electrons in the external conductors. The mechanism of electrical transfer in the solution is by means of electrically charged "particles" called ions. Positive ions (cations) travel toward the negative electrode (cathode) and negative ions (anions) travel toward the positive electrode (anode) when the potential is applied, thus completing the electrical circuit [37−40].
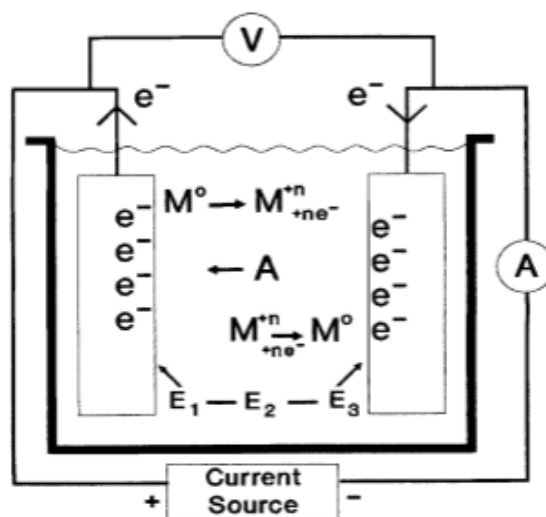
Figure 1.7 Illustration of the electrochemical deposition of Hap on a solid substrate, which is reprinted and modified based on the report [35].

The cathode or deposition reactions are characterized as reduction reactions since electrons are "consumed," and the valence states of the ions involved are reduced. The anodic reactions are oxidation reactions wherein electrons are liberated, and the valence states are increased. Each set of reactions represents half-cell reactions and proceeds independently of the other, limited by a condition of material balance, i.e., electrons liberated in the anode reactions must equal the number of electrons "consumed" in the cathode reactions. **Figure 1.8** shows the covering of the silicone rubber with the HAp.
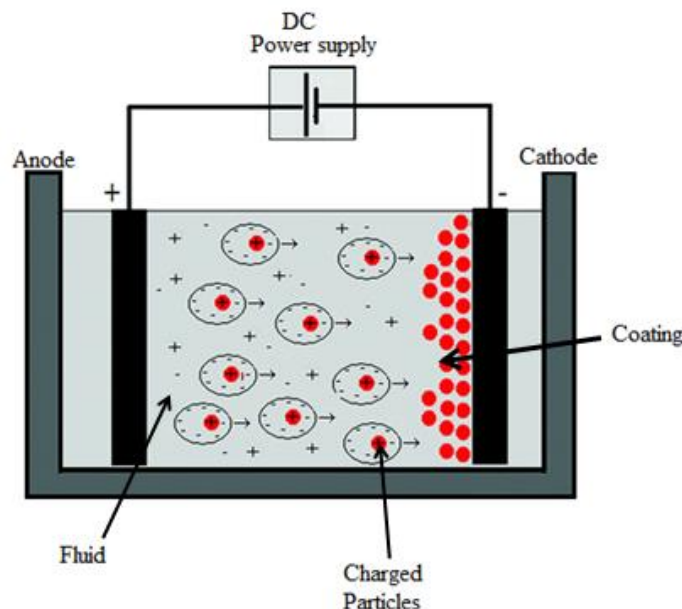
Figure 1.8   Scheme of the experiment set-up of electrophoretic deposition, which is reprinted and modified based on the report [41].

b) <u>Plasma Spray Process</u>:

Plasma has been successfully applied to chemically inert materials like polymers or silicon to graft various functional groups to the surface of the implant. Plasma spraying is most popular method due to its feasibility and low operational cost. Plasma sprayed HA coatings bear good mechanical properties, there are sprayed onto implantable devices to improve adhesion and bone healing.

Plasma Spray Process is basically the spraying of molten or heat softened material onto a surface to provide a coating (see **Figure 1.9**). The material in the form of powder is injected into a very high-temperature plasma flame, where it is rapidly heated and accelerated to a high velocity. The hot material impacts on the substrate surface and rapidly cools forming a coating. This plasma spray process carried out correctly is called a "cold process" (relative to the substrate material being coated) as the substrate temperature can be kept low during processing avoiding damage, metallurgical changes and distortion to the substrate material.

In general principles, the plasma spray gun comprises a copper anode and tungsten cathode, both of which are water cooled. Plasma gas (argon, nitrogen, hydrogen, helium) flows around the cathode and through the anode which is shaped as a constricting nozzle.

The plasma is initiated by a high voltage discharge which causes localized ionization and a conductive path for a DC arc to form between cathode and anode. The resistance heating from the arc causes the gas to reach extreme temperatures dissociates and ionizes to form a plasma. The plasma exits the anode nozzle as a free or neutral plasma flame (plasma which does not carry electric current) which is quite different to the Plasma Transferred Arc coating process where the arc extends to the surface to be coated. When the plasma is stabilized ready for spraying the electric arc extends down the nozzle, instead of shorting out to the nearest edge of the anode nozzle. This stretching of the arc is due to a thermal pinch effect. Cold gas around the surface of the water cooled anode nozzle being electrically non-conductive constricts the plasma arc, raising its temperature and velocity. The powder is fed into the plasma flame most commonly via an external powder port mounted near the anode nozzle exit. The powder is so rapidly heated and accelerated that spray distances can be in the order of 25 to 150 mm [42, 43].
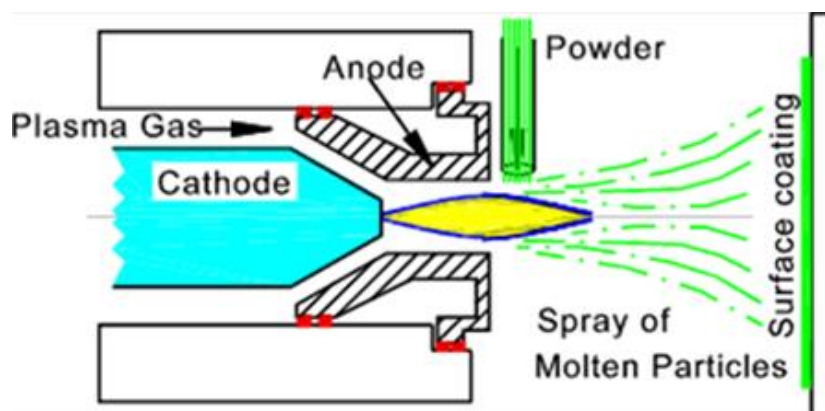
Figure 1.9   Schematic diagram of the plasma spray process, which is reprinted and modified based on the report by "Thermal Spray Coatings" [44].

1.4 Scope of This Study

In this study, the synthesis of zinc-substituted HAp (Zn: HAp) nanocrystals and subsequent formation of the nanocrystalline film on the biomedical polymer without using chemical reagents for investigating their biocompatibility as well as antibacterial properties as shown in **Figure 1.10**. It is focused that the synthesized material possesses the following characteristics:

1. Having biocompatibility and also has antibacterial activity. Because HAp is a material that has good biocompatibility and biodegradability because HAp is the main component of bones and teeth in mammals, it is pretended that with the addition of zinc ion (II) (Zn^{2+}), the HAp acquire the antibacterial ability by the dope in the host.

2. The synthesized material has to be nano-sized particles to fill the interspace. Because the particles are very small (nanometers), the space between them is lower and, therefore, the bacteria can no longer permeate through the interspace.

3. Development of a fixation technique without chemical reagents (e.g., Use of electric field, plasma treatment, thermos-compression). No silane coupling agents used are toxic to cells.

The thesis contains the four chapters. In "*Chapter 1*" in this chapter, it was suggested that the surface modification of the biomedical polymer (e.g., silicone resin) used as catheters is desired for improving the biocompatible and antibacterial properties. As the modification materials, hydroxyapatite ($Ca_{10}(PO_4)_3(OH)_2$) (HAp), which is crystallographically and chemically similar to the components of human's hard tissues, is a good candidate. Importantly, naturally-formed HAp is not absolutely pure and has some impurities of ions (Zn^{2+}, Mg^{2+}, K^+, etc.), which provides biocompatibility as well as antibacterial properties. In "*Chapter 2*", Zn: HAp nanocrystals were synthesized by a wet chemical method. In the method, the initial (Ca+Zn)/P ratio of 1.67 and 2.00 were adjusted from the reagents ($CaCl_2$, $ZnCl_2$, and K_2HPO_4) to resultantly form the stoichiometric and carbonate HAp nanocrystals, respectively. The initial $ZnCl_2$ was changed as the dopant concentration of Zn/(Ca+Zn) = 0.0, 2.5, 5.0 and 10 mol%. In "*Chapter 3*", an electrophoretic deposition at the optimized voltage of 100 V was used for the surface modification of biomedical polymers. In "*Chapter 4*", the nanocrystalline Zn: HAp films

were summarized to provide good biocompatibility as well as antibacterial properties on biomedical polymer surfaces, suggesting useful catheter surface modification technique.
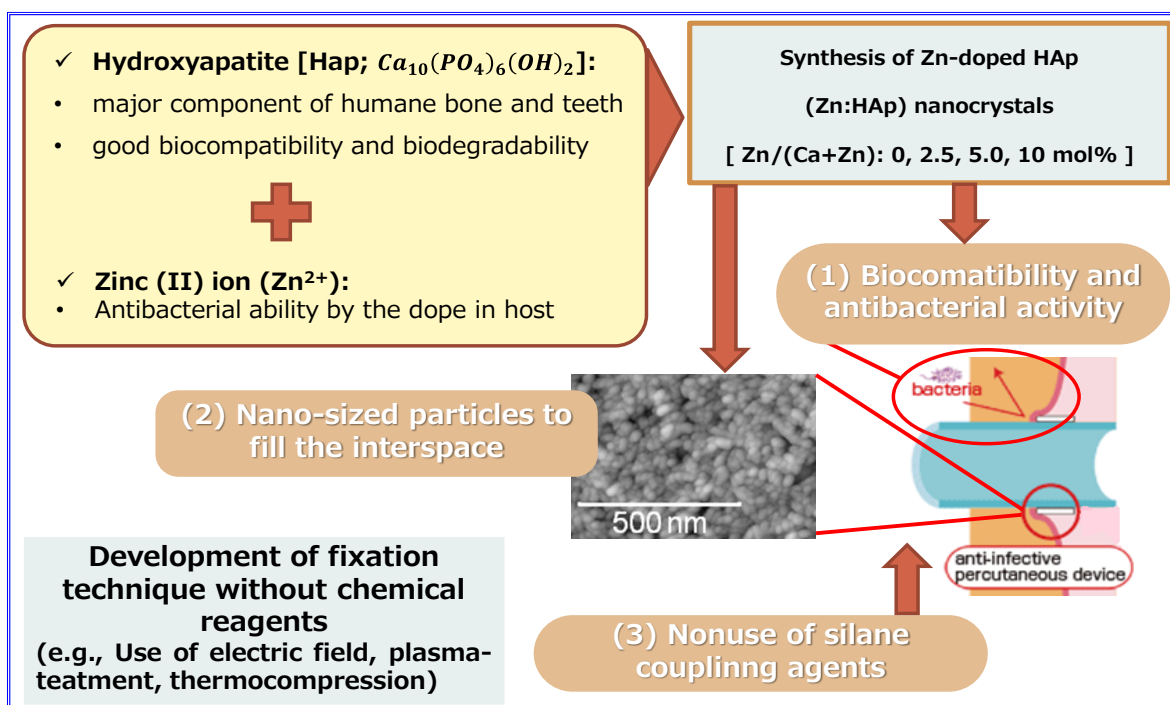
Figure 1.10 Scope of this study "Preparation and biological evaluation of nanocrystalline zinc-substituted hydroxyapatite films for medical applications", which will completely prevent the bacterial infection (i.e., down-growth) by indwelling Zn: Hap nanocrystals just beneath the skin.

REFERENCES

[1]   Gokal, R.; Khanna, R.; Krediet, R.; Nolph, K.Textbook of Peritoneal Dialysis, 2nd ed. Kluwer Academic Publishers

[2]   Álvarez, A.;Cortés, J.; Gómez, C.; Fernández, J.; Sossa, M.; Beltrán, F.; Mendieta, G.; Montúfar, F.; Ortiz, G.; Padilla, A.; Guías de práctica clínica para la prevención de infecciones intrahospitalarias asociadas al uso de dispositivos médicos (2010)

[3]   M. Espiaua,M.; Pujolb, M.; Campins-Martíc,M.; Planesd, A.; Peñab, Y.; Balcellsb, J.; Roquetab, J., An Pediatr, 74:3, 188 (2011).

[4]   World Health Organization (WHO), Report on the Burden of Endemic Health Care-Associated Infection Worldwide. A systematic review of the literature (2011)

[5]   Speranza, G.; Gottard, G.;Perderzolli, C.; Canteri, R.; Carli, E.; Lui, A.; Maniglio, D.; Brugnara, M.; Anderle, M.; Pasquardini, L. Role of chemical interactions in bacterial adhesion to polymer surface. Biomaterials, 25, 2029 (2004)

[6]   Monteiro, D.; Gorup L.; Takayima, A.; Filho, A.; Camargo, E.; Barbosa, D., International Journal of Antimicrobial Agents, 34, 103 (2009)

[7]   Tomazi, A.; Chollopetz, M., Rev. Latino-Am. Enfermagem 18:2 (2010)

[8]   Mah, T.; O'Toole, A., TRENDS in Microbiology, Vol.9, No.1 (2001)

[9]   Jefferson, K. What drives bacteria to produce a biofilm?, FEMS Microbiology letters, 236, 163 (2004)

[10] Houdt, R.; Michiels, Michiels, C., Research in Microbiology, 156, 626 (2005)

[11] Arciola, C., The International Journal of Artificial Organs, Vol. 32, no. 9, 533 (2009)

[12]Manufacturing technology of equally shaped and sized hydroxyapatite nanoparticle. http://sofsera.co.jp/english/tech3_e.html. (10/02/2015)

[13] Williams, D.,Medical Device Technology 14,8, (2003)

[14] Ghosh, S.; Banthia, A. Biocompatibility and antibacterial activity studies of polyamidoamine (PAMAM) dendron, side chain dendritic oligourethane (SCDOU), Wiley InterScience (2014)

[15] Biocompatibility Safety Assessment of Medical Devices: FDA/ISO and Japanese Guidelines". Mddionline.com. (02/2015)

[16] Furuzono, T.; Wang, P.; Korematsu, A.; Miyazaki, K.; Oido-Mori, J.; Kowashi, Y.; Ohura, K.; Tanaka, Kishida A., J Biomed Mater Res Part B: Appl. Biomater 65B, 217, (2002).

[17] Bierbaum, S.; Hintze, V.; Scharnweber, D., Biomatter 2:3, 132, (2012)

[18] Suslua, A.; Albayraka, Z. Bayirb, E.; Urkmezc, A.; Cocena, U., 64:9, 465 (2015)

[19] Damm, C.; Münstedt, H.; Rösch, A., Materials Chemistry and Physics, 108, 61 (2008)

[20] Lin, J.; Lin, W.; Li, S; Lin, C.; Hsu, S., ACS Appl. Mater. Interfaces, 5, 433, (2013)

[21] Suslua, A., Albayraka, A.; Bayirb, E.; Urkmezc, A.; Cocena, U., International Journal of Polymeric Materials and Polymeric Biomaterials, 64:9, 465, (2014)

[22] Aoki H. Science and Medical Applications of Hydroxyapatite. JAAS, 1991, 214pp.

[23] Valencia R., Espinosa R., Ceja I., Marín A., Rodyb,vol 2, no. 3, 1(2013)

[24] Matthew, J.;, Xingguo, C.; Sang, S.; Rajendra, Kumar.; Yi-Yeoun, K.; Michael, J.; Elliot P.; Laurie B., ScienceDirect, MSR-343,1, (2007)

[25] Jevtic, M.; Mitric, M.;kapin, S.; Jancˇar , B.; Ignjatovic, N.; Uskokovic, D. Crystal Structure of Hydroxyapatite Nanorods Synthesized by Sonochemical Homogeneous Precipitation, crystal growth &design, vol.8,no.7, 221, (2008)

[26] Orlovskii, V.; Komlev,V.; Barinov, S. Hydroxyapatite and Hydroxyapatite-Based Ceramics. Inorganic Materials, Vol. 38, No. 10, 973,(2002).

[27] Al-Jawad M, Steuwer A, Kilcoyne SH, Shore RC, Cywinski R, Wood, D., Biomaterials, 28, 2908, (2007)

[28] Elliott J C. Studies in inorganic chemistry 18: Structure and chemistry of the apatites and other calcium orthophosphates. Amsterdam: Elsevier, (1994)

[29] Massaro, C.; Baker, M.; Cosentino, F.; Ramires, P.; Klose, S.; Milella E., J Biomed Mater Res. 58, 651 (2001).

[30] Barralet, J.; Best, S.; Bonfield, W., J Biomed Mater Res, 41, 79, (1998)

[31] Romaña, D.; Castillo, C.; Diazgranados, D., Rev Chil Nutr , Vol. 37, No.2, 234 (2010)

[32]Food and nutrition board, Institute of medicine. Dietary Reference Intakes for Vitamin A, Vitamin K, Arsenic, Boron, Chromium, Copper, Iodine, Iron, Manganese, Molybdenum, Nickel, Silicon, Vanadium, and Zinc. National Academy Press 442-501(2001)

[33] Ardila, M.; Vargas, A.; Pérez j.; Mejía, L., Biosalud, Volumen 8, 47 (2009).

[34] Stanic, V.; Dimitrijevic, S.; Antic-Stankovic, J.; Mitric, M.; Jokic, B.; Plecas B.; Raicevc, S., Applied Surface Science 256, 6083 (2010)

[35] Norhidayu, D.; Sopyan, I.; Ramesh, S., ICCBT,24,257, (2008)

[36] Cox, S.; Jamshidi, P.; Grover, L.; Mallick, K., Materials science and Engineering c 35, 106 (2014)

[37] Schwartz, M. Deposition from Aqueous Solutions: An Overview

[38] Zhitomirsky, I.; Gal-or, L., Journal of materials science: materials in medicine, 8, 213, (1997)

[39] Sarkar, P.; Nicholson, P., j. AM. Ceram. Soc, 79, 8, 1987 (1996)

[40] Besra, L.; Liu, M. A review on fundamental applications of Electrophoretic deposition (EPD), Progress in Materials Science, 52, 1 (2007)

[41] Malika Ammam. RSC Adv, 2, 7333-46 (2012)

[42] Deram V, Minichiello C, Vannier RN, Le Maguer A, Pawlowski L, Murano D., 166, 153 (2003).

[43] Sun,L.; Berndt, C.; Khor, K.; Cheang, H.; Gross, K., J Biomed Mater Res, 62. 228 (2002)

[44] Thermal Spray Coatings.
http://www.roymech.co.uk/Useful_Tables/Manufacturing/Surf_Eng.html (22/05/2015)

Chapter 2

Wet Chemical Synthesis of Zinc-substituted Hydroxyapatite Nanocrystals

2.1 Introduction

The compositions of human bone is an inorganic/organic hybrid consisting of 70 %(wt) apatitic calcium phosphates and 30 % (wt) organic (largely collagen fibers), The apatitic calcium phosphate compounds of bone mineral consist of carbonate, a small amount of sodium, magnesium, and other trace elements. The submicroscopic crystals of calcium phosphate in bone resemble the crystal structure of synthetic apatite.

Hydroxyapatite $[Ca_{10}(PO_4)_6(OH)_2]$ (HAp) based bioceramics is successfully used as implants due to its chemical similarity with the inorganic constituent of biological hard tissue. It is present in bone, teeth and tendons for stability, hardness, and function to these organs. It's remarkable biocompatibility is because of its chemical similarity to the biological calcified tissue. The application of HAp as useful biocompatible materials largely depends on the purity and morphology of the powder. HAp [1] has been widely investigated for the application use as bone filling materials with collagen [2−5] and as drug delivery carriers [6−10]. The protein adsorption and cell adhesion on the surface are critical issues and has been investigated [11,12]. However, the detailed features attributed to the interfaces have not been clarified. Thus, *in situ* monitoring and understanding of the interfaces are of great importance for making the nature of biocompatibility clear. This study also will clarify several ambiguities of the interfacial phenomena between biomaterials and cells.

Many routes have been developed for the preparation of HAp like using hydrolysis, hydrothermal, precipitation route, sol-gel route, combustion synthesis, plasma, etc., but generally there are five principal methods to synthesize HAp and each method gives different characteristics of crystallinity of HAp; (a) wet method for synthesize small

crystalline or noncrystalline HAp powder, (b) dry method for preparing well-crystallized HAp, (c) hydrothermal method for obtain large, perfect single crystals of HAp, (d) hydrothermal method for obtain large, and perfect single crystals of HAp and (e) flux method for preparing big single crystals. The most widely used method is a wet method, which is characterized by its simplicity and low cost. Also, the purity of the final HAp powder and stoichiometry (molar ratio of Ca/P=1.67) can be well controlled in chemical the wet method [13].

Using solution reaction (from solution to solid), is available for mass production of small crystalline or noncrystalline HAp powder. Typically, there are 2 kinds of the wet chemical process in this method: one (i) involving a neutral reaction of acid and alkaline solution, and the other (ii) involves the reaction of calcium salts and phosphates salts. The typical chemical formulas for these processes are:

i. $10Ca(OH)_2 + 6H_3PO_4 \rightarrow Ca_{10}(PO_4)_6(OH)_2 + 18H_2O$

ii. $10Ca(NO_3)_2 6(NH_4)_2 HPO_4 + 2H_2O \rightarrow Ca_{10}(PO_4)_6(OH)_2 + 12NH_4NO_3 +$
    $8HNO_3$

The calcium source may be administered as aqueous solutions of $CaCl_2$, $Ca(NO_3)_2$, $CaCO_3$, $Ca(CH_3COO)_2$ or $CaSO_4.2H_2O$. As phosphate sources may be used aqueous solutions of $(NH_4)_2HPO_4$, $NH_4H_2PO_4$, K_2HPO_4, KH_2PO_4, Na_2HPO_4 or NaH_2PO4. The pH is controlled during synthesis by a flow of NH_3 gaseous or by adding aqueous solutions of NH_4OH, NaOH or KOH. Depending on the concentration of reactants, and temperature, there will be substantial variation in the molar Ca/P ratio and crystallinity of HAp obtained. The process is by slow addition of the reactants to avoid drastic changes in the reaction conditions.

For the biocompatibility, the investigation of carbonate ion, K ion, Zn ion substituted in the HAp structure is very important. CO_2 in the atmospheric air is absorbed by the alkaline aqueous solutions as CO_3^{2-} ion and eventually incorporated to HAp structure, replacing PO_4^{3-} ions or OH^- ions of the HAp ions. When the synthesis is performed in the presence of sodium or potassium ions, these partially substitute the Ca^{2+} ions into the product. These small substitutions in the HAp structure are important for the biocompatibility, which has been found to promote new tissue (e.g., bone) formation.

However, its use is often limited due to its slow osteointegration rate and low antibacterial activity, particularly where HAp has to be used for long-term biomedical applications. From these points, the incorporation of trace ions such as Ag, Zn, Ti, and Cu into HAp structures not only provides crystallinity but also improves their antimicrobial property [14, 15], as described in *Chapter 1*. Especially, Zn is present in all biological tissues, stimulates bone mineralization, and helps in pathological calcification. Bone is the main reservoir of Zn, which accounts for 28 % of the total Zn content in the body. Furthermore, Zn also plays a vital role in the maintenance of membrane structure, function, protein synthesis, DNA synthesis, mitosis, and cell proliferation [16−18].

In this chapter, the synthesis of Zn^{2+}-substituted HAp (Zn/HAp) nanocrystals with both biocompatibility and antibacterial activity were synthesized. Because the HAp to be synthesized must be nanocrystalline as described in *Chapter 1*, the wet chemical method was chosen because it is useful for preparing very small crystals of HAp, and because of the (Ca+Zn/)P ratios desired are high (1.67 and 2) were precipitated in alkaline solution due to under basic conditions. The process used for the synthesis of Zn: HAp was the wet chemical process based on the process (ii) as described above. The general chemical formula for this process is:

$$10CaCl_2 + 6K_2HPO_4 + 2H_2O \rightarrow Ca_{10}(PO_4)_6(OH)_2 + 12KCl + 8HCl$$
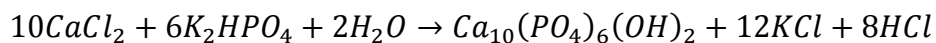
Furthermore, the Zn/HAp nanocrystals were successfully optimized for medical material surface modification, and the crystal growth at the higher Zn concentration (e.g., segregation at the HAp surfaces) was investigated.

2.2 Experimental Section

2.2.1 Materials

All the reagents used in the present investigations were used without further purification. Potassium phosphate dibasic trihydrate ($K_2HPO_4 \cdot 3H_2O$, 99.0 wt%), zinc chloride ($ZnCl_2$, 99.5 wt%), and sodium hydroxide (NaOH) as special grade chemicals were purchased from Wako Chemical Co., Ltd. Calcium chloride ($CaCl_2$, 95.0 wt%) as special grade chemical was purchased from Nacalai Tesque, Inc.

2.2.2 Synthesis of Zinc-substituted Hydroxyapatite Nanocrystals

2.2.2.1 Zinc-substituted Nanocrystals at the (Ca+Zn)/P molar ratio of 1.67 with the Zn/(Ca+Zn) Concentration of 0, 2.5, 5.0 and 10 mol%

In order to compare the biological properties of Zn: HAp nanocrystal films, two types of the initial molar ratios of (Ca+Zn)/P at 1.67 (Stoichiometric HAp) and 2.00 (carbonate HAp (CHA)) were synthesized. Ultrapure water and super grade chemicals were used for the synthesis without further purification.

The procedure for preparation of Zn ion-doped nanocrystals at the (Ca+Zn)/P molar ratio of 2.00 (Zn/(Ca+Zn) concentration: 0, 2.5, 5.0 and 10 mol%) was based on wet chemical method. As the starting materials, commercially guaranteed $CaCl_2$, $ZnCl_2$, $K_2HPO_4 \cdot 3H_2O$, and NaOH were used.

As shown in **Figure 2.1**, the stoichiometric Zn: HAp nanocrystals ((Ca+Zn)/P at 1.67) with the different initial Zn concentrations of 0, 2.5, 5.0 and 10 mol% were synthesized. Typically, 0.024 mol (5.48 g) of $K_2HPO_4 \cdot 3H_2O$ was added into Teflon vessel containing 100 mL of deionized water under magnetic stirring at room temperature for 60 min. After the complete dissolution of $K_2HPO_4 \cdot 3H_2O$, the mixture aqueous solution containing the total amount of 0.04 mol of both $CaCl_2$ and $ZnCl_2$ was slowly added into the aqueous K_2HPO_4 solution under magnetic stirring at 40 °C for 60 min at the drop rate of 5 ml/min with peristaltic pump (Masterflex, Cole-Parmer Instrument Co., Ltd.). Then, the pH value of the solution was adjusted to 12 using 1N-NaOH. The aging period with continuous agitation was one hour, and the obtained precursor solution was then refluxed at 40 °C for 24 h. The solution was centrifuged (10000 *g*, 15 min, 4 °C) to sediment solid product and

washed with ultrapure water 3 times. The washed product was dried in an oven at 100 ºC for 24 h. Here, the sample name was abbreviated as "1.67−Ymol%-Zn:HAp (Y=(Zn/(Ca+Zn))=0, 2.5, 5.0, 10)".

2.2.2.2 Zinc-substituted Nanocrystals at the (Ca+Zn)/P molar ratio of 2.00 with the Zn/(Ca+Zn) Concentration of 0, 2.5, 5.0 and 10 mol%

The carbonate Zn: HAp nanocrystals ((Ca+Zn)/P at 2.00) with the different initial Zn concentrations of 0, 2.5, 5.0 and 10 mol% were synthesized as follows. 0.024 mol (5.48 g) of $K_2HPO_4 \cdot 3H_2O$ was added into Teflon vessel containing 100 mL of deionized water under magnetic stirring at room temperature for 60 min. After the complete dissolution of $K_2HPO_4 \cdot 3H_2O$, the mixture aqueous solution containing the total amount of 0.048 mol of both $CaCl_2$ and $ZnCl_2$ was slowly added into the aqueous K_2HPO_4 solution under magnetic stirring at 40 °C for 60 min at the drop rate of 5 ml/min with a peristaltic pump. Then, the pH value of the solution was adjusted to 12. The aging period with continuous agitation was one hour, and the obtained precursor solution was then refluxed at 40 °C for 24 h. The solution was centrifuged to sediment solid product and washed with ultrapure water 3 times. The washed product was dried in an oven at 100 ºC for 24 h. Here, the sample name was abbreviated as "2.00−Ymol%-Zn:HAp (Y=(Zn/(Ca+Zn))=0, 2.5, 5.0, 10)".
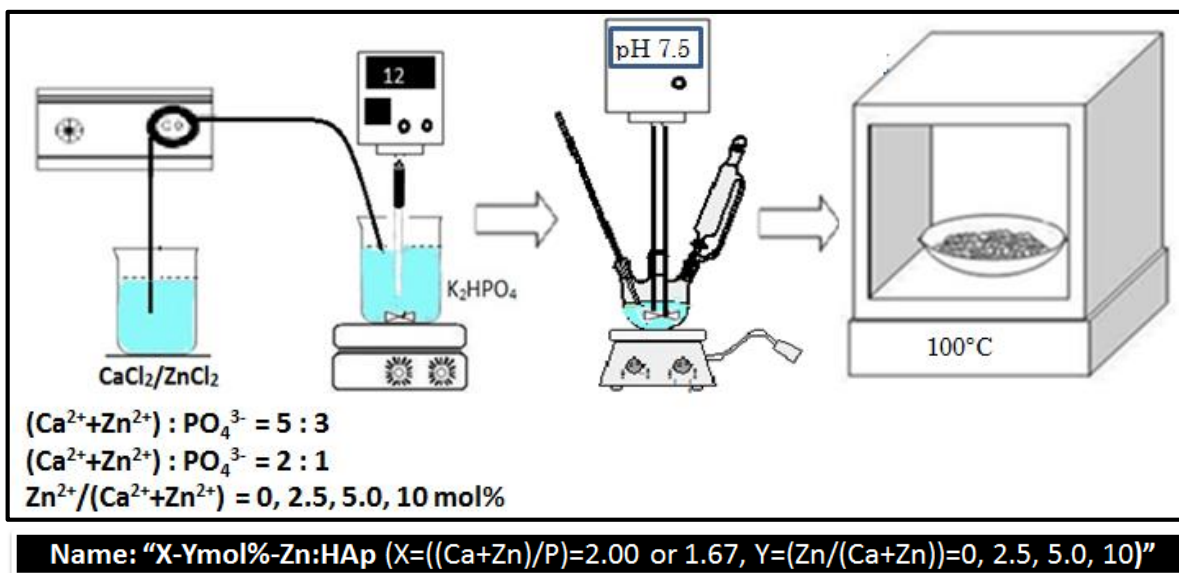
Figure2.1. Scheme of the synthesis of two types of Zn: HAp nanocrystals with the initial molar ratios of (Ca+Zn)/P at 1.67 (Stoichiometric HAp) and 2.00 (carbonate HAp).

2.2.3 Characterization

The content of the elements of two kinds of Zn: HAp nanocrystals with the Zn+Ca/P ratio of 1.67 and 2.00 was determined using a wavelength dispersive X-ray fluorescence spectrometry (XRF) (Primus, Rigaku Co., Ltd.). The chemical composition was analyzed and calculated based on from Ca, C, Zn, P, Cl, Na, K elements. Here, the chemical composition analysis of the whole nanocrystal is possible by an XRF, because the invasion depth is sufficiently longer (ca. 1 μm) as compared with the nanocrystal size.

Fourier Transform Infrared (FTIR) spectra were recorded on a Jasco FT/IR-4100 spectrometer. Spectra were obtained between wavenumbers 400–4000 cm^{-1} with an accumulation of 128 times and resolution of 2.0 cm^{-1}. The nanocrystal powder was diluted as a pellet by adequately-dried KBr powder.

The XRD patterns were recorded by a Smart Lab diffractometer (Rigaku Co., Ltd.) using monochromatized CuKα radiation. The primary optics is equipped with soller slits (0.04 rad), a divergence slit (1°) and a scattering slit (1 °), and the secondary optics is equipped with a receiving slit (0.1 mm), soller slits (0.04 rad), a graphite monochromator and a detector. The present phases were determined by comparing the x-ray patterns with

hydroxyapatite (JCPDS 9-432) standard. The lattice parameters of the Zn/HAps were determined by Rietveld refinement of the diffraction profiles with a PDXL2 program.

The crystallographic characteristics of the crystals can be determined from the X-ray diffraction's data. For the hexagonal cell parameters "*a*" and "*c*" of the crystallographic system of HAp, the relationship between the distance, d, of two adjacent net planes and the (hkl) Miller indices of the reflection planes, is given by the Bragg's law, **Eq. (1)** [13, 19].

$$d = \frac{1}{\sqrt{\frac{3}{4}*\frac{h^2+hk+k^2}{a^2}+\frac{l^2}{c^2}}} \tag{1}$$

The crystalline sizes of the Zn: HAp nanocrystals were estimated using the Scherrer equation as shown in **Eq. (2)**, where D_{hkl} indicates the crystalline size, λ is the x-ray wavelength (0.15418 nm), β is the full-width at half-maximum (in radians) of 200, 002 and 300 diffraction, and θ is the diffraction angle (Bragg's angle, degree), K is 0.9 [13, 20].

$$D_{hkl} = \frac{K\lambda}{\beta cos\theta} \tag{2}$$

The nitrogen (N_2) adsorption/desorption isotherms, and the BET surface area (S_{BET}), BJH pore size (r_{BJH}) and pore volume (*V*) of Zn:HAp nanocrystals with the different Zn ion concentrations were measured at 77 K using the dynamic triple point Brunauer-Emmett-Teller (BET) (30/70 He/N_2) based on the Micrometric TriStar II surface area and porosity equipment (Shimazu Co., Ltd.). A glass sample tube was filled with small pieces of the samples (100 mg). Prior to the measurement, the samples were degassed under vacuum at 393 K for 4 h. For each sample, the measurements were performed 3 times with conducting a 3-min leak check to ensure data reproducibility, sufficient sealing and complete drying of the specimens. The adsorption isotherm at the lower pressures ($p/p_0 < 1.0$) was systematically analyzed by the BET surface area evaluation method using the commercially available software.

The crystallite morphology from the precipitation reaction was observed by transmission electron microscopy (TEM) with a JEM-1400 (JEOL Co., Ltd.). The HAp nanocrystal ethanolic suspension was dropped onto a carbon-coated copper (Cu) grid (Cu 200-A mesh, Okenshoji Co., Ltd.) and the grid was dried in a desiccator under a nitrogen atmosphere for 1 day before the observation. The Zn/HAp nanocrystals were examined in

bright mode and using electron diffraction at magnifications typically up to ×1,000,000, using an accelerating voltage of 120 kV.

2.3 Results and Discussion

2.3.1 Chemical Composition

Table 2.1 shows the quantity (mass percent) of the synthesized Zn: HAp nanocrystals with the initial Ca+Zn/P molar ratio of 1.67 and 2.00, which are measured by XRF. Here, inorganic ion content in human bone is 55 wt% in the content the bone minerals, and the each atomic content of the inorganic composition is 34.0 wt% for Ca, 15.0 wt% for P, 1.6 wt% for C, 0.9 wt% for Zn, 0.2 wt% for Cl, 0.8 wt% for Na and 0.2 wt% for K, suggesting the importance of Zn substitution of ca. 1.0 wt% in the apatite structure HAp [21]. Thus, it is necessary to synthesize a biocompatible apatite, which has some minerals in the biological apatite. In this study, the most similar Zn: HAp to the biological apatite is the Zn: HAp nanocrystal with 2.5 mol% of Zn amount (initial Ca+Zn/P=1.67). In the samples, the content of calcium and phosphorus is decreasing with the increasing amount of Zn. On the other hand, the content of carbon is increasing with the increasing amount of Zn, indicating the inclusion of carbonate ion (e.g., CO_3^{2-}, HCO_3^-) in the crystal formation from the aqueous solution. The coexistence of carbonate ions in aqueous solution in addition to initial Ca-rich composition (in this study: Ca+Zn/P=2.00) often leads to difficulty in the precipitation of stoichiometric hydroxyapatite to form carbonate apatite-like biological apatite. The carbonate ion, when substituted for phosphate ion in HA mimics human bone mineral, is special interest: however, the substitution mechanism is not clear even though the A-type, B-type, and AB-type carbonate apatite are known so far. All the Zn: HAp nanocrystals in the initial Ca+Zn/P=2.00 have the more content of carbon, and the highest amount of carbon is in the 2.00-10.0mol%-Zn: HAp. The Initial Ca+Zn/P=2.00 exhibits the lowest content of phosphorous at 14.5 wt%, assuming that the carbonate ions are replacing the phosphate ions in the Zn: HAp nanocrystals. Thus, the Zn: HAp nanocrystals in the initial Ca+Zn/P=2.00 are thought to be B-type carbonate apatite.

Table 2.1 Contents (mass percent) of the elements in the synthesized Zn: HAp nanocrystals with the initial Ca+Zn/P molar ratio of 1.67 and 2.00.

	Ca (wt%)	P (wt%)	C (wt%)	Zn (wt%)	Cl (wt%)	Na (wt%)	K (wt%)
1.67-0mol%-Zn:HAp	34.4	15.8	3.11	0.0	0.53	0.12	0.02
1.67-2.5mol%-Zn:HAp	34.4	16.3	3.2	0.76	0.30	0.00	0.01
1.67-5.0mol%-Zn:HAp	33.0	16.3	2.65	1.43	0.20	0.00	0.02
1.67-10.0mol%-Zn:HAp	29.4	15.9	4.63	2.76	0.10	0.00	0.01
2.00-0.0mol%-Zn:HAp	37.3	15.7	3.31	0.00	0.20	0.74	0.20
2.00-2.5mol%-Zn:HAp	35.3	14.6	4.15	0.75	0.00	0.56	0.14
2.00-5.0mol%-Zn:HAp	35.0	14.6	4.44	1.46	0.00	0.31	0.12
2.00-10.0mol%-Zn:HAp	32.9	14.5	4.99	2.87	0.00	0.47	0.61

In the XRF results, the molar percentages of the elements found in both types of Zn: HAp nanocrystals were shown in **Table 2.2**. The resultant chemical compositions of the Zn: HAp nanocrystals synthesized from the initial (Ca+Zn)/P molar ratios equal to 1.67 and 2.00 were calculated. From the mean values of Zn, Ca and P contents obtained by XRF, the calculated resultant Zn+Ca/P molar ratio was 1.65 for the stoichiometric HAp and 1.94 for nonstoichiometric carbonate HAp. In the Zn: HAp nanocrystals, the Zn+Ca/P molar ratio decreased with increasing the Zn ion amount, being this decrease more marked in the nonstoichiometric HAp as shown in **Figure 2.2**. The decrease in the Zn+Ca/P molar ratio was attributed to the inclusion of carbonate ion in the synthesis. The stoichiometric chemical composition of (Ca+Zn)/P exhibits the wider range of Zn concentration, and the Ca and Zn ion rich composition of (Ca+Zn)/P (= 2.00) induced the carbonate ion inclusion.

This increase in carbonate ions in this HAp can also be observed in the FTIR spectra, resulting in the decrease in the amount of Zn concentration.

Table 2.2   Initial and resultant chemical compositions of the Zn: HAp nanocrystals synthesized from the initial different molar ratios.

Initial molar (Ca+Zn)/P ratio	Initial Zn conc. (mol%)	Resultant Ca (mol %)	Resultant Zn (mol%)	Resultant P (mol %)	Resultant C (mol %)	Resultant (Ca+Zn)/P ratio	Resultant Zn conc. (mol %)
1.67	0.0	0.86	0.00	0.52	0.26	1.65	0.00
	2.5	0.86	0.01	0.53	0.27	1.64	1.15
	5.0	0.82	0.02	0.53	0.22	1.58	2.38
	10.0	0.73	0.04	0.51	0.39	1.51	5.19
2.00	0.0	0.93	0.00	0.48	0.24	1.94	0.00
	2.5	0.88	0.01	0.47	0.37	1.89	1.12
	5.0	0.87	0.02	0.47	0.35	1.85	2.24
	10.0	0.82	0.04	0.47	0.42	1.83	4.65
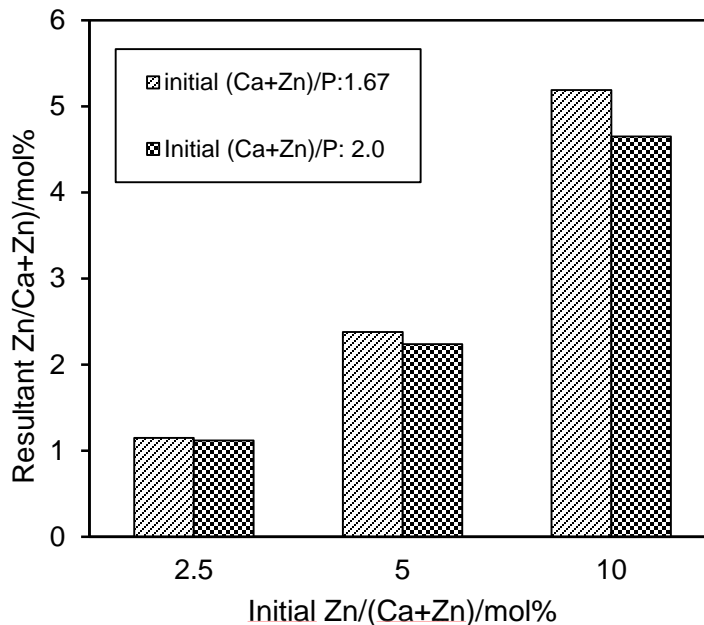
Figure 2.2 Initial and resultant Zn/(Ca+Zn) molar concentrations of the Zn:HAp nanocrystals

2.3.2 Infrared Spectroscopic Analysis

FTIR characterization was carried out for the samples to study the spectral characteristics indicative of the chemical bonding in the synthesized Zn: HAp nanocrystals as shown in **Figure 2.3** and **Figure 2.4**.

From the infrared spectra of stoichiometric Zn: HAp nanocrystals with a chemical composition of (Ca+Zn)/P (= 1.67) in **Figure 2.3**, the absorption bands, are assigned as follows. The peak observed around 3530 cm^{-1} is due to the presence of structural hydroxyl group (−OH bond) in the hydroxyapatite structure. This peak is mainly due to O−H stretching vibration in the Zn: HAp structure, even though the band at around 3400 cm^{-1}, which is attributed to surface OH group of Zn: HAp as well as adsorbed water molecules, was observed. The spectral shape due to the band at around 1150 cm^{-1} would associate with low crystallinity due to the small crystallite sizes and lattice imperfection. The main bands at 1076 cm^{-1}, 1030 cm^{-1}, 957 cm^{-1}, 601 cm^{-1}, 572 cm^{-1} and 460 cm^{-1} are assigned to vibrations of the phosphate group, PO$_4^{3-}$ [22-24]. In the details, the first peak a 1087cm^{-1} proceeds from a triple degenerated asymmetric stretching mode vibration; the component of this triple degenerated vibration of the P−O bond of the phosphate group appear at 1030

47

cm^{-1} [23]. The peak at 957 cm^{-1} is assigned to a no degenerated symmetric stretching mode of the P−O bond of the phosphate group, PO$_4$. The double peak at 601 cm^{-1} and 572 cm^{-1} are assigned to a triple degenerated bending mode of the O−P−O. The weak peaks at 460 cm^{-1} and the shoulder at 460 cm^{-1} are components of the doubly degenerated bending mode of the phosphate group, PO$_4$. These bands and assignments are summarized in **Table 2.3.**
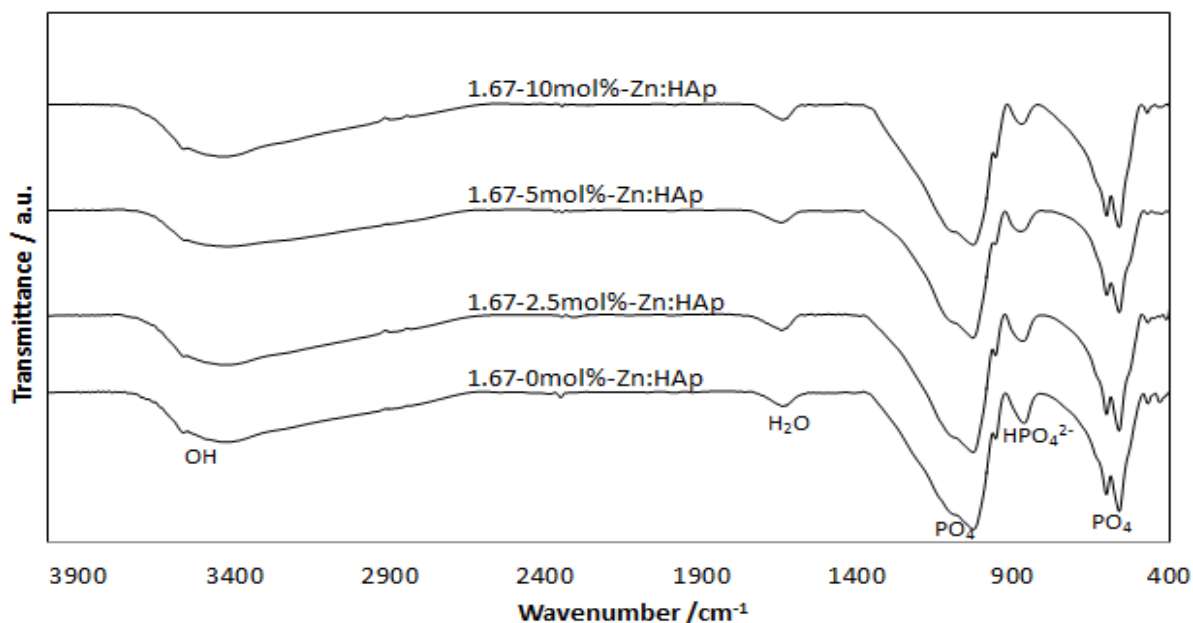
Figure 2.3 FT-IR spectra of the 1.67-Zn: HAp nanocrystals synthesized from the different initial Zn concentrations at 0, 2.5, 5.0 and 10.0 mol%.

Table 2.3 Infrared absorption assignments for the Zn: HAp nanocrystals.

Peak (cm^{-1})	Assignment
3572 (w)	Stretching mode, ν_s, of the hydroxyl group
2070 (w)	Harmonic overtone or combination band
2000 (w)	Harmonic overtone $2*\nu_3$ or combination band $\nu_1 + \nu_{3b}$
1154 (w)	Harmonic overtone or combination band
1087 (s)	Triply degenerated asymmetric stretching mode, ν_{3a}, of the P−O bond of the phosphate group

1046 (s)	Triply degenerated asymmetric stretching mode, ν_{3b}, of the P–O bond of the phosphate group
1032 (sh)	Triply degenerated asymmetric stretching mode, ν_{3c}, of the P–O bond of the phosphate group
962 (w)	Non-degenerated symmetric stretching mode, ν_1, of the P–O bonds of the phosphate group
631 (m)	Vibrational mode, ν_L, of the hydroxyl group
602 (s,shp)	Triply degenerated bending mode, ν_{4a}, of the O–P–O bonds of the phosphate group
574 (s,sh)	Triply degenerated bending mode, ν_{4b}, of the O–P–O bonds of the phosphate group
561 (s)	Triply degenerated bending mode, ν_{4c}, of the O–P–O bonds of the phosphate group
472 (w)	Double degenerated bending mode, ν_{2a}, of the O–P–O bonds of the phosphate group
462 (w,sh)	Double degenerated bending mode, ν_{2b}, of the O–P–O bonds of the phosphate group
361 (w, sh)	HAp lattice vibration mode or combination band, $\nu_1 - \nu_4$
355 (sh)	Translational mode, ν_T, of the hydroxyl group (ν_3)
342 (w, sh)	Translational mode, ν_T, of the hydroxyl group (ν_3)

w: weak, m: medium, s: strong, sh: shoulder, shp: sharp

For the Zn: HAp nanocrystals with the chemical composition of (Ca+Zn)/P (= 2.00), the infrared spectra in **Figure 2.4**, the bands and assignments are almost the same that for the stoichiometric Zn: HAp nanocrystals with the chemical composition of (Ca+Zn)/P (= 1.67). However, the double peaks at around 1440 and 1420 cm^{-1} [25, 26] appeared, and the bands is attributed to symmetric and asymmetric carbonate ions (CO_3^{2-}) in the apatite structure. The carbonate ions were possibly derived from atmospheric carbon dioxide and dissolved into the solution, even though the Zn: HAp was synthesized in the absence of carbonate ions. This HAp type can be called as "carbonate HAp (CAP)," which can be

classified into type B CAP [25] because the carbonate ions were substituted into HAp structure. The bands at around 1440 and 1420 cm^{-1} are attributed to the symmetric mode with its transition moment parallel to the C–O bond (ν_s) and the asymmetric mode with its transition moment perpendicular to the same C–O bond (ν_{as}). The variation in the relative band ratio (ν_s/ν_{as}) with increasing the initial Zn amount is attributed to changes in the bonding state of the carbonate ions in the HAp surface.
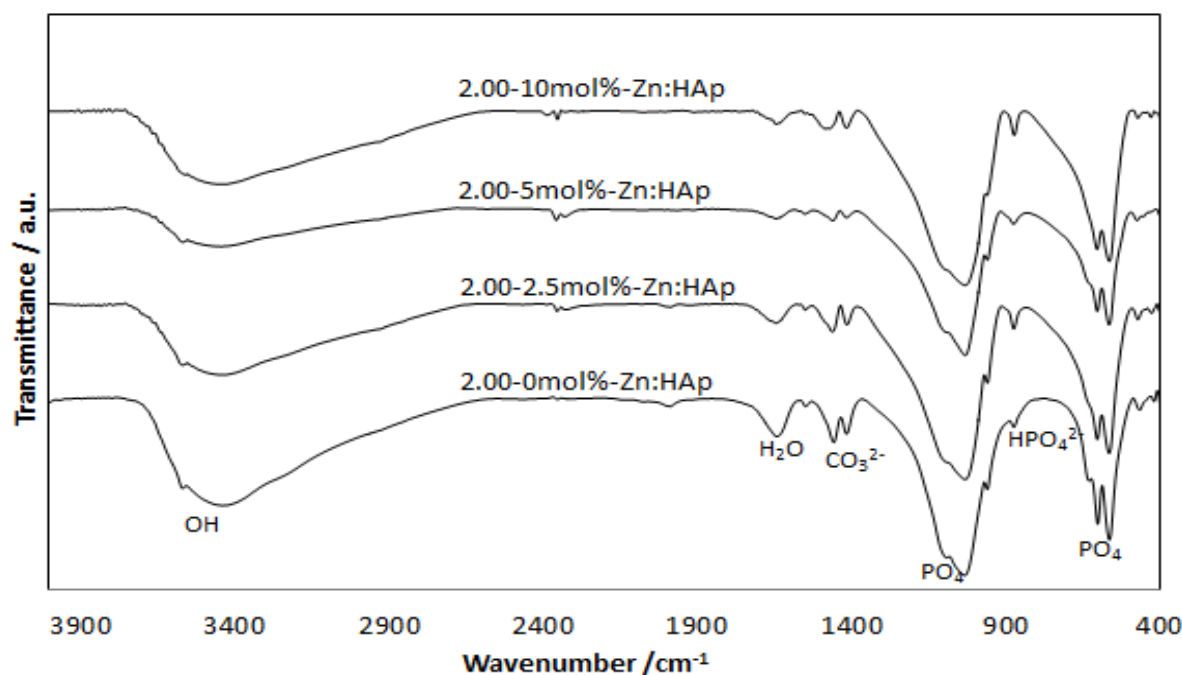
Figure 2.4 FT-IR spectra of the 2.00-Zn: HAp nanocrystals synthesized from the different initial Zn concentrations at 0, 2.5, 5.0 and 10.0 mol%.

2.3.3 Crystallinity

2.3.3.1 X-ray diffraction analysis

From the data of the X-ray diffraction patterns as are shown in **Figure 2.5** and **Figure 2.6**, the crystallographic characteristics of the crystals can be determined. For both Zn:HAp nanocrystals (initial (Ca+Zn)/P molar ratio =1.67 and initial (Ca+Zn/P) molar ratio=2.00), all the XRD peaks were assigned to a HAp single phase as shown in **Table 2.4**, which are summarized as the main peaks observed for the stoichiometric Zn:HAp and carbonate

Zn:HAp. As are shown in **Figure 2.5** and **Figure 2.6**, with the increase in the amount of Zn ion, the peaks are broadening. The broadening of the peaks was attributed to decreased crystallinity of the crystals because of the Zn ion substitution into Ca site of HAp, indicating that the Zn ion with the ion radius of 0.6 nm is part of the HAp structure with replacing the Ca ion with the ion radius of 0.1 nm [27, 28]. These results have high initial growth rates of the crystals with good crystallographic characteristics, but the presence of Zn ion affected the crystalline size and also is expected to be affected the total surface area of the crystals.
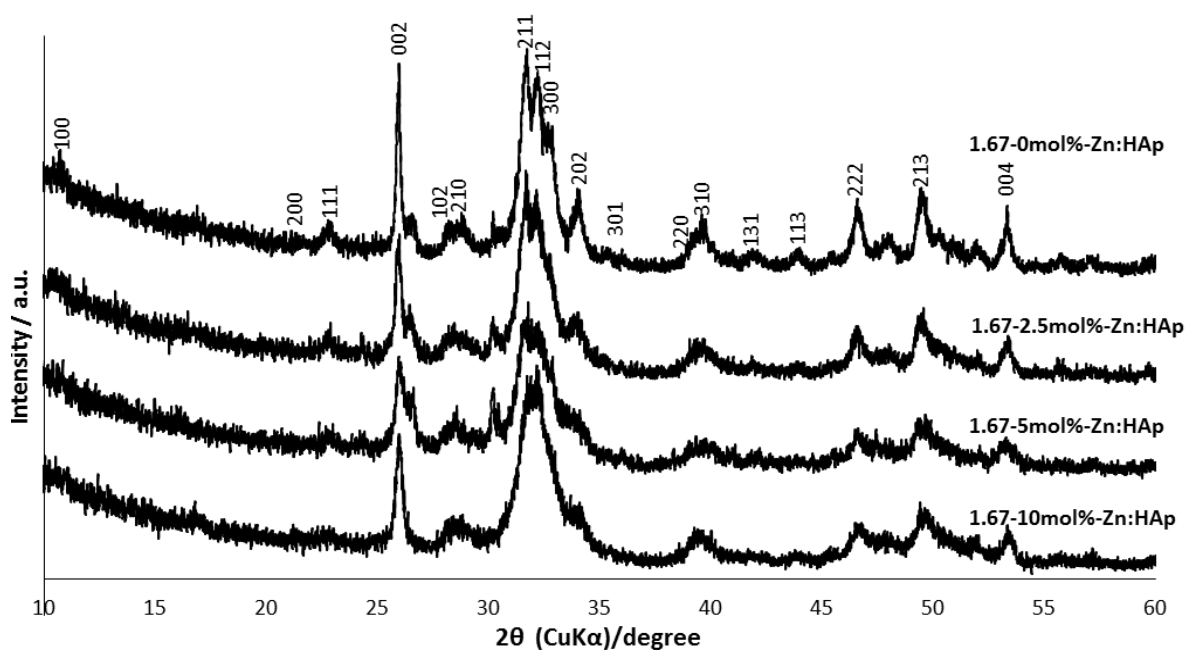
Figure 2.5 XRD patterns of the 1.67-Zn: HAp nanocrystals synthesized from the different initial Zn concentrations at 0, 2.5, 5.0 and 10.0 mol%.

Table 2.4 List of the main peaks observed in XRD patterns for the stoichiometric Zn: HAp and carbonate Zn: HAp nanocrystals, which were assigned as referred to the miller index in the JCPDS card of No. 9-432 and No. 19-272, respectively. Here, the *"I"* means the intensity of the pattern, and the I_1 means the most intensive peak in the patterns.

Stoichiometric Zn: HAp			Carbonate Zn: HAp		
$\frac{I}{I_1}$(%)	d(Å)	Miller Index of the Corresponding Reflection	$\frac{I}{I_1}$(%)	d(Å)	Miller Index of the Corresponding Reflection
40	3.440	002	25	3.46	002
100	2.814	211	100	2.78	211, 112
60	2.778	112	40	2.68	300
60	2.720	300	16	2.23	310
30	1.943	222	16	1.93	232,. 401
40	1.841	213	16	1.84	213
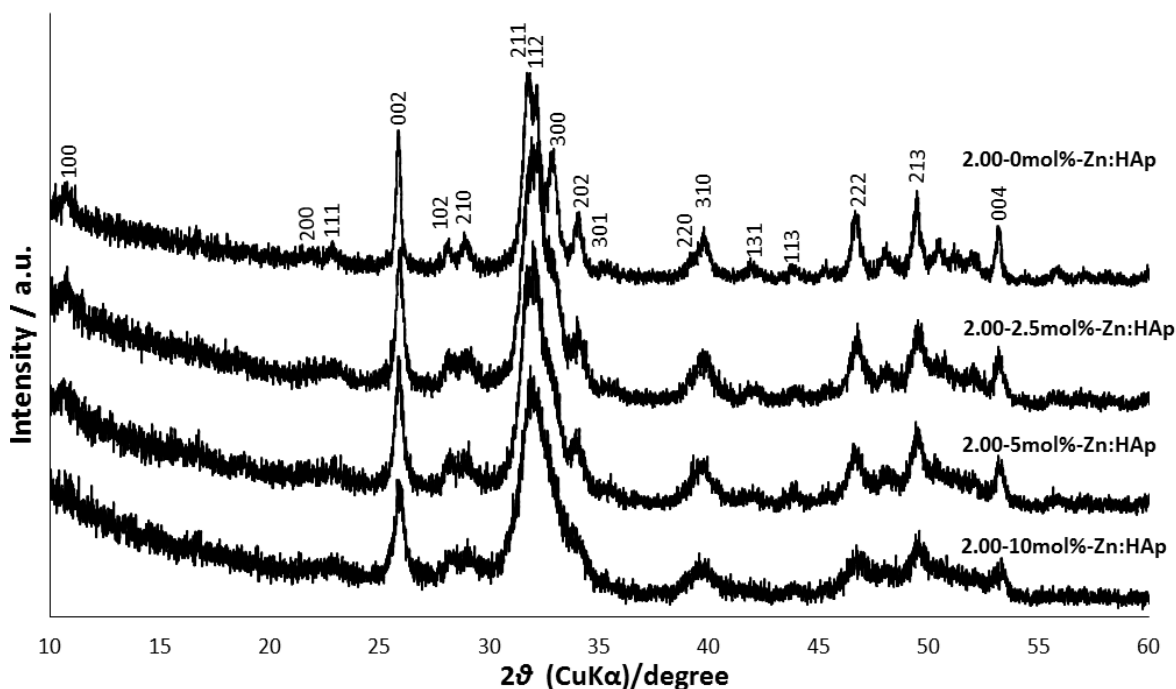
Figure 2.6 XRD patterns of the 2.00-Zn: HAp nanocrystals synthesized from the different initial Zn concentrations (0, 2.5, 5.0 and 10.0 mol%).

The calculated hexagonal unit cell $a = b$ and c for the two kind of Zn:HAp nanocrystals are shown in **Table 2.5**. For the initial Zn:Hap nanocrystals with the molar ratio of (Ca+Zn)/P=1.67 are $a = b = 9.40$ Å and $c = 6.88$ Å, and for initial Zn:HAp nanocrystals with the molar ratio of (Ca+Zn)/P=2.00 are $a = b = 9.43$ Å and $c = 6.88$ Å. The values of the stoichiometric Zn:HAp of th is study are not far from those found in the literature ($a = 9.41$ Å, $c = 6.88$ Å). However, the slight decrease in a lattice would be attributed to the carbonate ion substitution into HAp to form B-type carbonate apatite [13, 29]. In the detail, a decrease in length of the a- axis in **Figure 2.5 (a)** in the unit cell could indicate that HAp crystals contain Zn ions and that coincide with the increased amount of Zn ion. The faces of the crystal witch are defined by the a and c unit cell axes contribute to more than 90 % of the HAp total surface , for that reason it is expected that with the integration of the Zn ion, the morphology of the crystals, the surface area and the behavior of the crystals during kinetic crystal growth studies will be affected.

The resultant crystalline sizes (d_{200}, d_{002} and d_{300}) of the Zn: HAp nanocrystals are shown in **Table 2.6**. The peaks that correspond to d_{200} are bordering with the increase in the Zn ion to be difficult to calculate the d_{200} values. As seen in **Figure 2.7 (b),** the lattice parameters (a and c) as well as the crystalline sizes (d_{300} and d_{002}) decreased with the increasing Zn amount, indicating that the Zn ion addition suppresses the HAp crystal growth to form smaller crystals [27-28, 30]. Especially, the "a" lattice parameter dramatically decreased with the increase in the Zn amount, indicating the smaller a plane and needle-like shape nanocrystals.

Table 2.5 Lattice parameters of the Zn: HAp nanocrystals with the different initial concentrations, which is calculated from XRD patterns.

Initial molar (Ca+Zn)/P ratio	Initial Zn conc. (mol%)	a (=b) (Å)	c (Å)
1.67	0	9.40	6.88
	2.5	9.33	6.88

	5.0	9.42	6.83
	10.0	9.28	6.83
2.00	0	9.43	6.88
	2.5	9.24	6.91
	5.0	9.27	6.91
	10.0	9.29	6.70

Table 2.6 Crystalline sizes of the Zn: HAp nanocrystals with the different initial concentrations, which is calculated from XRD patterns.

Initial molar (Ca+Zn)/P ratio	Initial Zn conc. (mol%)	d_{200} (nm)	d_{002} (nm)	d_{300} (nm)	d_{002}/d_{300}
1.67	0	17	40	20	2.0
	2.5	14	14	5.4	2.6
	5.0	---	13	5	2.6
	10.0	---	24	5.7	4.0
2.00	0	7	34	15	2.3
	2.5	---	21	6	3.5
	5.0	---	20	5.6	3.6
	10.0	---	18	4.6	3.9
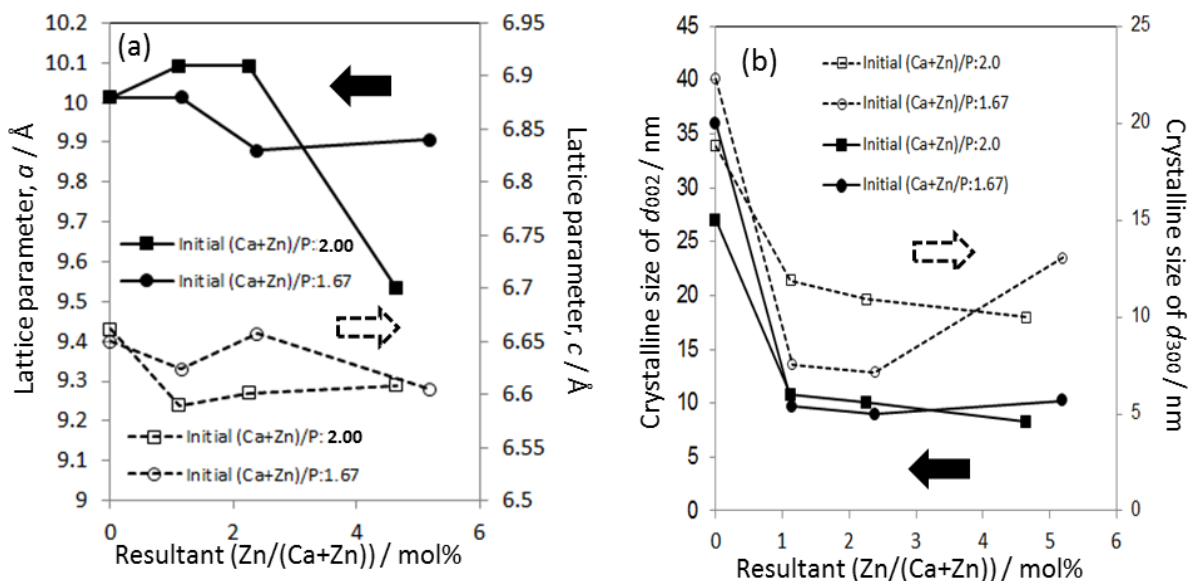
Figure 2.7 (a) Lattice parameters (*a* and *c*) and (b) crystalline sizes (d_{002}) and (d_{300}) of the Zn: HAp nanocrystals with the different Zn ion concentrations.

2.3.4 Nanostructures

2.3.4.1 Nitrogen Adsorption and Desorption Behaviors

The surface area (S_{BET}), BJH pore size (r_{BJH}), and pore volume (*V*) obtained of 1.67-Zn: HAp and 2.00-Zn: HAp nanocrystals with the different Zn ion concentrations (0, 2.5, 5 and 10 mol%) are summarized in **Table 2.7** and **Table 2.8**. These S_{BET} and *V* are changed with the increasing amount of the substituted Zn ion, resulting in the increased surface area and pore volume. Especially, the S_{BET} of the 2.00-Zn: HAp nanocrystals varied from 87 to 118 m^2/g. The higher surface area implies that the sample consists of small crystals and/or has low crystallinity (i.e., high surface concentration of steps, kinks, and vacancies in the crystals). The pore size is almost same as the increasing amount of the substituted Zn ion, suggesting the pores confined by the nanocrystal aggregation forms.

Table 2.7 BET surface area (S_{BET}), BJH pore size (r_{BJH}), and pore volume (*V*) of 1.67-Zn: HAp nanocrystals with the different Zn ion concentrations.

Sample name	S_{BET} (m^2 g^{-1})	$2r_{BJH}$ (nm)	V x 10^{-3} (ml g^{-1})
1.67-0.0mol%-Zn:HAp	78	9.7	4.7
1.67-2.5mol%-Zn:HAp	82	9.8	4.8
1.67-5.0mol%-Zn:HAp	85	9.8	5.3
1.67-10mol%-Zn:HAp	112	9.8	6.4

Table 2.8 BET surface area (S_{BET}), BJH pore size (r_{BJH}), and pore volume (*V*) of the 2.00-Zn: HAp nanocrystals with the different Zn ion concentrations.

Sample name	S_{BET} (m^2 g^{-1})	$2r_{BJH}$ (nm)	V x 10^{-3} (ml g^{-1})
2.00-0.0mol%-Zn:HAp	87	10.6	4.5
2.00-2.5mol%-Zn:HAp	99	10.6	4.7
2.00-5.0mol%-Zn:HAp	100	10.5	5.4
2.00-10mol%-Zn:HAp	118	9.7	6.3

The N_2 adsorption and desorption isotherms of 1.67- and 2.00-Zn: HAp nanocrystals are shown in **Figure 2.8** and **Figure 2.9**, respectively. Generally, there are many different isotherm shapes depending on the type of adsorbent/absorbate and intermolecular interactions between the gas and the solid surface. The Brunauer, Deming, Deming and Teller (BDDT) classification has also become the basis of the modern IUPAC classification of adsorption isotherms, which consist of six broad categories. The isotherms of this study are similar to the Type II, indicating the adsorption on a nonporous or microporous adsorbent with strong adsorbate-adsorbent interactions (unrestricted monolayer-multilayer adsorption).

In the higher Zn-substituted concentration samples, there is a small hysteresis loop, which is due to the filling of the mesoporous structures and is governed by the capillary condensation phenomenon as well as by the percolative properties [31]. The hysteresis loop type (IUPAC classification) corresponds to isotherm type H_1, which is obtained from agglomerates of spherical particles of uniform in the sizes and shapes [31], indicating the agglomerates of smaller-sized Zn: HAp nanocrystals. The hysteresis loop is gradually opening a little more with the increasing Zn ion amount, indicating the increase in porosity, which is also reflected in the increase of pore volumes as shown in **Table 2.7** and **Table 2.8**.

The pore size is not charged with increasing the Zn concentration as shown in **Figure 2.10** and **Figure 2.11**. The opening in the hysteresis loop is above the initial isotherm (initial), so the pre-hysteresis zone is not affected.
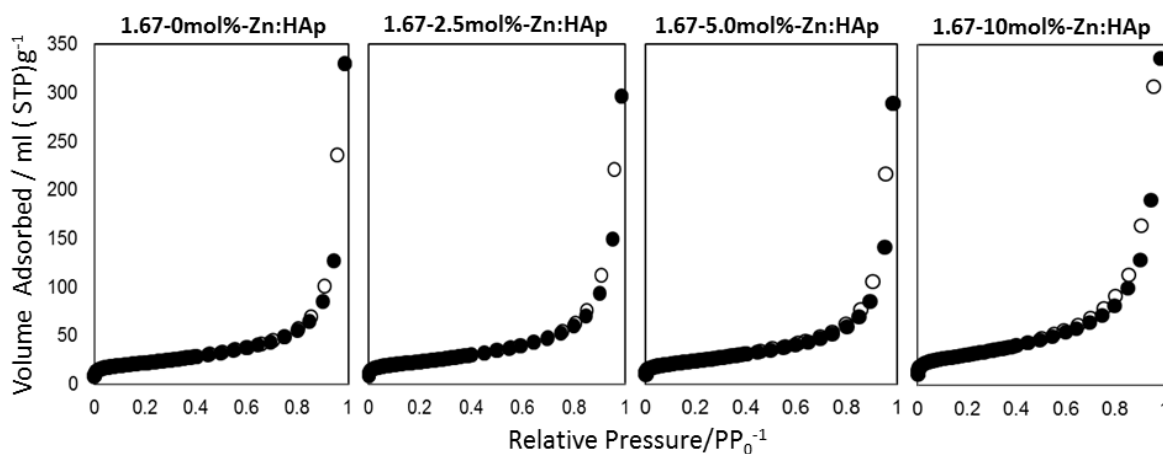
Figure 2.8 Nitrogen adsorption (closed circles) and desorption (open circles) isotherms of the 1.67-Zn: HAp nanocrystals with the different Zn ion concentrations.
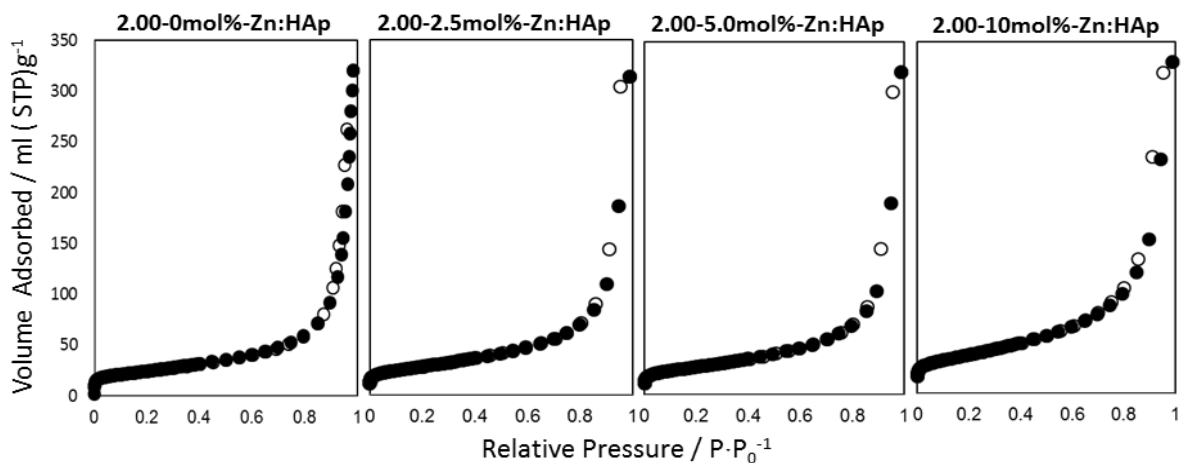
Figure 2.9 Nitrogen adsorption (closed circles) and desorption (open circles) isotherms of the 2.00-Zn: HAp nanocrystals with the different Zn ion concentrations.
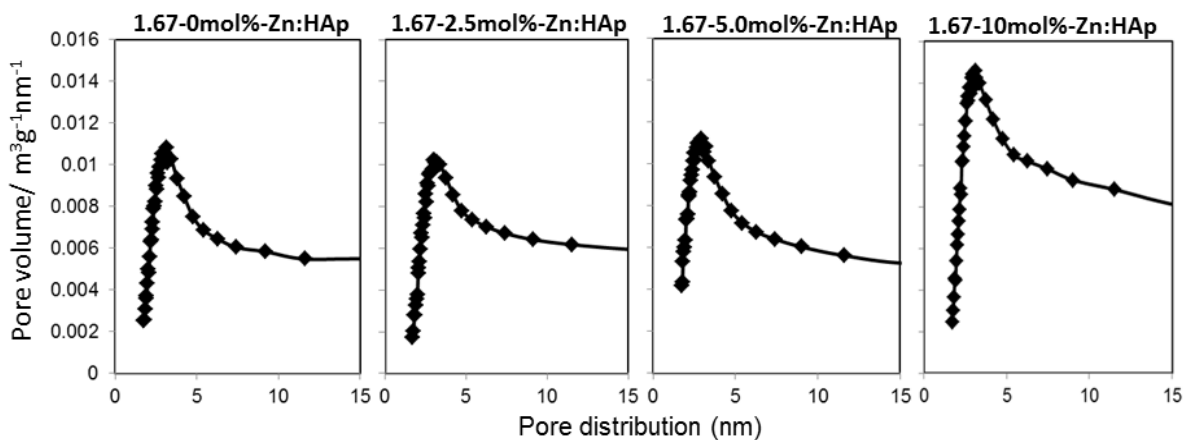
Figure 2.10 Pore size distributions of the 1.67-Zn: HAp nanocrystals with the different Zn ion concentrations.
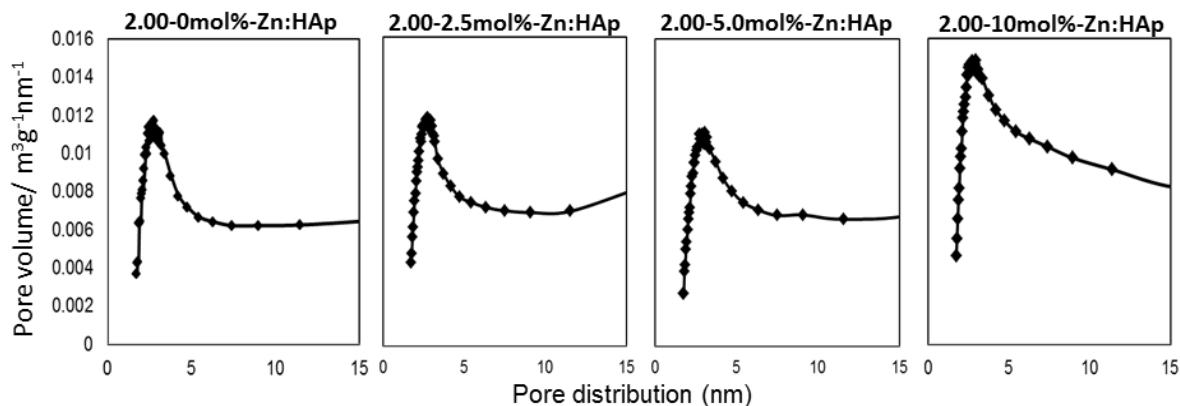
Figure 2.11 Pore size distributions of the 2.00-Zn: HAp nanocrystals with the different Zn ion concentrations.

2.3.4.2 Transmission Electron Microscope Observation

TEM micrographs of the 1.67- and 2.00-Zn: HAp nanocrystals with the different Zn ion concentrations (0, 2.5, 5 and 10 mol%) are shown in **Figure 2.13** and **Figure 2.14** respectively. In the micrographs, the initial 1.67- and 2.00-Zn: HAp nanocrystals have the typical prism needle-like shape morphologies, although the prism is more marked in the stoichiometric HAp, indicating the reflection in hexagonal crystalline structure. The needle-like shapes were changed to particulate shapes with increasing the Zn ion amount [32]. Zn-substituted CHA nanocrystals exhibit the particulate shapes. All the nanocrystals exhibit the smaller crystalline sizes less than 100 nm. The crystal sizes from the TEM observation correspond to those from the XRD patterns, indicating the single crystal of one particle.
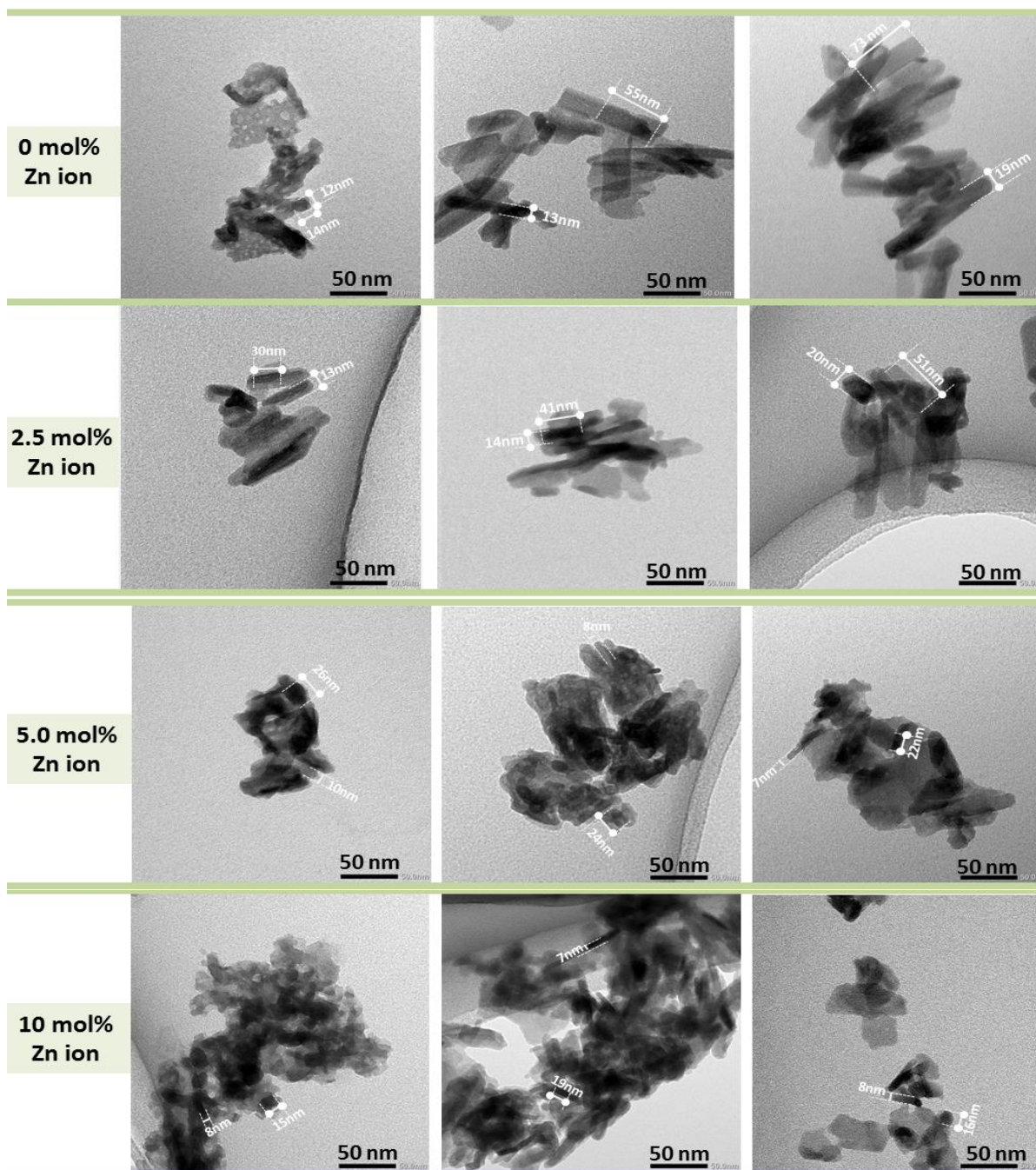
Figure 2.12 TEM photographs of the 1.67-Zn: HAp nanocrystals with the different Zn ion concentrations. Three photographs at the different positions were showed for one concentration. The representative crystalline sizes were marked in the photographs.
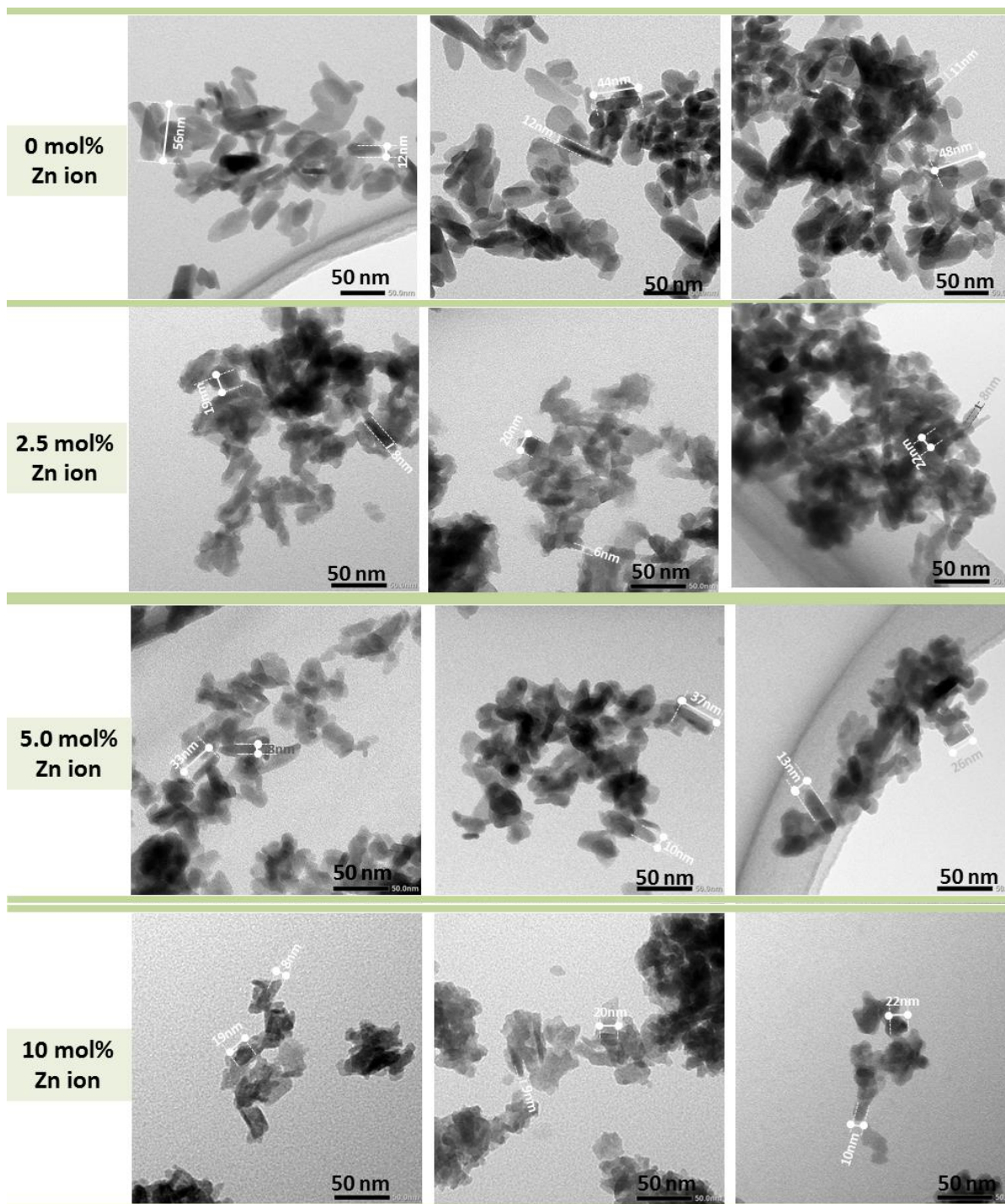
Figure 2.13 TEM photographs of the 2.00-Zn: HAp nanocrystals with the different Zn ion concentrations. Three photographs at the different positions were showed for one concentration. The representative crystalline sizes were marked in the photographs.

2.4 Conclusion

Two types of Zn-substituted hydroxyapatite nanocrystals were successfully obtained; the initial molar ratios of (Ca+Zn)/P at 1.67 (stoichiometric HAp) and 2.0 (carbonate HAp: CHA) were prepared. The nanocrystals at the initial concentration ((Ca+Zn)/P = 1.67) exhibit the wider range of Zn-substituted concentration, and the substituted Zn concentration to Ca sites is the range between 1 and 5 mol%. On the other hand, the nanocrystals at the initial Ca and Zn ion rich composition ((Ca+Zn)/P = 2.00) induced the carbonate ion including. These crystals are monocrystalline because the crystalline sizes measured by XRD match to those by TEM, and the crystalline sizes are less than 100 nm. The crystalline sizes (d_{100} and d_{200}) decreased with the increasing Zn amount, indicating that the Zn ion addition suppresses the crystal growth to form smaller crystals. The increasing Zn amount also resulted in the increasing of the surface area and pore volume because of the lower crystallinity. TEM micrographs showed that the needle-like shapes were changed to particulate shapes with increasing the Zn ion amount.

References

[1]   Kay M., Young R. *Nature* 204, 1050 (1964)

[2]   Kikuchi M., Itoh S., Ichinose S., Shinomiya K., and Tanaka J. *Biomaterials* 22, 1705 (2001)

[3]   Letic-Gavrilovic L., Piattelli A., and Abe K. *Journal of Materials Science: Materials in Medicine* 14, 95 (2003)

[4]   Liao S., Cui F. *Tissue Engineering* 10, 73 (2004)

[5]   Yunoki S., Ikoma T., Monkawa A.,. Ohta K, Kikuchi M., Sotome S.,. Shinomiya K, Tanaka J. *Materials Letters.* 60, 999 (2006)

[6]   Paul W., Sharma C. *Journal of Biomaterials Applications* 17, 253 (2003).

[7]   Kim H., Knowles J., Kim H. *Journal of Biomedical Materials Research B* 74B, 686 (2005)

[8]   Mizushima Y., Ikoma T., Tanaka J., Hoshi K., Ishihara T., Ogawa Y., Ueno A. *Journal of Controlled Release* 110, 260 (2006)

[9]   Ikoma T., Tonegawa T., Watanabe H.,. Chen G., Tanaka J., Mizushima Y. *Journal of Nanoscience and Nanotechnology* 7, 822 (2007)

[10]   Tagaya M., Motozuka S., Kobayashi T., Ikoma T., and Tanaka J. *Industrial and Engineering Chemistry Research* 51, 11294 (2012)

[11]   Yongli C., Xiufang Z., Yandao G., Nanming Z., Tingying Z., Xinqi S. *Journal of Colloid and Interface Science* 214, 38 (1999)

[12]   Kandori K., Miyagawa K., and Ishikawa T. *Journal of Colloid and Interface Science* 273, 406 (2004)

[13]   Hideki, Aoki. "Science and Medical Applications of Hydroxyapatite". JAAS,1991,214pp.

[14]   F. Bir, H. Khireddine, A. Touati, D. Sidane, S. Yala, H. Oudadesse, Applied Surface Science 258 7021–7030 (2012)

[15]   E. Boanini, M. Gazzano, A. Bigi, Acta Biomaterialia 6 1882–1894 (2010)

[16]   Kumar G., Thamizhavel A., Yokogawa Y., Kalkura S., Girija E. Materials Chemistry and Physics 134 1127–1135 (2012)

[17]   Ann L., Mahmud S., Bakhori S. Applied Surface Science 265 137–144 (2013)

[18] Thian E., Konishi T., Kawanobe Y., Lim P.,. Choong C, Ho B., Aizawa M. Journal of Materials Science: Materials in Medicine 24 437–445 (2013)

[19] World Journal of Nano Science and Engineerin, 2, 154-160 (2012)

[20] EIA Journal, ISSN 1794-1237 Num. 5 p. 109-118. Junio (2006)

[21] American Journal of Materials Science, 3(5): 130-135 (2013)

[22] Jorurnal of Biomedical Materials Research, 662(4):600-12 (12/2002)

[23] Singh A, Purohit KM Chemical Synthesis, Characterization and Bioactivity Evaluation of Hydroxyapatite Prepared from Garden snail (Helix aspersa). J Bioprocess Biotechniq 1:104 (2010)

[24] American Journal of Materials Science, 3(4): 84-90 (2013)

[25] J Biomed Mater Res. Jul;41(1):79-86 (1998)

[26] J. Res. Natl. Inst. Stand. Technol. 109, 553-568 (2004)

[27] Environ. Sci.Technol, 39, 4042-4048(.2005)

[28] Chemical Engineering Journal 162 487-494 (2010)

[29] Journal of Solid State Chemistry 144, 272-276 (1999)

[30] J Biomed Mater Res B Appl Biomater. May 15;65(2):217-26. (2003)

[31] Tip Magazine Specializing in Chemical and Biological Sciences, Vol. 9, no. 2 diciembresin month, pp. 90-95 (2006)

[32] Liga Berzina-Cimdina and Natalija Borodajenko. Research of Calcium Phosphates Using Fourier Transform Infrared Spectroscopy, Infrared Spectroscopy - Materials Science, Engineering and Technology, Prof. Theophanides Theophile (Ed.), ISBN: 978-953-51-0537-4, InTech, (2012)

Chapter 3

Fabrication of Nanocrystalline Zinc-substituted Hydroxyapatite Films on Biomedical Polymers and Their Fibroblast Compatibility and Antibacterial Properties

3.1 Introduction

Up to now, lots of antibacterial agents have been investigated for applications in medical applications. Among them, zinc (Zn) salts are commonly used because they are inexpensive, stable and environmentally friendly. Zn has been proved to inhibit bacteria growth. However, the antibacterial effect of Zn ions is limited by poor retention because the Zn level decreased drastically within 30–60 min after being delivered to the soft tissue, mucosa or dental plaque following dental hygiene practices. Thus, hydroxyapatite (HAp; $Ca_{10}(PO_4)_6 (OH)_2$) is most important biomaterials due to their excellent biocompatibility. Once Zn exists in the remineralization layer, the antibacterial agent can retain for a relatively long time and release abundant Zn ions. Furthermore, the Zn-containing tooth surface will also restrict bacterial attachment and prevent the formation of calculus. Thus, the coating of HAp on the catheters is important.

The ceramic bioactive coatings consist of mainly HAp. The role of apatite layer is to inhibit the negative interaction of living tissue with metal implants, which are implemented in the defective place and improve its biointegration, i.e. speeds up the healing process, penetration of bone tissue [1]. HAp powders can be applied to the metal substrates by plasma sprayed, magnetron sputtering, EPD, enameling techniques and other methods [2]. HAp practices show good adhesion and overgrowth of the implant with bone an HAp layer of only a few micrometers represent a sufficient thickness [1, 3].

Layers of a thickness of a few micrometers as far as several tenths of micrometers can be deposited from HAp suspension depending on process conditions [1]. The interest in EPD for biomedical applications stemmed from a variety of reason such a low-cost, the possibility of deposition of stoichiometric, high purity material to a degree not easily

achievable by other processing techniques, the possibility of forming coatings and bodies of complex shape, like short formation time, requiring simple apparatus, coatings with uniform thickness, no requirement for binder burnout as the green coating contains few or no organics [3−6].

For nonuse of chemical reagents (e.g., silane coupling agent), EPD technique is useful. The EPDis a colloidal process wherein different materials, like ceramic bodies, were shaped directly from a stable colloid suspension by a direct current (DC) electric field [4]. The EPD is a combination of two processes. The motion of charged particles in a suspension under the influence of an electric field. The migration involves the properties of the colloidal dispersion (bath conductivity, viscosity, particle concentration, size distribution and surface charge density) and an actual field strength in the bath [4–7]. The coagulation of particles generates a dense mass. This step proceeds by a complex superposition of electrochemical and aggregation phenomena [4–7]. The depositing electrode and the shape were required, and it is designed such that deposit release is facilitated. The degree of stoichiometry in the power used controls the degree of stoichiometry in the electrophoretic deposit. Thus, the usage of EPD for biomedical materials is very important.

In this chapter, the EPD of Zn-substituted HAp nanocrystals on silicone rubber film, performed in ethanol as a suspension medium, and the biocompatibility and antibacterial properties of coating films were investigated using NHI3T3 fibroblasts and *E*. coli DH5α, respectively.

3.2 Experimental Section

3.2.1 Materials

Synthetized Zn-substituted HAp nanocrystals [the initial (Ca+Zn)/P ratio=1.67 and initial (Ca+Zn)/P ratio=2 and Zn concentration of 0, 2.5, 5.0 and 10.0 mol%] was used. Ethanol 99.5% (mass/mass) was purchased from Wako Co., Ltd. Inc. Silicon transparent conductive film (Kyohritsu Electronic Industry Co. Ltd) and silicone catheters (uc 25c-12, (Junkosha Inc.), SH No. 7 (Create Medic Co. Ltd.) and 2 ways catheter No. 26, (Cliny Co.)

were used. For cell culture, phosphate buffered saline (PBS, Dullbecco Co., Ltd), 0.05 w/v% trypsin-0.053 M-ethylenediaminetetraacetate (trypsin-EDTA, Gibco), formaldehyde (37 vol %, Wako Co., Ltd.) Dulbecco´s modified eagle medium (DMEM without sodium pyruvate, Gibco) were used. NIH3T3 mouse embryonic fibroblast cells (RCB1862) purchased from BioResource Center of Japan. FBS was purchased from Bioscience Co., Ltd. (product number: 12603C, lot no. 6D0975: SAFC). For the antibacterial test, 6-cm-petri dish (CELLSTAR dish, Greiner bio-one Co., Ltd. code No. 628160) and cover glass #1 (size: 18 mm×18 mm, Matsunami glass Co., Ltd., code No. : C218181) was used.

3.2.2 Film Formation of Zn-Substituted Hydroxyapatite Nanocrystals on Biomedical Substrates and Catheters by Electrophoretic Deposition.

Pre-preparation of polymer substrate: Before the EPD is carried out the preparation of the polymer, which consisted of covering the surface of the silicone polymer with a very thin titanium layer. Using DC sputtering can deposit very thin layers of material from a "target" (titanium) that is a source onto a "substrate" such as a silicone rubber. DC diode sputtering system is constituted by a pair of flat electrodes. One of the electrodes is the cathode and the other anode. On the cathode side facing the plasma the target, that it is desired to evaporate, is located, and the other face is cooled with water. In the anode was placed the substrate (silicone rubber) on which is desired to evaporate. In a DC diode sputtering system, Argon is ionized by a strong potential difference, and these ions are accelerated to a target. After impact, target atoms are released and travel to the substrate where they form layers of atoms in the thin-film.

Preparation of suspension: Removal of the Cl^- ions and others impurities from the powders is very important because it can affect the suspension stability and deposition characteristics; [5] for that reason the Zn-substituted HAp nanocrystals was washed three times with ethanol (99.5 % (mass/mass), Wako Co., Ltd.) before EPD. The suspension was prepared by the dispersion of 1 wt% of the Zn-substituted HAp nanocrystals in pure ethanol (99.5 % (mass/mass), Wako Co., Ltd.).

EPD process of Zn-substituted HAp nanocrystals on the substrate: For the purpose of clean the materials; the electrode and the silicone rubber surfaces were

undergone to UV/Zone treatment for 5 min. The coating was deposited onto silicone substrates from suspensions containing 1 wt% of Zn-substituted HAp nanocrystals (initial $(Zn+Ca)/P = 1.67$ and 2 with $Zn/(Ca+Zn) = 0, 2.5, 5.0$ and 10.0 mol%), dispersed in pure ethanol (99.5 % (mass/mass), Wako Co., Ltd.).The suspensions had been ultrasonically agitated before EPD process for 3 minutes while deposition was carried out without stirring. The Zn-substituted HAp nanocrystals were deposited onto the silicone substrates (transparent silicon conductive film), and catheters surface through EPD method, (shown in **Figure 3.1**) at a deposition time of 1 min, and an electrode distance of 1 cm. In order to obtain the best coating, the different DC voltage were applied at 10, 50 and 100 V/cm, following by the ultrasonication in 20 mL of ethanol for 1 minute and the subsequent wash in 20 mL of ethanol¸ to remove excess of Zn-substituted HAp nanocrystals. The coated samples were dried in air for 1h at room temperature.
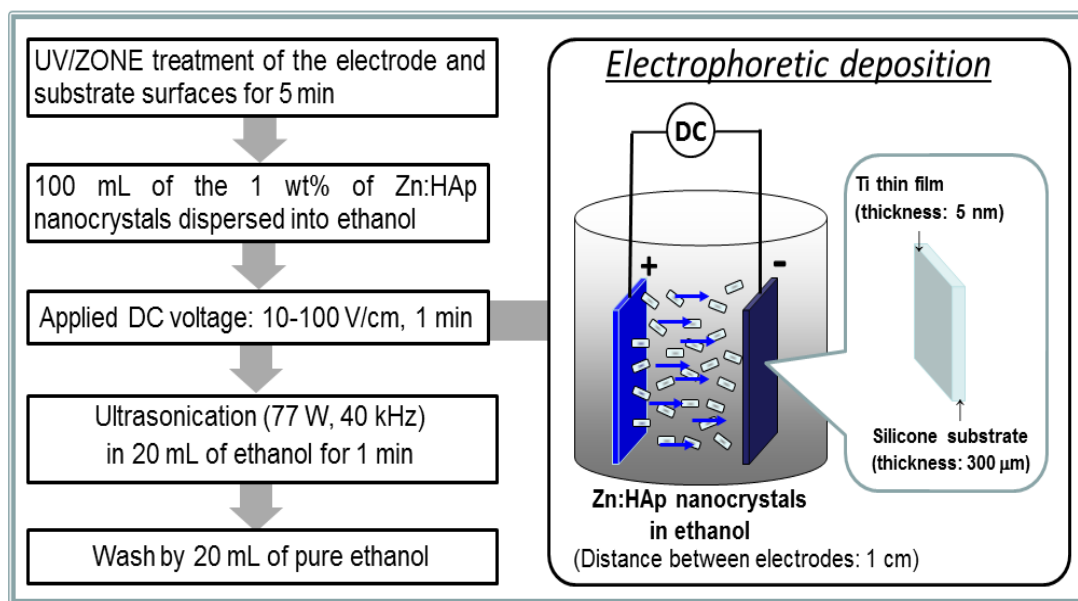
Figure 3.1. Scheme of the EPD procedure of nanocrystalline Zn: HAp nanocrystals on biomedical silicone substrates. The very thin film coating of Ti on biomedical polymer has been usually conducted for providing antistatic function.

EPD process of Zn-substituted HAp nanocrystals on biomedical catheters: Suspensions containing 1 wt% of Zn-substituted HAp nanocrystals (initial $(Zn+Ca)/P = 1.67$ and 2 with $Zn/(Ca+Zn) = 0, 2.5, 5.0$ and 10.0 mol%), dispersed in pure ethanol (99.5

% (mass/mass), Wako Co., Ltd.) was deposited onto catheters substrates (uc 25c-12, (Junkosha Inc.), SH No. 7 (Create Medic Co. Ltd.) and 2 ways catheter No. 26, (Cliny Co.Ltd.). The suspensions had been ultrasonically agitated before EPD process for 3 minutes while deposition was carried out without stirring. The EPD system consists in a beaker that had contained a solution of 1 wt% of Zn-substituted HAp nanocrystals was placed in the center of the vessel, a cylinder made of aluminum foil and in the center of this cylinder of this cylinder was placed a catheter tube piece. The aluminum foil was connected to the anode and the cathode connected Catheter. The deposition time was 1 min and an electrode distance of 1 cm. with the purpose to obtain the best coating the different DC voltage were applied at 10, 50 and 100 V/cm, following by the ultrasonication in 20 mL of ethanol for 1 minute and the subsequent wash in 20 mL of ethanol¸ to remove excess of Zn-substituted HAp nanocrystals. The coated samples were dried in air for 2h at room temperature.

The procedure of dissolution behavior test for the long term: First EPD process of nanocrystalline Zn: HAp on a polymer substrate, 100 V for 1 minute. The obtained nanocrystalline Zn: HAp films were placed in a petri dish and covered for 2 mL of DMEM medium, and it was put to incubate at 37°C and 5% CO_2 for 5, 7 and 10 days. Then using an AFM could determine the mechanism of dissolution of the nanocrystalline Zn: HAp in the film.

3.2.3 Fibroblast Cell Culture

The cell culture was conducted as shown in **Figure 3.2**. First the samples were kept in phosphate buffered saline (PBS) for three hours and then sterilized with ethanol 50 and 70 vol% of concentration for 12 h each of them, then rinsed twice with PBS 30 min, and finally swelled in Dulbecco's modified Eagle's medium (DMEM) for 30 minutes two times; before the seeding procedure. NIH 3T3 mouse embryonic fibroblast cells were cultured at 37°C, 95% relative humidity and 5% CO_2 environment. The culture medium was 90% Dulbecco's modified Eagle's medium (DMEM) supplemented with 10% fetal bovine serum (FBS) and 1% penicillin/streptomycin. The cells were cultured in a cell culture flask containing 15 mL of the FBS dispersed into DMEM at 10 vol% (10%

FBS/DMEM). The cells were incubated at 37 °C in a humidified atmosphere of 5% CO_2 and subcultured every 7 days with 1 mL of the trypsin-EDTA. After being washed with 15 mL of PBS and treated with 1 mL of the trypsin-EDTA for 10 min at 37 °C, the cells were dispersed in 15 mL of PBS, separated by centrifugation (2000 rpm, 2 min), and dispersed in 15 mL of 10% FBS/DMEM. The centrifugation and dispersion were carried out twice. The number of cells in the suspension was counted and adjusted to the seeding density of 0.8×10^4 cells·mL^{-1}.The suspension was seeded on nanocrystalline Zn: HAp films on polymer substrates, which were [(Ca+Zn)/P ratio=1.67 and Zn conc.=0mol%], [(Ca+Zn)/P ratio=1.67 and Zn conc.=2.5mol%], [(Ca+Zn)/P ratio=1.67 and Zn conc.=5.0mol%], [(Ca+Zn)/P ratio=1.67 and Zn conc.=10mol%], [(Ca+Zn)/P ratio=2.00 and Zn conc.=0mol%], [(Ca+Zn)/P ratio=2.00 and Zn conc.=2.5mol%], [(Ca+Zn)/P ratio=2.00 and Zn conc.=5.0mol%], and [(Ca+Zn)/P ratio=2.00 and Zn conc.=10mol%] in Petri tissue culture dish 35×10 mm, at a density of 8×10^3 cells/cm^2. Polystyrene tissue culture (PS) dish was used as control and polydimethylsiloxane (PDMS) as a polymer reference. The cells were used for imaging and characterization purposes after 72 h of culture.
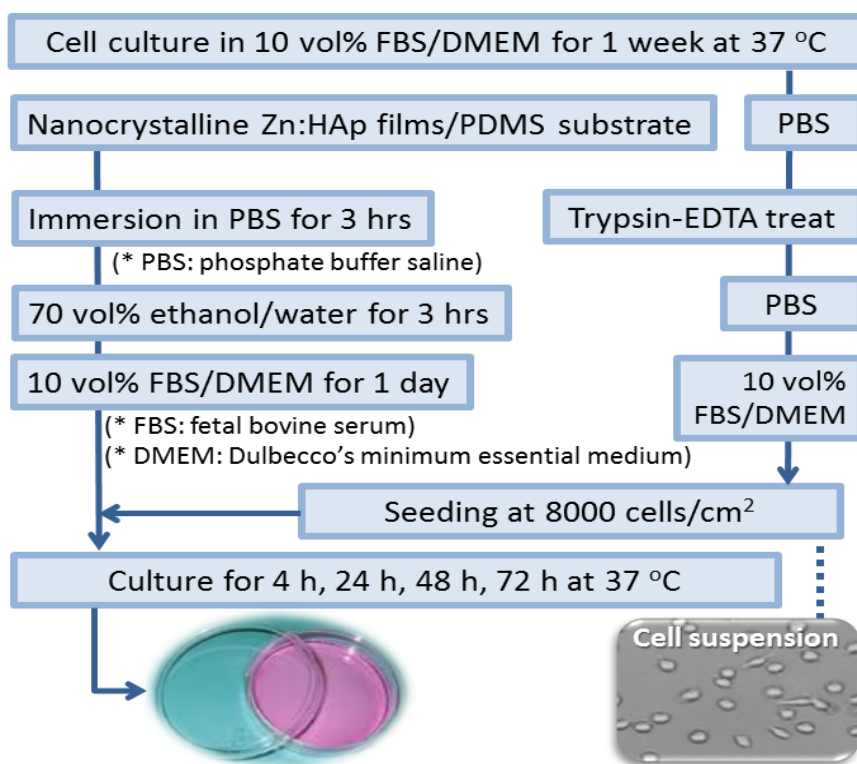
Figure 3.2. Scheme of the procedure for fibroblast cell culture.

3.2.4 Antibacterial Test

The antibacterial text of the nanocrystalline Zn: HAp films on polymer substrates, which were [(Ca+Zn)/P ratio=1.67 and Zn conc.=0mol%], [(Ca+Zn)/P ratio=1.67 and Zn conc.=2.5mol%], [(Ca+Zn)/P ratio=1.67 and Zn conc.=5.0mol%], [(Ca+Zn)/P ratio=1.67 and Zn conc.=10mol%], [(Ca+Zn)/P ratio=2.00 and Zn conc.=0mol%], [(Ca+Zn)/P ratio=2.00 and Zn conc.=2.5mol%], [(Ca+Zn)/P ratio=2.00 and Zn conc.=5.0mol%], [(Ca+Zn)/P ratio=2.00 and Zn conc.=10mol%], and [reference: polymer substrate], were conducted using Escherichia coli (E. coli DH5α) purchased from Takara Bio Co., Ltd.

Preparation of LB medium and LB plate: LB medium and LB plate kit were purchased. LB culture medium solution was prepared by mixing Tryptone (Becton, Dickinson, and Company (BD) Co., Ltd., code No. : 211705), Yeast Extract (BD) Co., Ltd., code No.: 211705), and NaCl (Wako Co., Ltd., code No. : 191-01665). The LB medium was prepared by dissolving 10 g of tryptone, 5 g of yeast extract and 10 g of NaCl in 950 mL of deionized water and adjusting the pH of the medium to 7.0 using 1N-NaOH to bring the volume up to 1 L. The medium was treated by an autoclave before the culture. On the other hand, LB plate culture medium for preparing colony plate was prepared by adding Agar (Wako Co., Ltd., code No.:010-15815) into LB culture medium solution, and the resulting solution was casted on sterile 10-cm- petri dish (AS ONE Co., Ltd., code No.: 3-1491-01). LB plate was prepared by adding 15 g/L agar before the autoclaving in the same preparation procedure to LB medium as above. After the autoclaving, the liquid at the temperature of 55 °C was poured into petri dishes (diameter: 10 cm). After harden, the plate was inverted and stored at +4 °C in the dark.

Pre-culture of *E. coli* DH5α: For coating of the cultured colony solution on the LB plate in the dish, T-shape spreading pole (product name: bacteria spreader, AS ONE Co., Ltd., code No. : 2-6424-04) was used. The *E. coli* DH5α bacteria were cultured in a plastic cell culture dish (diameter: 10 cm) with LB medium plate containing 10 mL of LB medium at 37 °C in a humidified air atmosphere, and then sub-cultured every 2 days to finally keep the cultured *E. coli* DH5α bacteria at 4ºC. After being washed with 15 mL of LB medium,

the bacteria were dispersed in 15 mL of PBS, separated by centrifugation (2000 rpm, 2 min). The centrifugation and dispersion were carried out twice.

Preparation of Bacteria Liquid: Based on a McFarland turbidimetric method, the bacteria liquid was adjusted by McFarland standard solution. The McFarland No. 3 solution was prepared in the admixture solution of 1 wt%-$BaCl_2$/water (0.3 mL) and 1 wt%-H_2SO_4/water (9.7 mL). As a result, the turbidity by a turbidimetric measurement (CO7500 Colorimeter UK, Biochrom Ltd.) was 26 % of transmittance at 590 nm (0.4 of absorbance at 590 nm) and 1.0×10^9 CFU(Colony Forming Unit)/mL of number of bacteria, indicating that the prepared bacteria liquid of *E. coli* DH5α was McFarland standard turbidity No. 3. Then, the diluted dispersion solution of *E. coli* DH5α was prepared at the concentration of 1.0×10^8 CFU/mL (900 μL), 1.0×10^7 CFU/mL (900 μL) and 1.0×10^6 CFU/mL (900 μL).

Exposure and culture, "first culture", of *E. coli* DH5α on the samples (see Figure 3.3): The sample films were which were pre-sterilize by 70 vol%-ethanol/water solution and then dried inside the clean bench. 50 μL of the *E. coli* DH5α bacterial liquid at the concentration of 1.0×10^6 CFU/mL (i.e., 5.0×10^4 CFU) was seeded on the sample film surface in 60-mm-cell-culture-dish. The seeded surface layer was immediately put over and homogeneously coated by a speeding stick. The surfaces were softly capped by a cover glass (area: 18 mm × 18 mm), and the culture dishes were put in a closed container with the 100 % of humidity and continuously pre-cultured for 17 h at room temperature.
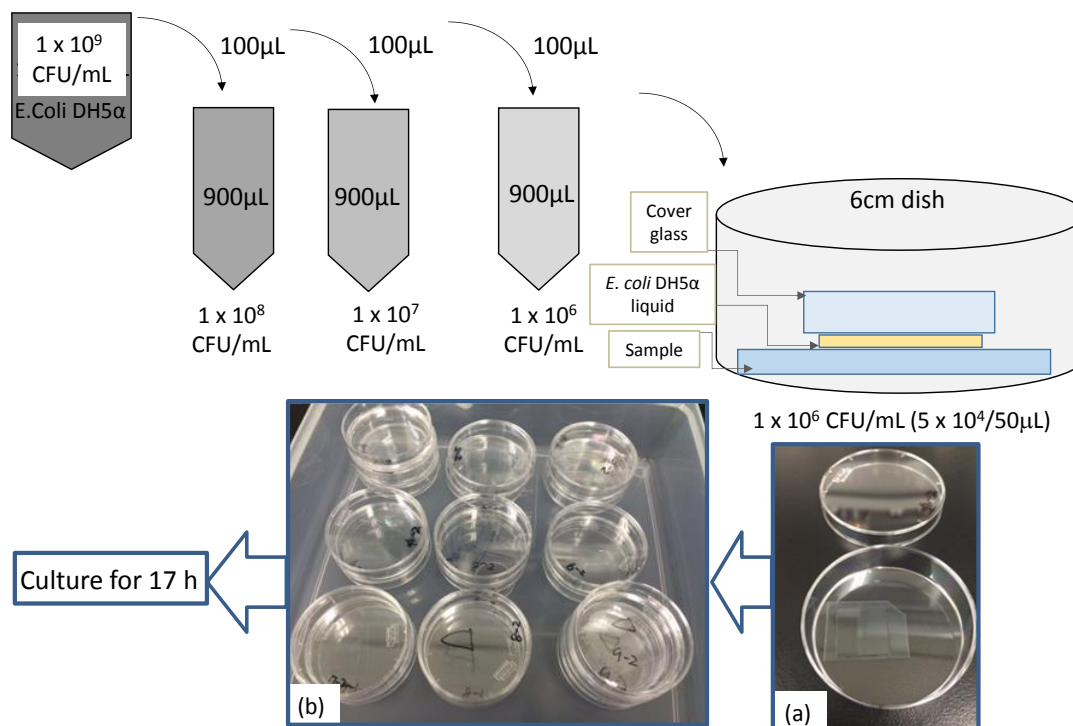
Figure 3.3. The experimental procedure of the exposure and culture (called as " the first culture") of E. coli DH5α on the sample films, and the photographs of (a) sample surface and (b) container surface at the starting.

Extraction of *E. coli* DH5α bacteria from the samples and the subsequent viable bacterial growth culture, "second culture", (see Figure 3.4): After the pre-culture, the cover glass/*E. Coli* DH5α bacteria/sample film substrate was moved into 10 mL of LB medium in 50-mL-tube-container and oscillated in order to extract all the *E. coli* DH5α bacteria (ca. 5.0×10^4 CFU) and prepare the dispersion medium solution (i.e., secondary bacteria liquid). Then, 200 μL of the secondary bacterial liquid (ca. 1000 CFU/200 μL), 200 μL of the 10-fold-dilution liquid (ca. 100 CFU/200 μL), 200 μL of 100-fold-dilution liquid (ca. 10 CFU/200 μL) were adjusted by LB medium and the liquid (200 μL) was seeded on the solid and dry state agar gel medium, which is a commercially-available LB agar plate, at three different concentrations. The seeded surface layer was immediately put over and homogeneously coated by a speeding stick. The culture of viable bacteria was conducted at 37 °C under air with 100 %-humidity for 24 h, and then the number of the viable bacteria was counted.
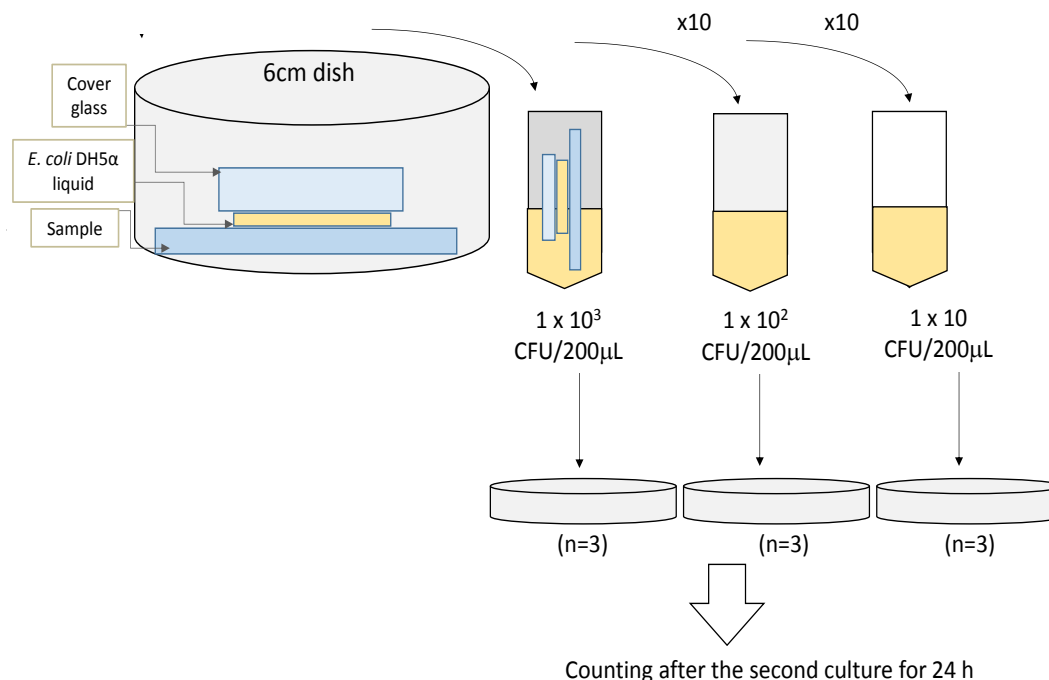
Figure 3.4. Scheme of the experimental procedure of the extraction of *E. coli* DH5α bacteria from the sample films and subsequent viable bacterial growth culture (called as " the second culture").

3.2.5 Characterization

3.2.5.1 Surface Properties of Nanocrystalline Zn: substituted Hydroxyapatite Films

The nanocrystalline Zn:substituted HAp films were characterized by X-ray diffractometers (TF-XRD), using Cu-Kα radiation in a "Smart Lab" diffractometer, Rigaku Co. Ltd. with the data analyzed using the Smart Lab Guidance program (measure condition: current: 60 mA, voltage: 40 kV, step: 0.02, scan rate: 3 degrees/min). The Atomic Force Microscope (AFM) was used to analyze the topography of the silicone rubber substrate and nanocrystalline Zn: substituted HAp films. The nanostructures and surface viscoelastic properties were analyzed by an atomic force microscope (AFM; Nano cube, SII Investments, Inc.) in an area of 1.0×1.0 μm^2. A silicon probe mounted on a cantilever (SII Micro Cantilever SI-AF01, SII Investments, Inc.) was employed. The surface roughness (R_{rms}) was calculated by the root mean squares in the Z-range images. The software used for the calculations of coverage percent and roughness is Spise 132. Fourier Transform Infrared (ATR-FTIR) spectra of nanocrystalline Zn: substituted HAp films were recorded

on a Jasco FT/IR-4100 spectrometer. The spectra were obtained between wavenumbers 400–4000 cm^{-1} with an accumulation of 128 times and resolution of 2.0 cm^{-1}.

From scanning, the AFM equipment developed a front image and a three-dimensional image of the morphology. Once the morphological image was made, obtained, the roughness of the area and of the line was obtained, in the parameters of mean roughness (equation (1)) and mean square roughness (equation (2)), respectively, as follows:

$$R_a = \sum_{n=1}^{N} \frac{|z_n - \bar{z}|}{N} \tag{1}$$

$$R_{rms} = \sqrt{\frac{\sum_{n=1}^{N}(|z_n - \bar{z}|)^2}{N-1}} \tag{2}$$

where z_n is a segment height, $\bar{z}$ is average height of all segments, and N is the number of segments. Roughness provides the information about area roughness trend across the swept area, whereas the roughness of the line yields the roughness value in a selected trajectory [11]. In this study, the R_{rms} was used.

3.2.5.2 Fibroblast Compatibility

The samples were imaged using an inverse microscope (Olympus CKX41). The images were analyzed for cell elongation and directionality using Cellsens software digital imaging software. To measure cell area, the cell boundaries were marked. Aspect ratio, long axis, and cell density were also measured. Approximately 50 cells were analyzed for each sample, and ten images were analyzed to obtain an unbiased estimate of the cell density and morphology. The results presented herein were based on three independent experimental runs.

3.2.5.3 Antibacterial Activity

As the characterization method of the antibacterial properties, the viability rate of the viable bacterial growth in the second culture was investigated by measuring the number of viable Escherichia coli, which is famous evaluation method. The number was averaged between three same sample films (n=3). The colony was counted by CO7500 Colorimeter as a counting meter (Biochrom Co., Ltd., code No.: 80-3000-43).

3.3 Results and Discussion

3.3.1 Characterization of Nanocrystalline Zn-substituted Hydroxyapatite Films

3.3.1.1 Surface Properties

Surface changes with the EPD process: AFM observation was performed for the polymer substrate films. **Figure 3.5** shows the AFM topographic images of the silicone rubber surface after and before the DC sputtering diode method. The roughness areas showed a highly-ordered pattern. Surface roughness in the film change from is 0.6 ± 0.3 nm to 1.2 ± 0.4 nm after the DC sputtering, because of the deposition of titanium in silicone substrate. The titanium layer (controlled thickness: 5 nm) is so thin that the silicon substrate continues to be transparent (80−90 %). Titanium has a number of impressive properties, including the ability to bind with human bone in a process called biointegration or osseointegration, and does not generate toxic to the human body, in addition, titanium gives conductive properties to the silicone substrate (transparent conductive film), which will facilitate the accession of HAp on the silicone substrate.
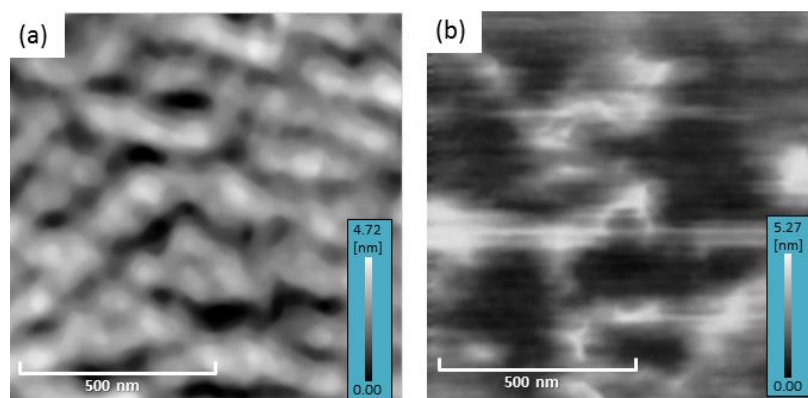
Figure 3.5. AFM topographic images (area: 1.0×1.0 μm^2) of the silicone substrates (a) before and (b) Ti deposition and the surface roughnesses are 0.6 ± 0.3 nm and 1.2 ± 0.4 nm, respectively.

Before EPD process, the polydimethylsiloxane (PDMS) used as a polymer substrate had a slightly brownish tonality after EPD with nanocrystalline Zn-substituted HAp, the film acquired a totally white hue and after ultrasonication had a slight blue coloration and

continued been transparent and flexible the coated film (see **Figure 3.6**). The flexibility of the film is important in biomedical applications especially those related to implants and catheters to avoid causing discomfort and to prevent damaging the tissue.
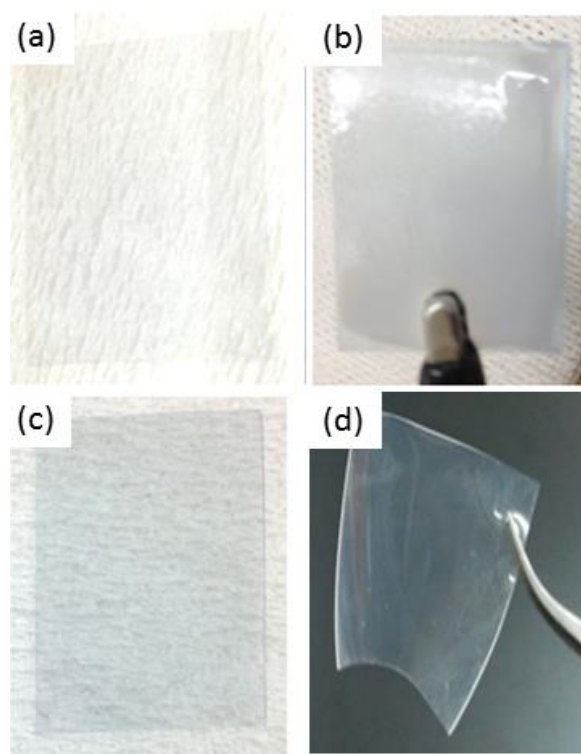
Figure 3.6. Photographs of the PDMS substrates (a) before and (b) after the EPD, and (c) after the ultrasonication, indicating the maintain of flexible state in folding back as shown in (d).

Because it is a desire to apply this material in biomedical applications, such as a coating of catheters, it is important to test the adhesion of the Zn-substituted HAp nanocrystals on the surface of the catheter using EPD for ascertains the viability of coverage. Three types of the catheter (pieces) were used, which were coated with Zn-substituted HAp nanocrystals using the EPD process. The results were similar to those observed previously with the transparent conductive film. After EPD with Zn-substituted HAp nanocrystals, pieces of the three types of catheters had white color and after ultrasonication were of a slightly less dark than the initial color (see **Figure 3.7**). This is because the catheters are not only silicone rubber compounds but also have an external layer (cover) which is a composite, which gives them semiconducting properties and

enables nanocrystalline Zn-substituted HAp is easily deposited on the surface of the catheter.
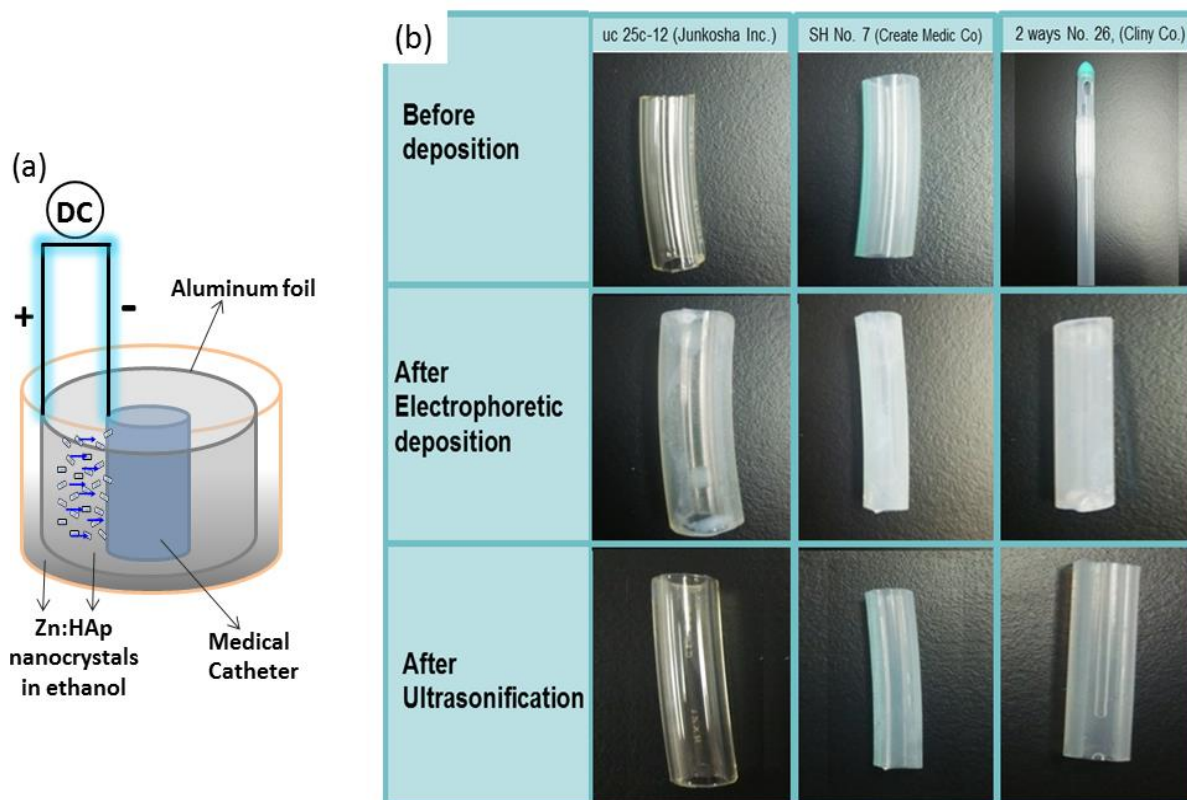
Figure 3.7. (a): scheme of the EPD procedure of nanocrystalline Zn: HAp nanocrystals on biomedical catheters. (b): Photographs of three kinds of the commercially-available medical catheters (a) before and (b) after the EPD at the applied voltage of 100 V for 1 min, and (c) after the subsequent ultrasonication for 1 min.

AFM images of nanocrystalline Zn-substituted HAp films: In order to obtain the best surface coating, DC voltage from 10, 50 and 100 V were applied, **Figure 3.8** shows the results of the coating of 1.67-Zn: HAp nanocrystals at the applied different DC voltages wherein 10 V, the surface was almost bare, and nanocrystals only remain sporadically. In 50 V, the sensor surface was almost covered with Zn- substituted HAp nanocrystals, but there were not perfect, there were spaces without covering. In 100 V, the sensor surface was completely covered with Zn- substituted HAp nanocrystals for that reason the optimum voltage condition is 100 V. HAp deposits obtained at the applied voltage below the critical saturated voltage showed preferable deposition of fine particles, [8] because smallest

particles reached the highest electrophoretic velocity, and, therefore, these were preferential deposited. [9] Both kinds of Zn- substituted HAp nanocrystals present good adherent and continuous coating after the deposition without cracks.

The deposit weight W in the EPD process could be described by the equation (3):

$$W = \frac{C\mu U t}{d} \tag{3}$$

where C and μ are particle concentration and mobility, respectively. t is deposition time, and d is the distance between the electrodes. U is as follows:

$$U = U_{ap} - U_{dep} \tag{4}$$

where U_{ap} = applied voltage, U_{dep}= voltage drop in deposit. The electrophoretic mobility can be determined by the equation (5):

$$\mu = \frac{\xi\varepsilon}{4\pi\eta} \tag{5}$$

where ξ= zeta potential, ε= dielectric constant, and η=viscosity of the medium [10].

The surface covering rate and roughness changes by the nanocrystalline Zn-substituted HAp ((Zn+Ca)/P ratio =1.67 and initial (Zn+Ca)/P ratio =2.00) with Zn concentration of 2.5, 5.0 and 10.0 mol% are shown in **Figure 3.9**, prepared from the different coating voltages of 10 V, 50 V, and 100V. From the viewpoint of the applied voltage, 100 V is the best. The percent of covering surface rate in all the nanocrystalline Zn-substituted HAp films was increased with the increased applied. The optimum voltage was 100 V. In both kind of HAp (initial (Zn+Ca)/P ratio =1.67 and initial (Zn+Ca)/P ratio =2.00), the high result was obtained with the concentration of 5 mol% of Zn. The nanocrystalline Zn-substituted HAp film with initial (Ca+Zn)/P ratio=1.67 in the different voltages always obtain higher surface coverage rate percent than nanocrystalline Zn-substituted HAp film with initial (Ca+Zn)/P ratio=2.00 nevertheless the highest amount of surface coverage rate percent was nanocrystalline Zn-substituted HAp film with initial (Ca+Zn)/P ratio=1.67 containing 5 mol% of Zn at 100 V (100% of surface coverage rate). With regard to surface roughness for both HAps (initial (Zn+Ca)/P ratio =1.67 and initial (Zn+Ca)/P ratio =2.00) containing 2.5 and 10 mol% of Zn with the increase of voltage the amount of surface roughness was increased, at 100 V was the highest amount, but in this

case the nanocrystalline Zn-substituted HAp films (initial (Zn+Ca)/P ratio =1.67 and 2.00) with initial (Ca+Zn)/P ratio=2.00 had higher surface roughness than nanocrystalline Zn-substituted HAp film with initial (Ca+Zn)/P ratio=1.67   and for the nanocrystalline Zn-substituted HAp films containing 5mol% of Zn the amount of surface roughness was decreased with the   increased voltage applied. The minimum surface roughness was nanocrystalline Zn-substituted HAp film with initial (Ca+Zn)/P ratio=1.67 containing 5mol% of Zn at 100 V (2.8 nm), that means that this sample is perfectly covered and fewer holes and breaks continent, i.e., is smooth. This change could be because the particle size of the Zn: HAp nanocrystals, because smallest particles reached the highest electrophoretic velocity, and, therefore, these were the preferential deposited [9].
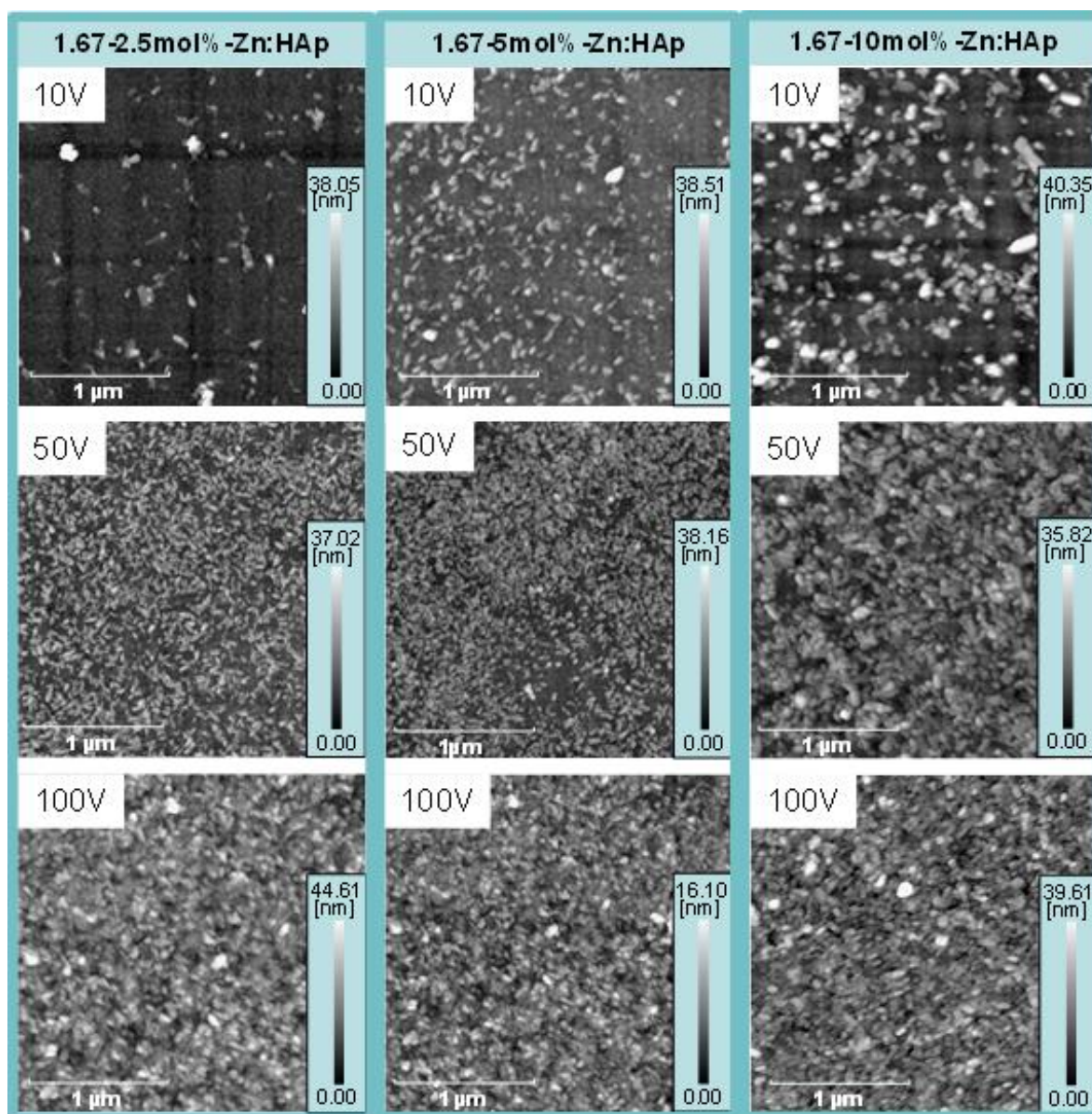
Figure 3.8. Representative AFM topographic images (area: 2.5×2.5 μm^2) of the 1.67-Zn: HAp nanocrystals electrophoretically prepared from the different coating voltages of 10, 50 and 100 V in ethanol. In the 10-V, the surface was almost bare, and the nanocrystals only remain sporadically. In the 50-V, the sensor surface was almost covered with nanocrystals, which were not perfect. In the 100-V, the sensor surface was completely covered with HAp nanocrystals and the optimum voltage condition is 100-V.
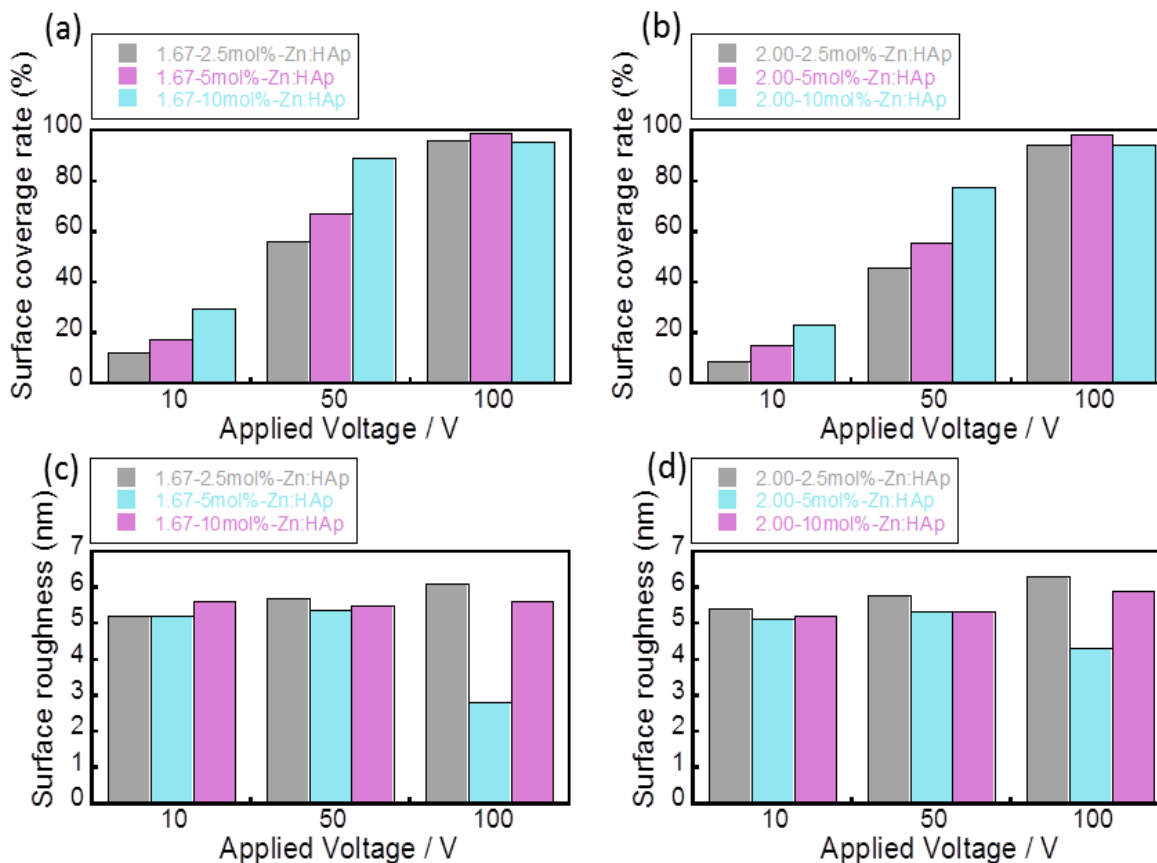
Figure 3.9. (a and b) surface coverage rates and (c and d) roughness changes from the AFM topographic images (area: 2.5 × 2.5 μm^2) of the nanocrystalline (a and c)1.67-Zn: HAp and 2.00-Zn: HAp films prepared from the different coating voltages (10 V, 50 V, and 100 V).

FT-XRD and ATR-FTIR analyzes of nanocrystalline Zn-substituted HAp films: The structure for FT- XRD characterizations is a nanocrystalline Zn: HAp which were [(Ca+Zn)/P ratio=1.67 and Zn conc.=0mol%], [(Ca+Zn)/P ratio=1.67 and Zn conc.=2.5mol%], [(Ca+Zn)/P ratio=1.67 and Zn conc.=5.0mol%], [(Ca+Zn)/P ratio=1.67 and Zn conc.=10mol%], [(Ca+Zn)/P ratio=2.00 and Zn conc.=0mol%], [(Ca+Zn)/P ratio=2.00 and Zn conc.=2.5mol%], [(Ca+Zn)/P ratio=2.00 and Zn conc.=5.0mol%], [(Ca+Zn)/P ratio=2.00 and Zn conc.=10mol%] were deposited on 250 μm-thick silicone conductive films (polymer substrate). The FT-XRD spectra were of nanocrystalline Zn-substituted HAp on polymer substrate films are showing in the **Figure 3.10 (a)** and **3.11 (a)**, the peaks at 18°, 23° and 27° correspond to the (110), (020) and (120) lattice planes,

respectively [12–13]. The figure suggests that the nanocrystalline Zn-substituted HAp has a defective structure or particles are very small [14]. It is not very clear that 2θ region, perhaps the thick of the nanocrystalline Zn-substituted HAp is too small, and the amorphous peaks of the polydimethylsiloxane are very marked in both XRD spectra.

From the infrared spectra of both kind of Zn- substituted HAp film ((Ca+Zn)/P ratio=1.67 and 2.00) in **Figure 3.10 (a)** and **(b)**, the absorption bands are assigned as follows. The spectral shape due to the band at around 1150 cm^{-1} would associate with low crystallinity due to the small crystallite sizes and lattice imperfection. The main bands at 1076 cm^{-1}, 1030 cm^{-1} are assigned to vibrations of the phosphate group, PO_4^{3-} [15–17]. In the details, the first peak a 1076cm^{-1} proceeds from a triple degenerated asymmetric stretching mode vibration; the component of this triple degenerated vibration of the P−O bond of the phosphate group appear at 1030 cm^{-1} [16]. However, the peaks at around 1440 and 1420 cm^{-1} [18, 19] appeared, and the bands is attributed to symmetric and asymmetric carbonate ions (CO_3^{2-}) in the apatite structure.
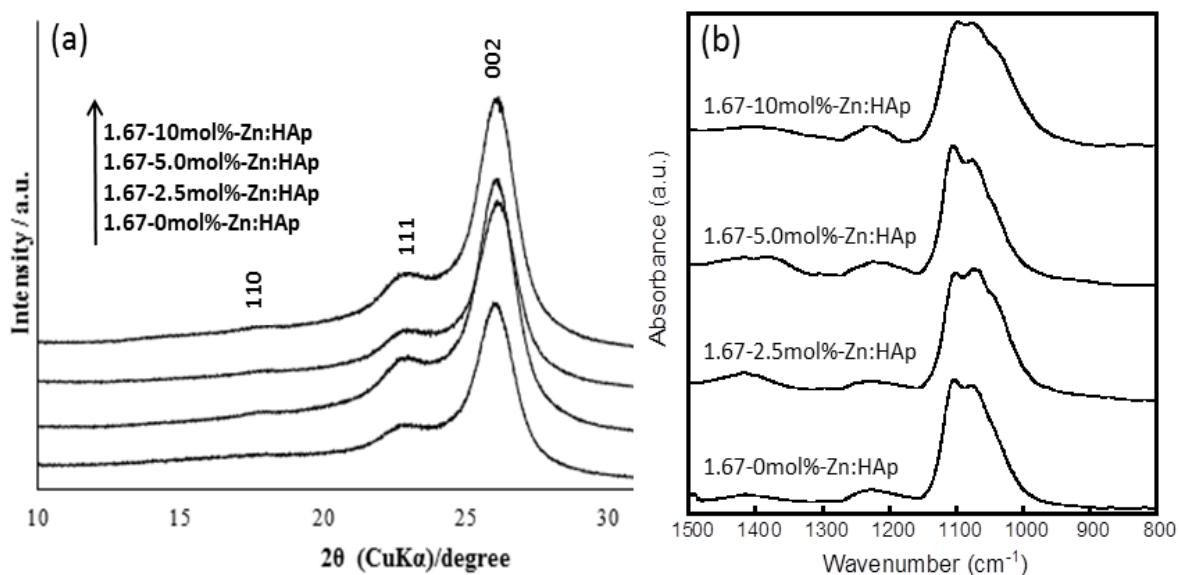
Figure 3.10. (a): Thin film XRD (TF-XRD) patterns and (b) FT-IR spectra of an attenuated total reflection (ATR) mode of the nanocrystalline 1.67-Zn: HAp films with the different initial Zn concentrations at 0, 2.5, 5.0 and 10 mol %. In the TF-XRD, the higher 2θ region were not clear due to the amorphous peak of poly(dimethylsiloxane).
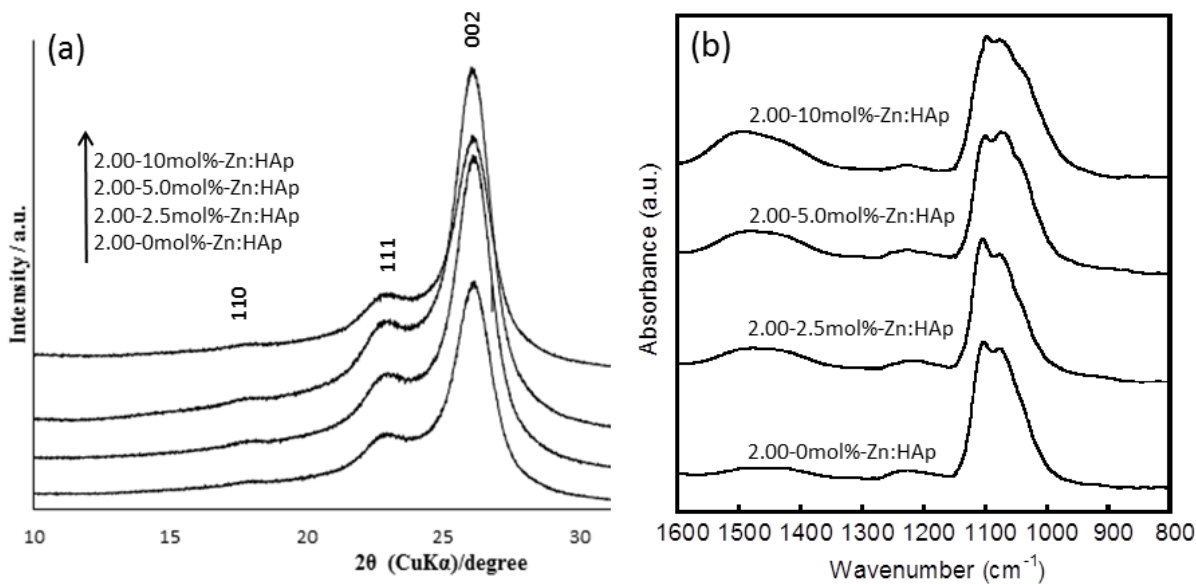
Figure 3.11. (a): Thin film XRD (TF-XRD) patterns and (b) FT-IR spectra of an attenuated total reflection (ATR) mode of the nanocrystalline 2.00-Zn: HAp films with the different initial Zn concentrations at 0, 2.5, 5.0 and 10 mol %.

3.3.1.2 Insight into Electrophoretic Deposition

The principal driving force for EPD is the charge on the particle and the electrophoretic mobility of the particles in the solvent under the influence of an applied electric field, the disadvantage in that it cannot use water as the liquid medium, because the application of voltage in water causes evolution of hydrogen and oxygen gases at the electrodes which adversely affect the quality of the deposits formed.

Two groups of parameters determine the characteristic of EPD process: (i) those related to the suspension (the particles most remain completed dispersed and stable for homogeneous and smooth deposition), and (ii) those related to the process including the physical parameters such as electrical nature of the electrodes, the electrical conditions (voltage/intensity relationship, deposition time, etc.) [5]. For have stability in the suspension it is necessary a particulate surface charge. This stability can be result of the following 4 processes [4]:

    a) Dissociation or ionization of surface groups on the particles.

    b) Readsorption of ionized surfactants.

    c) Adsorption of ionized surfactants.

d) Isomorphic substitution.

The mechanism of suspension stability in HAp in ethanol could involve three steps: (i) adsorption of ethanol molecules in undissociated form onto the basic surfaces sites of the oxide particles; (ii) dissociation of the adsorbed ethanol molecules by hydrogen ions transferring to the surface sites; and (iii) desorption of $C_2H_5O^-$ anions from the solution, leaving the particles positively charged. Zn: HAp being basics in nature.

The mechanism of EPD is summarized in the **Figures 3.12** and **3.13**. Absorb an undissociated the ethanol molecule onto their surface. This absorbed alcohol ionizes into a protonated alcohol and an ethoxide ion. The protonated alcohol dissociates, thereby leaving the proton on the particle surface. The dissociated alcohol and ethoxide ion desorb into the solution, leaving the Zn: HAp particle positively charged in solution. 'The negatively-charged ethoxide ion and positively–charged ZnHAp nanocrystals were easily formed in ethanol (see **Figure 3.12**). These positively –charged ZnHAp nanocrystals are moved towards the cathode under applied field during EPD experiments.
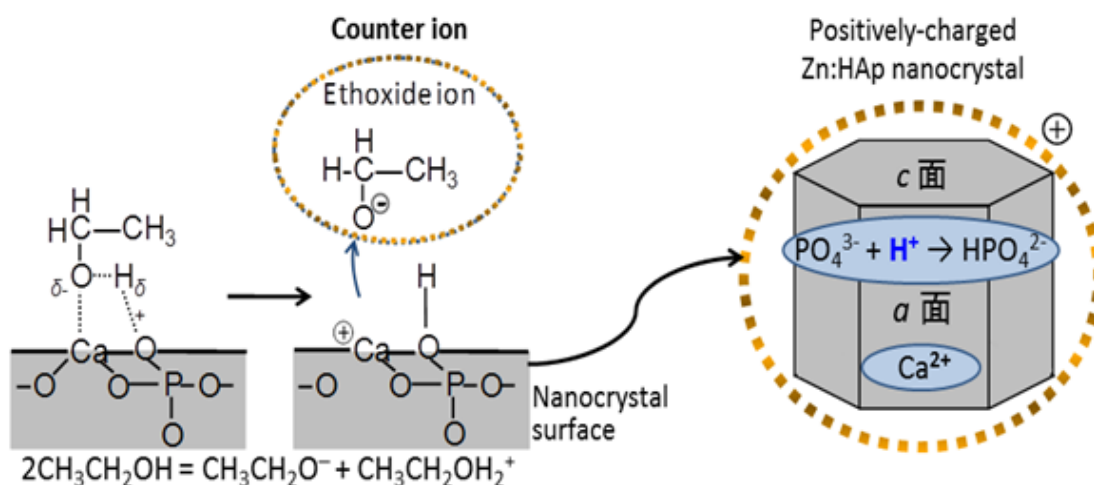
Figure 3.12. Formation of ethoxide ion mechanism on the Zn: HAp surface in ethanol. The ethanol molecule adsorbs on the phosphate group of the Zn: HAp surface to generate ionic dissociation. Thus, the negatively-charged ethoxide ion and positively-charged Zn: HAp nanocrystals were formed in the ethanol.

Derjaguin and Landau [20] and Verwey and Overbeek [21] developed a theory (DLVO, see **Figure 3.13**. **(a)**) to describe the stability of colloid suspension using the

repulsive energy concepts and London-van der Waals (LVDW) attractive energy. According to this theory, the stability of a colloidal system is determinate by the total energy of interaction, determinate by the sum of electrical double layer repulsive forces (F_R) and van der Waals attractive forces (F_V) which the particles experience as they approach one another.

Charged particles attract oppositely charged (i.e., counterions) around the particle (see **Figure 3.13**. **(b))**; this is the "atmosphere" plus the article are the "biosphere". When a particle moves in the liquid, some ions in the lyosphere fluid-mechanically "shear off", and the resultant potential is the zeta potential [4].

When two particles approach, double layers overlap and local ionic concentration increase, thus lowering the system entropy [5]. If F is the force of interaction between two flat double layers separated by distance (D), the latter is the result of differences in ionic concentration between the double layer and the bulk of the solution. F has two components, the electrostatic force (resulting from the energy change) and the osmotic force (entropic in origin) [4–6].

Because the attractive force follows a power law, it dominates at small separations. A primary (deep) minimum (F_1) in the interaction energy curve results at particle/particle contact (D=0 in **Figure 3.13**. **(a)**). As a particle separation increases, double layer repulsion dominates [4, 6]. Thus, the total interaction energy exhibits a peak of height energy barrier E_B, that is the energy barrier to particles coagulation. A secondary shallow minimum (F_2) also develops because, at large distances, the attractive energy again dominates [4, 22]. If particles approach closer than the primary energy barrier (E_B), they will adhere irreversibly. The secondary minimum also can result in coagulation, but the adhesion is weak and reversible, (soft agglomerates, as is shown in **Figure 3.13**. **(c)**).
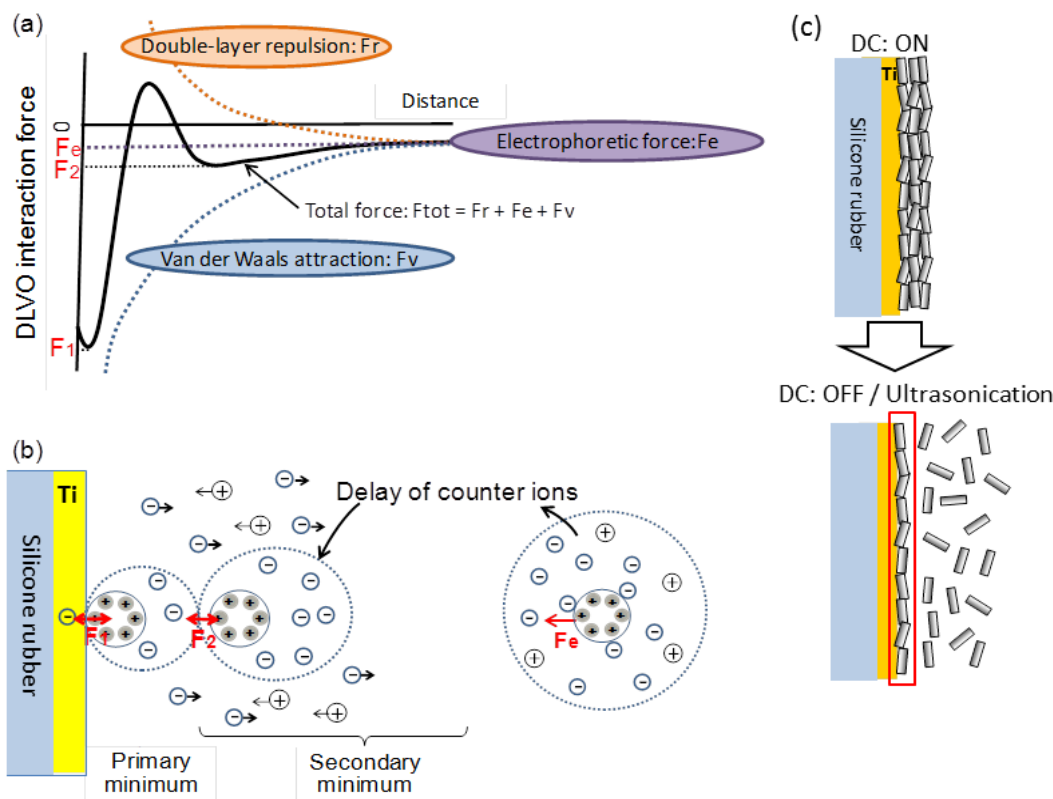
Figure 3.13. Schematic illustrations of (a) DLVO interaction force as a function of distance and (b) deposition mechanism in ethanol, and (c) resultant EPD system at the monolayer.

3.3.1.3 Stability in Cell Culture Solution

The stability of the surface was closely related to both reactions of association and dissociation of calcium and phosphate in tissue culture medium. Ca-deficient HAp, which has a similar crystal structure to HAP with a Ca/P ratio less than 1.67, was generated by degradation and reforming of the surface layer. The stability of the surface structure was considered to be the dominant factor for the enhancement of the adhesiveness of cells on nanocrystalline Zn-substituted HAp ceramics [23]. For that reason, a small experiment was conducted to evaluate the stability of the film in the culture medium.

The nanocrystalline Zn- substituted HAp in a polymer film was immersed in the culture medium (DMEM) for two weeks, and the stability of the Zn-substituted HAp film was evaluated at 5, 7 and 10 days using AFM measurements. The results are shown in the **Figure 3.14** where it is seen as that the Zn-substituted HAp [initial (Ca+Zn)/P ratio= 1.67)]

is dissolving day by day, the surface roughnesses are decreasing with the immersion over time: 6.3 nm, 4.1 nm and 1.3 nm for 5, 7 and 10 days, respectively. Similar results were obtained for Zn-substituted HAp [initial (Ca+Zn)/P ratio= 2)] but in this kind of HAp, the dissolution was little faster, (see **Figure 3.15**) were after the immersion the surface roughnesses are 6.5 nm, 2.3 nm, and 1.8 nm for 5 days, 7 days and 10 days, respectively.
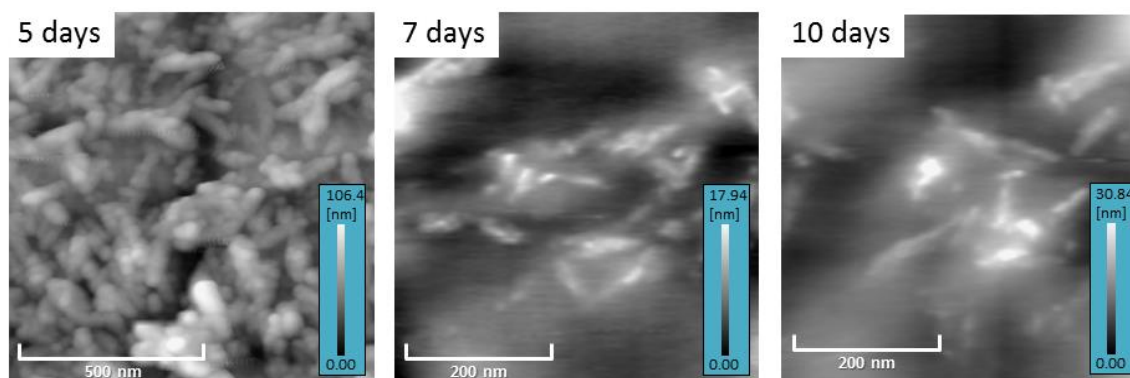
Figure 3.14. AFM topographic images of the nanocrystalline 1.67−Zn: HAp films (with the initial Zn/(Zn+Ca)=10 mol%) after the immersion in DMEM for 10 days and the surface roughnesses are 6.3 nm, 4.1 nm and 1.3 nm for 5, 7 and 10 days, respectively.
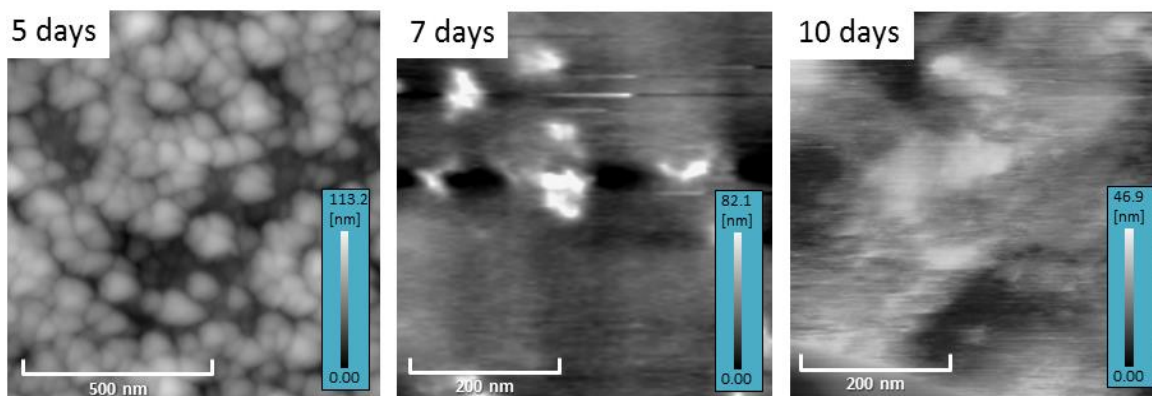
Figure 3.15. AFM topographic images of the nanocrystalline 2.00−Zn: HAp films (with the initial Zn/(Zn+Ca)=10 mol%) after the immersion in DMEM for 10 days and the surface roughnesses are 6.5 nm, 2.3 nm, and 1.8 nm for 5 days, 7 days and 10 days, respectively.

3.3.2 Fibroblast Compatibility

Because the NIH 3T3 fibroblast can synthesize the extracellular matrix for animal tissue and are common cells of connective tissue in an animal, NIH 3T3 fibroblasts were used for determining the biocompatibility with the nanocrystalline Zn-substituted HAp films. A phase-contrast light microscope was used for obtaining the micrographs of the NIH 3T3 fibroblasts on the nanocrystalline Zn-substituted HAp film and for determining the effect on cell adhesion, morphology and cell density on the nanocrystalline Zn-substituted HAp films.

The cell density of the fibroblast cells on different nanocrystalline Zn-substituted HAp films (initial (Zn+Ca)/P ratio= 1.67 and 2.00 and with the Zn concentration of 0, 2.5, 5.0 and 10.0 mol %) were compared and showed in the **Figure 3.16**. Before 72 h in all cases, the results obtained in the nanocrystalline Zn-substituted HAp films were higher than the observed on PS dish used as a control surface. In almost all the samples, the cell density increases with increasing duration time. After 72 h the all the nanocrystalline Zn-substituted HAp films with initial (Ca+Zn)/P =2 exhibit a high cell density much higher than the PS dish, but the Zn-substituted HAp films with initial (Ca+Zn)/P =1.67 exhibit a very low amounts of the cell density smaller than the PS dish. The smallest cell density was the Zn-substituted HAp films with initial (Ca+Zn)/P =1.67 with Concentration of Zn of 10 mol% and in all the culture time the maximum adhesion was observed in the Zn-substituted HAp films with initial (Ca+Zn)/P =2.00 with Zn concentration of 5.0 mol%. This proves that the calcium deficient Hydroxyapatit, because it is carbonated, is more biocompatible than stoichiometric HAp and apparently the addition of Zn to a concentration of 5 mol% might promote adhesion of fibroblasts cell adhesion. As expected, the films of PDMS were no cell growth.
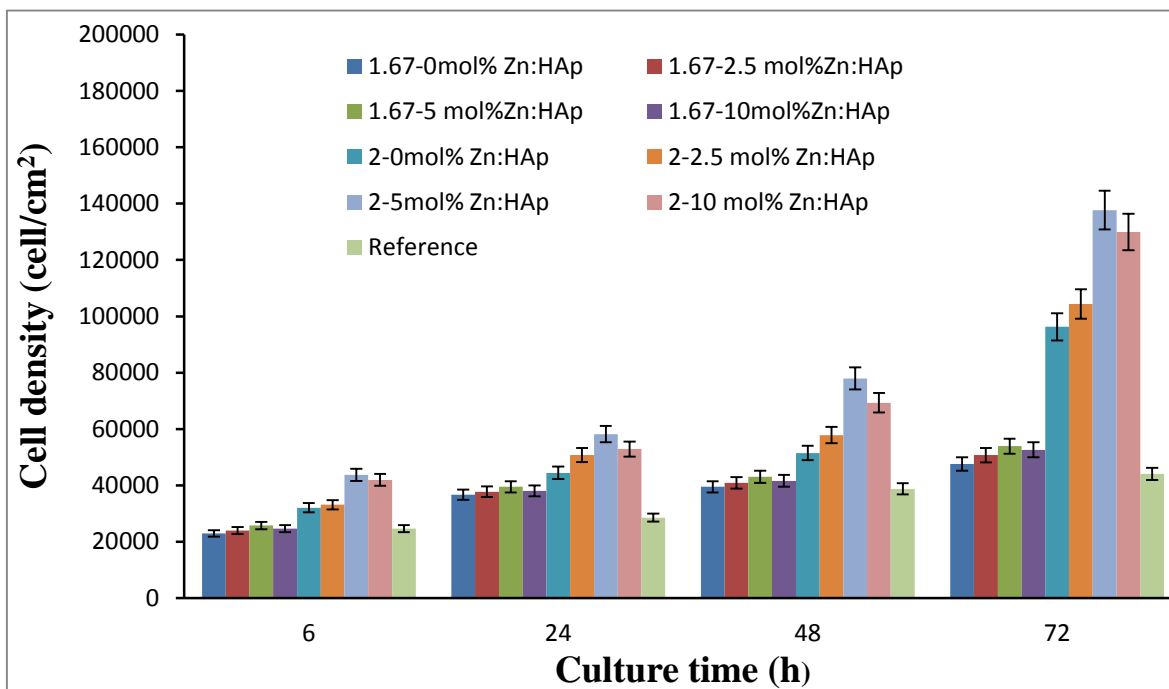
Figure 3.16 Cell density on the nanocrystalline Zn: HAp films with the different Zn concentrations at 0.0, 2.5, 5.0 and 10 mol% to the Ca sites of HAp structure, and the reference to PDMS film.

Figures 3.17, 3.18 and **3.19** show phase-contrast light images of the nanocrystalline Zn-substituted HAp films structure containing 0, 2.5, 5.0 and 10.0 mol % of Zn at the culture time of 72 h. Phase-contrast light images revealed a growing pattern of the adhered NIH 3T3 cells on the nanocrystalline Zn-substituted HAp films and PDMS used as a reference. The nanocrystalline Zn-substituting HAp films exhibit better fibroblast adherence at 72 h than the PDMS used as a reference (see **Figure 3.19**). In **Figure 3.17** the micrographs show the adhered cells on the nanocrystalline 1.67−Zn: HAp films with different Zn concentrations where the cell number of cells increased with the increased amount of Zn ion, but at 10 mol% the number of cells decreased a little. But in figure 3.18 show that the cells on nanocrystalline 2.00−Zn: HAp films with different Zn concentrations increased significantly during culture time. However cells to multiply significantly on nanocrystalline 2.00−Zn: HAp films as compared to nanocrystalline 1.67−Zn: HAp films, demonstrating that the carbonate ion-containing the nanocrystalline

2.00−Zn: HAp films play an important role in the adhesion and biocompatibility of the cells.
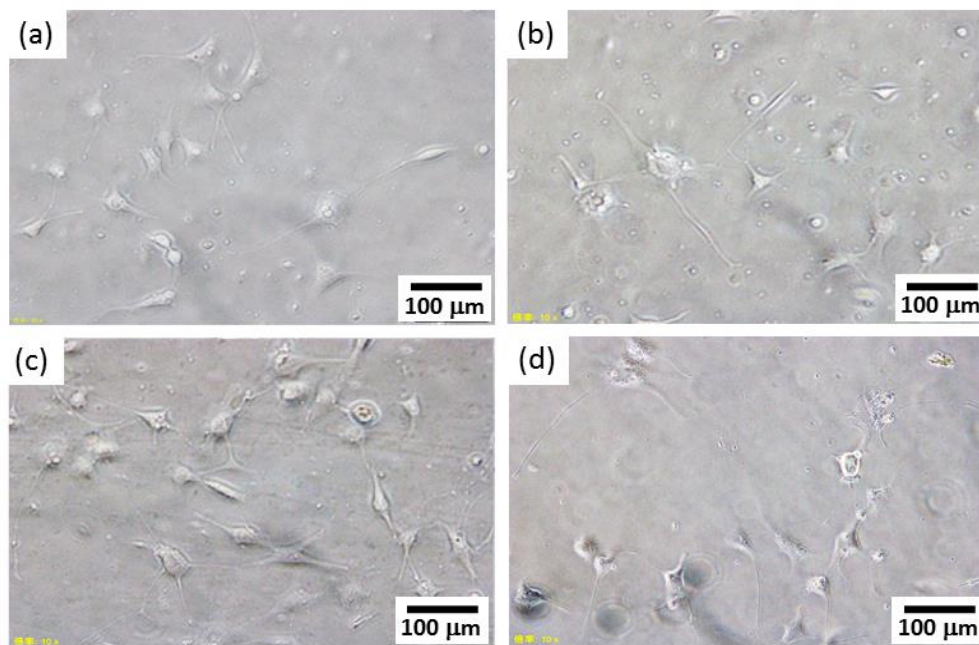
Figure 3.17 Low-magnification photographs (×40) of the cells adhered on the nanocrystalline 1.67−Zn: HAp films with the different Zn concentrations at (a) 0.0, (b) 2.5, (c) 5.0 and (d) 10 mol% to the Ca sites of HAp structure at the culture time of 72 h.
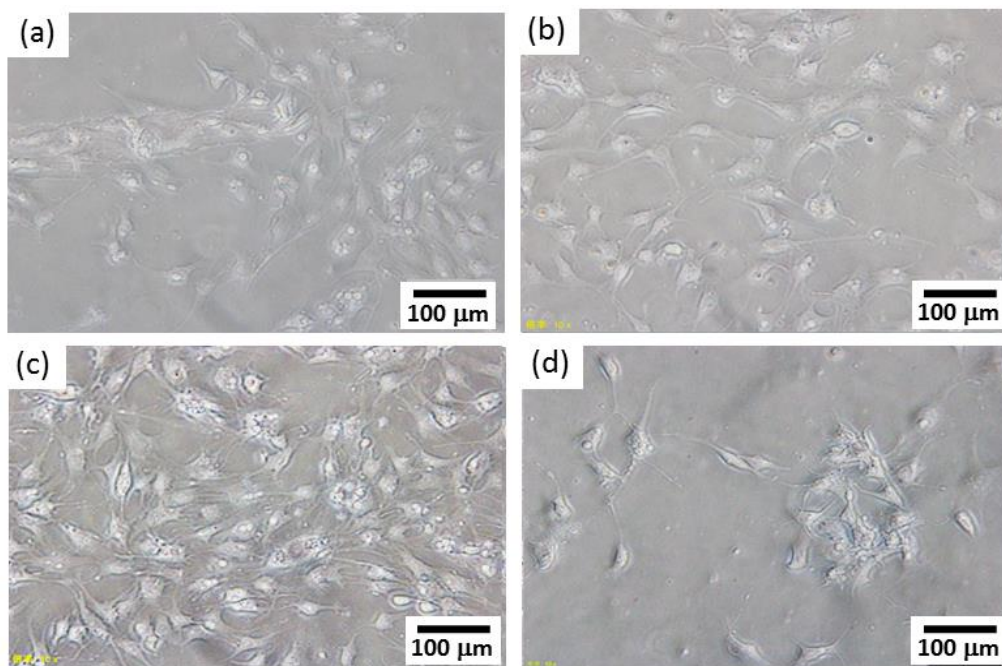
Figure 3.18 Low-magnification photographs (×40) of the cells adhered on the nanocrystalline 2.00−Zn: HAp films with the different Zn concentrations at (a) 0.0, (b) 2.5, (c) 5.0 and (d) 10 mol% to the Ca sites of HAp structure at the culture time of 72 h.
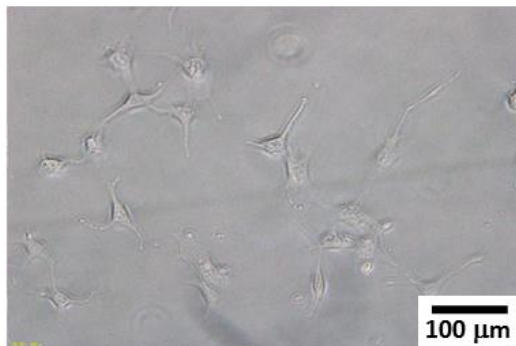
Figure 3.19 Low-magnification photographs (×40) of the cells adhered to the PDMS film as the reference at the culture time of 72 h.

It was observed that the values of cell area (see **Figure 3.20**), aspect ratio (see **Figure 3.21**) were high in the nanocrystalline Zn-substituted HAp films. At 72 h of culture time, the cell area of the nanocrystalline 1.67−Zn: HAp films was higher compared with the nanocrystalline 2.00−Zn: HAp films in contrast the aspect ratio of the nanocrystalline 1.67−Zn: HAp films is lower than nanocrystalline 2.00−Zn: HAp films and showed a

difference compared with PDMS used as control. In fact, all the nanocrystalline Zn-substituted HAp films showed higher results than the reference (PDMS). In addition, it was reported that because adhesion and spreading of anchorage-dependent cells are prerequisite for cell viability and proliferation [24, 25], the reduction of the aspect ratio on the surface with higher contact angle might be expected to result in lower cell densities, especially at early time points in the culture time. The cell morphology results at 72 h of culture time of the cells adhered on the nanocrystalline 1.67−Zn: HAp films with the different Zn concentrations are shown in **Figure 3.22**, cells adhered on the nanocrystalline 1.67−Zn: HAp films in **Figure 3.23** and for the PDMS in **Figure 3.24**. The cells were attaching and stretching well on the ZnHAp films, this phenomenon was supported by the micrographs, indicating filopodia projecting from the cells edges for ZnHAp; indicated that the nanocrystalline Zn-substituted HAp films could provide a suitable environment to promote and enhance the platelet adhesion.

Figure 3.20 Area of the cell adhered on the nanocrystalline Zn: HAp films with the different Zn concentrations at 0.0, 2.5, 5.0 and 10 mol% of the Ca sites of HAp structure, and the reference to PDMS film.

Figure 3.21 Aspect ratio of the cell adhered on the nanocrystalline Zn: HAp films with the different Zn concentrations at 0.0, 2.5, 5.0 and 10 mol% to the Ca sites of HAp structure, and the reference to PDMS film.
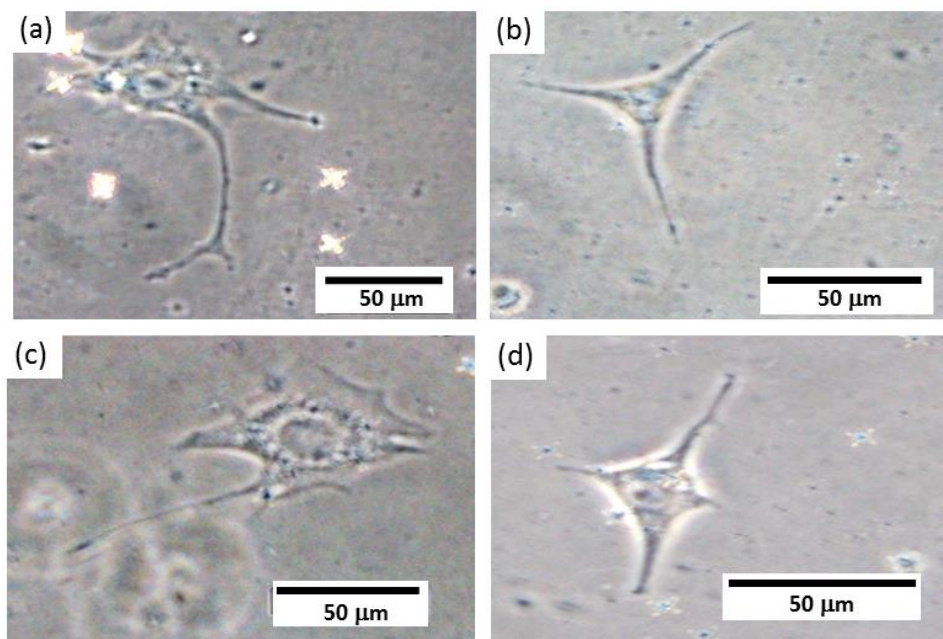
Figure 3.22 High-magnification photographs (×200) of the cells adhered on the nanocrystalline 1.67−Zn: HAp films with the different Zn concentrations at (a) 0.0, (b) 2.5, (c) 5.0 and (d) 10 mol% to the Ca sites of HAp structure at the culture time of 72 h.
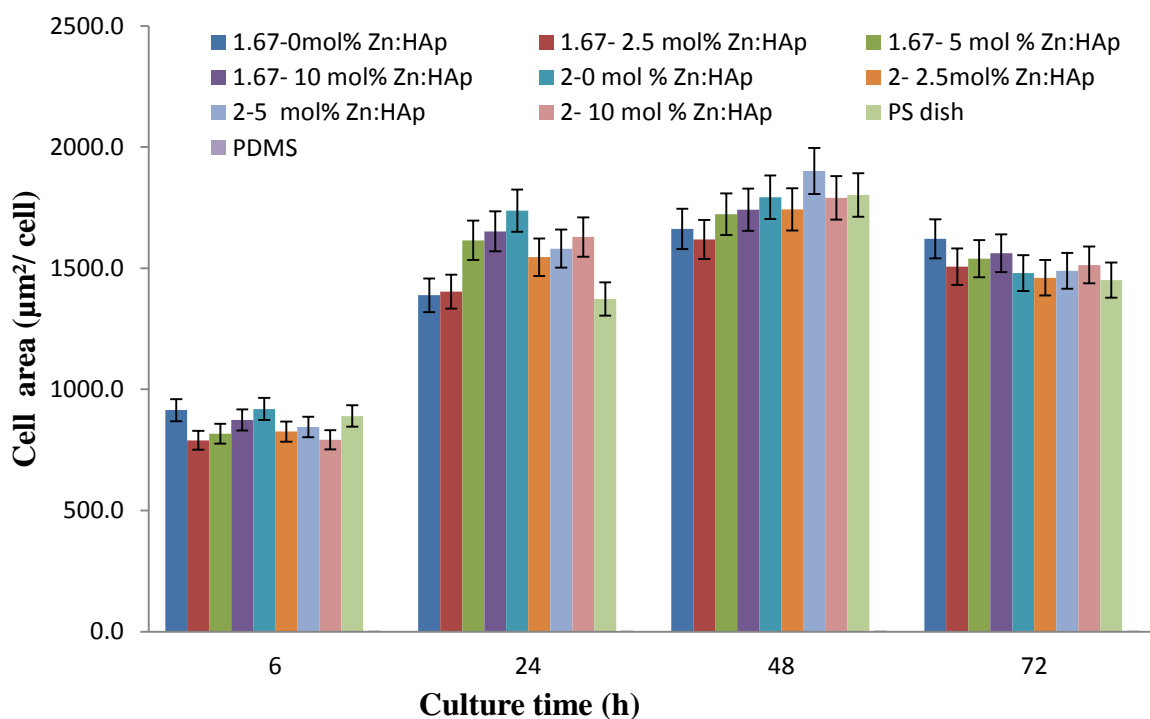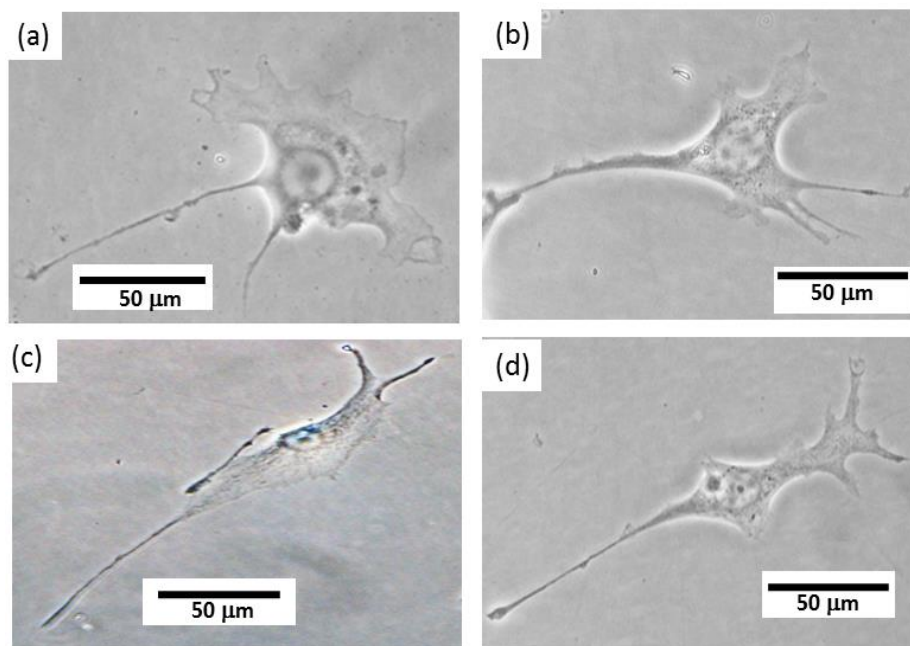
Figure 3.23 High-magnification photographs (×200) of the cells adhered on the nanocrystalline 2.00−Zn: HAp films with the different Zn concentrations at (a) 0.0, (b) 2.5, (c) 5.0 and (d) 10 mol% to the Ca sites of HAp structure at the culture time of 72 h.
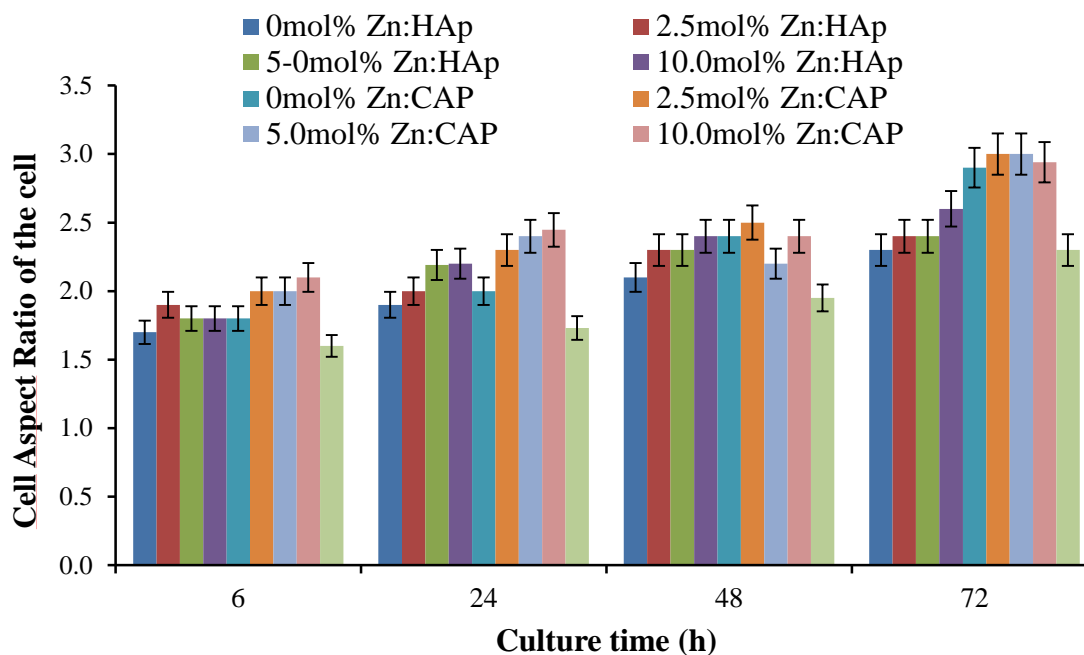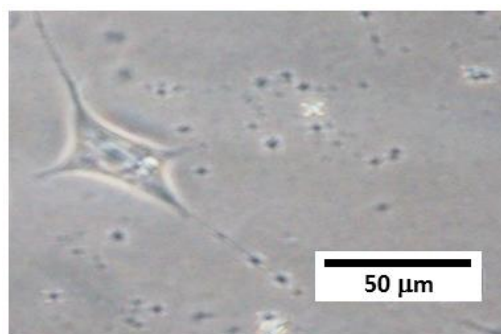

Figure 3.24 High-magnification photographs (×200) of the cells adhered to the PDMS film as the reference at the culture time of 72 h

3.3.3 Antibacterial Activity

The photographs of LB plate surfaces after the viable bacterial growth of the second culture was shown in **Figure 3,25**. After 24 h of culture, bacterial growth was observed in all LB plates, including the polymer substrate used as a reference, nevertheless there was a reduction in viable cells of *E. coli* DH5α in samples containing Zn (nanocrystalline Zn-

substituted HAp films with Zn concentration of 2.5, 5.0 and 10.0 mol%) unlike samples had no Zn nanocrystalline Zn-substituted HAp films with Zn concentration of 0 mol%).

In **Figure 3.25** the results of nanocrystalline Zn-substituted HAp films with initial (Ca+Zn)/P ratio=1.67 are observed where, even the last dilution (10 CFU/plate), had quite a few viable *E. coli* DH5α colonies. The Zn-substituted HAp films with initial (Ca+Zn)/P ratio=1.67 at the Zn concentration of 2.5, 5.0 and 10.0 mol% presented better antibacterial activity since both plates bacterial inhibition halos were observed in the second dilution (100 CFU /plate), and were made more marked in the third dilution (10 CFU / plate). Of these films which showed higher bacterial activity was nanocrystalline Zn-substituted HAp film with Zn concentration of 10 mol%.

It is noted that the nanocrystalline Zn-substituted HAp films with initial (Ca+Zn)/P ratio=2.00 had a higher antibacterial activity compared to nanocrystalline Zn-substituted HAp films with initial (Ca+Zn)/P ratio=1.67. Unlike the nanocrystalline Zn-substituted HAp films with initial (Ca+Zn)/P ratio=1.67, in nanocrystalline Zn-substituted HAp films with initial (Ca+Zn)/P ratio=2.00 the bacterial inhibition halos began to be observed from 1000 CFU/plate, and these halos were becoming larger as going increasing dilution CFU/plate and in the third dilution (10 CFU/plate) viable cells of *E. coli* DH5α were dramatically less. The nanocrystalline Zn-substituted HAp films with initial (Ca+Zn)/P ratio=2.00 with a Zn concentration of 5 mol% exhibits good bacterial inhibition at a dilution of 10 CFU/plate, however the Zn concentration of 10 mol% shows better bacterial inhibition, with this concentration of Zn which antibacterial shows improved antibacterial activity in this study. In the nanocrystalline Zn-substituted HAp films with initial (Ca+Zn)/P ratio=2.00, the viable *E. coli* DH5α colonies were scattered unlike the nanocrystalline Zn-substituted HAp films with initial (Ca+Zn)/P ratio=1.67 where the viable *E. coli* DH5α colonies was focalized.
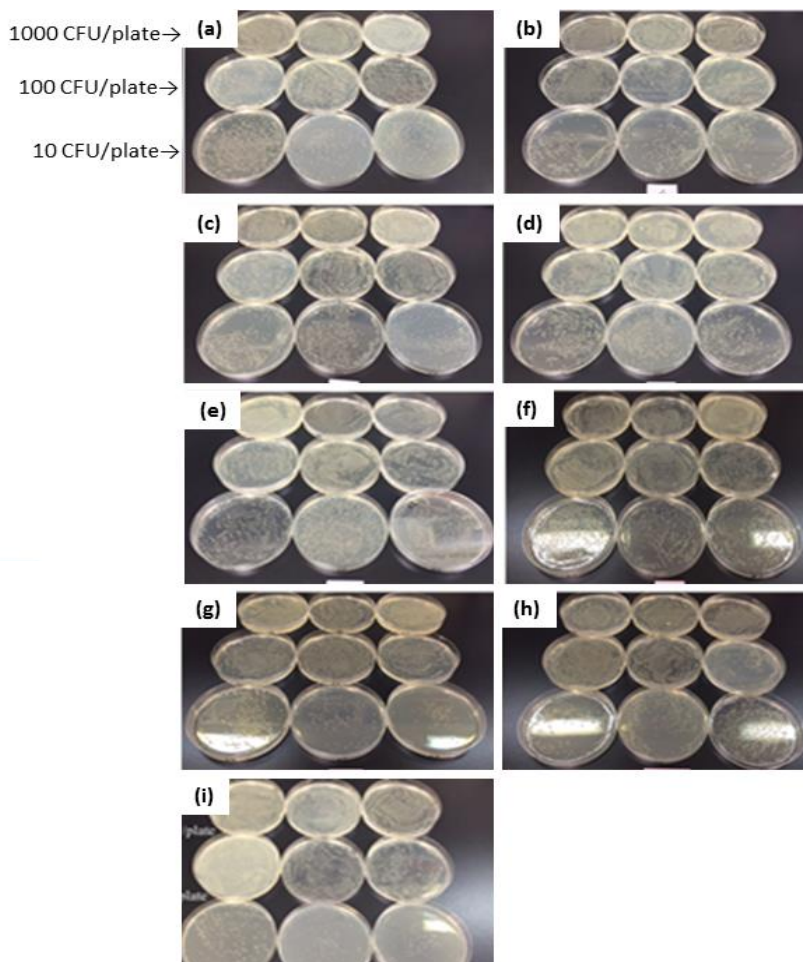
Figure 3.25. Photographs of the culture state of *E. coli* DH5α after the second culture vs. the sample films of (a) [(Ca+Zn)/P ratio=1.67 and Zn conc.=0mol%], (b) [(Ca+Zn)/P ratio=1.67 and Zn conc.=2.5mol%], (c) [(Ca+Zn)/P ratio=1.67 and Zn conc.=5.0mol%] and (d) [(Ca+Zn)/P ratio=1.67 and Zn conc.=10mol%], (e) [(Ca+Zn)/P ratio=2.00 and Zn conc.=0mol%], (f) [(Ca+Zn)/P ratio=2.00 and Zn conc.=2.5mol%], (g) [(Ca+Zn)/P ratio=2.00 and Zn conc.=5.0mol%], (h) [(Ca+Zn)/P ratio=2.00 and Zn conc.=10mol%], and (i) [reference: PDMS film], were abbreviated as the "initial molar ratio (Zn+Ca)/P─initial Zn concentration".

A viable number of the viable *E. coli* DH5α after the second culture depending on the sample films is shown in **Figure 3.26.** In this case, the number of the viable *E. coli* DH5α colonies was lower for all the nanocrystalline Zn-substituted HAp films with initial (Ca+Zn)/P ratio=1.67 than for nanocrystalline Zn-substituted HAp films with initial (Ca+Zn)/P ratio=2.00.

200 µL of the secondary bacteria liquid (ca. 10 CFU/200 µL) was seeded on the LB agar plate was cultured for 24 h, and the number of the viable bacteria after the culture was shown in **Figure 3.27**.

Because the nanocrystalline Zn-substituted HAp films with initial (Ca+Zn)/P ratio=2.00 exhibits greater biocompatibility, it was expected that the film containing no Zn (nanocrystalline Zn-substituted HAp films with initial (Ca+Zn)/P ratio=2.00 with Zn concentration of 0 mol%) had a higher number of bacteria than Zn-substituted HAp films with initial (Ca+Zn)/P ratio=1.67, which seen in **Figure 3.27** the film has more than 1000 viable *E. coli* DH5α colonies. In all films, it can be seen that Zn ion has an antibacterial activity effectively because all films containing Zn had a decrease in the number of viable *E. coli* DH5α colonies and this decreased in viable *E. coli* DH5α colonies is more notorious with the increment of Zn ion amount. For both kind of films (nanocrystalline Zn-substituted HAp films with initial (Ca+Zn)/P ratio=1.67 and initial (Ca+Zn)/P ratio=2.00), the sample that showed higher antibacterial activity was that had a Zn concentration of 10 mol%. Nevertheless, the nanocrystalline Zn-substituted HAp films with initial (Ca+Zn)/P ratio=2.00 with a concentration of 10 mol% showed the highest antibacterial ability. These results are consistent with those presented in the previous experiment (see **Figure 3.25)**

Two ways of antibacterial activity derived from (1) the Zn ion by its toxicity and (2) the reactive oxygen caused by catalysis was implied in the Zn ion substitution. However, the detailed mechanism isn't understood yet. There is little elution because the Zn ion is substituted into the HAp crystal. Thus, it seems not to notify the enough concentration of Zn ion which indicates an antibacterial activity in the bacterial liquid. When doing the released Zn ion test, it'll be possible to investigate the mechanism. When the activated oxygen evolution with the Zn ion catalysis is thought, there is no report on the reactive oxygen radical species by the Zn ion substituted in the HAp crystal, and the possibility is low. Otherwise, Nan *et al.* [26] reported that membranes of E. coli were seriously damaged after in contact with the stainless steel containing copper ions, thereby causing nutrients, proteins, and other essential components of the cytoplasm within the bacteria to 'leak out' and hence, resulting cell death [27, 28].

Because the Zn ions is also a heavy metal, it was hypothesized that in this study, Zn^{2+} ions would behave similarly to Cu^{2+} ions to form strong bonds with the membrane proteins of *E. coli* DH5α causing structural changes to the several membranes, thereby affecting proper nutrient/protein transport through the nuclei via the membranes and hence, contributing to cell death. The mechanism in which how Zn interacts with the bacteria's membrane and thereby, activates antimicrobial property, have to be investigated further. In addition to cytotoxic nature, biocompatibility is one important factor for the application in tissue engineering. Therefore, as Table 3.1 lists biocompatibility and cytotoxicity properties that are presented.
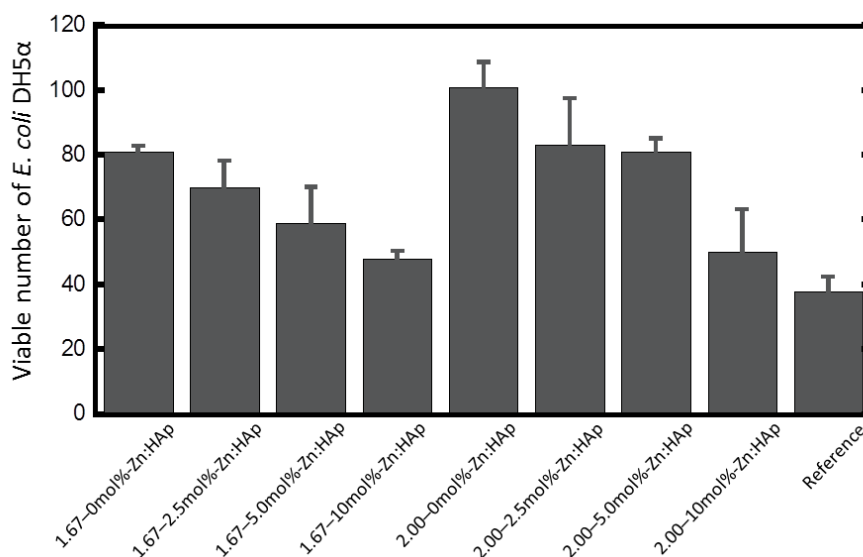
Figure 3.26. Viable number of the viable *E. coli* DH5α after the second culture depending on the sample films (reference: PDMS film), which were abbreviated as the "initial molar ratio (Zn+Ca)/P─initial Zn concentration" at the lower seeding concentration (first culture: 1×10^3 CFU/mL (5×10^2 CFU/50 uL) and second culture: 5 CFU/200uL).
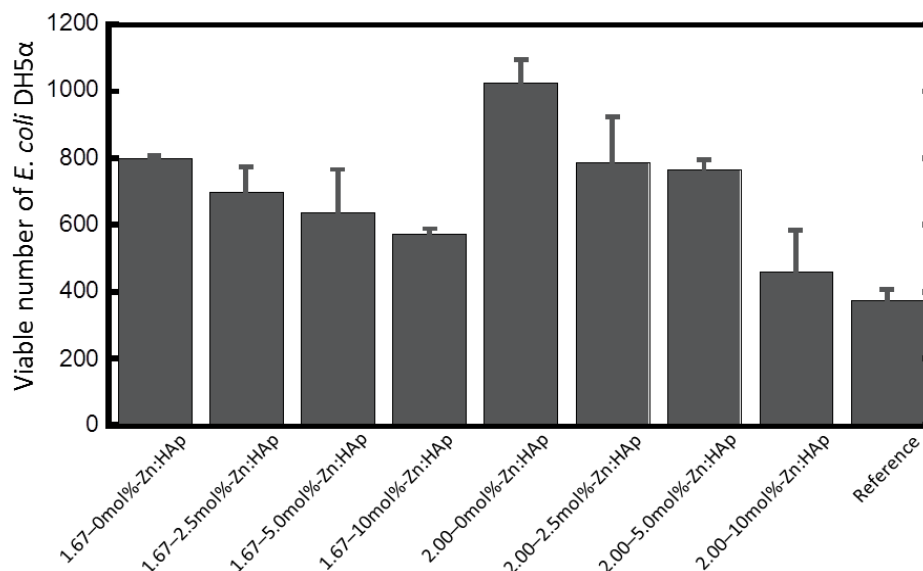
Figure 3.27. Viable number of the viable *E. coli* DH5α after the second culture depending on the sample films (reference: PDMS film), which were abbreviated as the "initial molar ratio (Zn+Ca)/P—initial Zn concentration" at the higher seeding concentration (first culture: 1×10^6 CFU/mL (5×10^4 CFU/50 uL) and second culture: 1×10 CFU/200uL).

Table 3.1 Evaluation of biocompatibility and cytotoxicity properties of nanocrystalline Zn-substituted HAp films.

	Fibroblast Compatibility				Antibacterial activity
	Initial Cell Adhesion	Cell Density	Area of Cell	Aspect Ratio	
1.67-0mol%-Zn: HAp film	*Regular*	*Regular*	*Good*	*Good*	*Regular*
1.67-2.5mol%-Zn: HAp film	*Regular*	*Regular*	*Good*	*Good*	*Good*
1.67-5.0mol%-Zn: HAp film	*Regular*	*Regular*	*Good*	*Regular*	*Good*
1.67-10mol%-Zn: HAp film	*Regular*	*Bad*	*Good*	*Good*	*Very Good*

2.00-0mol%-Zn: HAp film	*Good*	*Good*	*Good*	*Very Good*	*Regular*
2.00-2.5mol%-Zn: HAp film	*Good*	*Good*	*Good*	*Good*	*Good*
2.00-5.0mol%-Zn: HAp film	*Very Good*	*Very Good*	*Good*	*Very Good*	*Good*
2.00-10.0mol%-Zn: HAp film	*Good*	*Good*	*Good*	*Good*	*Very Good*
Reference	*Bad*	*Bad*	*Good*	*Good*	*Very Good*

3.4 Conclusion

Nanocrystalline Zn-substituted HAp (initial (Ca+Zn)/P ratio=1.67 and initial (Ca+Zn)/P ratio=2.00) containing 0, 2.5, 5.0 and 10.0 mol% was successfully deposited on a polymer substrate by EPD without using chemical reagents. The optimum voltage condition for EPD was 100 V, obtaining a uniform film without cracks. Nevertheless, a dissolution of the nanocrystalline Zn-substituted HAp (initial (Ca+Zn)/P ratio=1.67 and initial (Ca+Zn)/P ratio=2.00) in the films occurs within two weeks. The in vitro cellular response for nanocrystalline Zn-substituted HAp films (initial (Ca+Zn)/P ratio=1.67 and initial (Ca+Zn)/P ratio=2.00) indicated an increase in the growth of NIH3T3 fibroblasts. The nanocrystalline Zn-substituted HAp films (initial (Ca+Zn)/P initial (Ca+Zn)/P ratio=2.00) showed better biocompatibility than nanocrystalline Zn-substituted HAp films (initial (Ca+Zn)/P ratio=1.67); demonstrating that Zn: HAp calcium deficient was an excellent bioactive material. The sample how showed the best biocompatibility with the fibroblast was the nanocrystalline Zn-substituted HAp films (initial (Ca+Zn)/P initial (Ca+Zn)/P ratio=2.00 containing 5.0 mol% of Zn. These findings demonstrated that the substitution of Zn in minute amount (5.0 mol%) into HAp, plays a significant role in promoting cell growth and differentiation. Nevertheless, the mechanism in which how Zn affects the biological response requires further investigation. From the antibacterial study, it was demonstrated that viable *E. coli* DH5α bacteria reduction could be observed in the nanocrystalline Zn-substituted HAp films. Nanocrystalline Zn-substituted HAp films (initial (Ca+Zn)/P initial (Ca+Zn)/P ratio=2.00 containing 10.0 mol% of Zn had the highest antibacterial activity. All these findings confirmed the enhanced bioactivity and antibacterial property of nanocrystalline Zn-substituted HAp films (initial (Ca+Zn)/P initial (Ca+Zn)/P ratio=2.00 as an alternative biomaterial to phase-pure HAp, and also that nanocrystalline Zn-substituted HAp films (initial (Ca+Zn)/P initial (Ca+Zn)/P ratio=2.00 had better biocompatibility and antibacterial activity than nanocrystalline Zn-substituted HAp films (initial (Ca+Zn)/P initial (Ca+Zn)/P ratio=1.67. Because of the nanocrystalline Zn-substituted HAp films could be deposited easily in polymer substrate without using chemical reagents and it was confirmed the enhanced bioactivity and antibacterial property these materials could use as a covering material for biomedical applications.

References

[1]   Plesiingerová B., Súcik G., Maryska M., Horkavcová D. Ceramics- Silikáty 51 [1] 15–23 (2007)

[2]   Hlavác J. Ceramics- Silikáty 43 133(1999)

[3]   Feng Z., Su Q. J. Mater. Sci. Tchnol., 19 [1] (2003)

[4]   Sakar P., Nicholson P. J.Am. Ceram. Soc. 79 [8] 1987–2002 (1996)

[5]   Besra L., Liu M. Progress in Materials Science 52. 1–61 (2007)

[6]   Schwartz M. Journal of The Electrochemical Society – J ELECTROCHEM SOC , vol. 112, no. 1, 1965

[7]   Lazic M., Simovic K., Miskovic-Stankovic V., Jovanici P., Kicevic D. J. Serb. Chem. Soc. 69 (3) 239–249 (2004)

[8]   Feng Z., Su Q. J.Mater. Sci.Technol. 19 [1] 30–32 (2003)

[9]   Plešingerová B., Súèik G., Maryška M., Horkavcová D. Ceramics − Silikáty 51 (1) 15–23 (2007)

[10] Zhitomirsky I., Gal-Or L. Journal of Materials Science: Materials in Medicine 8 213–21 (1997)

[11] Cardona Q., Oliveros C., Arias D., Devia A., Arcilla J., Álvarez F. Cenicafé, 59 (3) 204–213 (2008)

[12] Kuribara K., Wang H.,Uchiyama N., Fukuda K., Yokota T., Zschieschang U., Jaye C., Fischer D., Klauk H., Yamamoto T., Ikeda M., Kuwabara H., Sekitani T., Loo Y., Someya T. Nature Communications 3, 723 (2012)

[13] Tian L., Fathi E., Tarighat R., Sivoththaman S. Semicond. Sci. Technol. 28 (10) 105004 (2013)

[14] Plešingerová B., Súèik G., Maryška M., Horkavcová D. Ceramics − Silikáty 51 (1) 15–23 (2007)

[15] Jorurnal of Biomedical Materials Research, 662(4):600–12 (12/2002)

[16] Singh A, Purohit KM. J Bioprocess Biotechniq 1:104 (2010)

[17] American Journal of Materials Science, 3(4): 84–90 (2013)

[18] J Biomed Mater Res. Jul;41(1):79–86 (1998)

[19] J. Res. Natl. Inst. Stand. Technol. 109, 553–568 (2004)

[20] Deryaguin B., Landau L. Acta Physicochim USSR 14:633 (1941)

[21] Verwey E., Overbeek J. Amsterdam: Elsevier (1948)

[22] Corni I.,Ryan M., Boccaccini A. Journal of European Ceramic Society 28 1353–1367 (2008)

[23] Suzuki T.,Yamamoto T., Toriyama M., Nishizawa K., Yokogawa Y., Mucalo M., Kawamoto Y., Nagata F., and Kameyama T. Journal of Biomedical Materials Research, Vol. 34, 507–517 (1997)

[24] Salem, A. K.; Tendler, S. J.; Roberts, C. J. Journal of Biomedical Materials Research, Vol, 61, 2002, pp. 212–218.

[25] . Tamada, Q, Ikada, J. Colloid Interface Sci, Vol, 155, 1993, pp. 334–339.

[26] Nan L, Liu Y, Lu M, Yang K. J Mater Sci Mater Med. 19 3057–62 (2008)

[27] Stanic V, Dimitrijevic S, Antic-Stankovic J, Mitric M, Jokic B, Plecas I, Raicevic S. Appl. Surf. Sci. 256 6083–9 (2010)

[28] Hian E., Konishi T., Kawanobe Y.,Lim P., Choong C., Aizawa B. J Mater Sci Mater. Med. 24 437–445 (2013)

Chapter 4

Summary and Future Perspectives

4.1 Summary

A hospital-acquired infection is usually one that first appears three days after a patient is admitted to a hospital or other health care facility. In the problems, it has been thought that the low bioaffinity of medical catheters often causes bacterial infection through the permeation interspaces between catheters and skin tissues. Thus, the surface modification of the biomedical polymers used as catheters is desired for improving the biocompatible and antibacterial properties. As the modification materials, hydroxyapatite $(Ca_{10}(PO_4)_3(OH)_2)$ (HAp) is a good candidate. HAp ceramics are remarkable by the great amount of applications that have like ability to absorb certain organic compounds, and therefore have been used as adsorption separation agents for proteins and nucleic acid, in chromatography column resins, toothpaste additives, gas sensor components, catalysis, fertilizers industry, pharmaceutical products, water treatment processes but his most important application that also has widely been used as bone substrates and as coating on metallic implants and self-setting bone cements because of its good biocompatibility, bioactivity and osteoconductivity. From the 70's started to investigate the use of HAp as osteoinductive material, is a material that induces new bone formation. Currently used successfully bovine bone graft or autologous (patient's own bone) as filler or implant in cases of missing bone. In order to improve the characteristics and properties of the HAp,

HAp has been doped with various metal ions. Especially, with zinc (Zn) doping into calcium phosphate structure not only give the better mechanical strength of calcium phosphate implants but also antibacterial properties could be acquired. The main chemical components of HAp include calcium and phosphate; however, the natural HAp containing minimum percentages of sodium, chloride, carbonate and magnesium, which play a major role in the function of bone remodeling. This is why it is not considered a pure apatite-based on this background.

In "**Chapter 1**: *General Introduction*" a brief introduction of percutaneous devices and the problems with bacterial infections that occur due to the low biocompatibility between silicone rubber (that is the most common material of which catheters are made) and human tissues, and problems encountered in current technologies. The structures and properties when the HAp is doped with a hetero element and when is doped with Zn ion (II) and the fixation technique of these Zn: HAp nanocrystals on a silicone rubber film without using chemical reagents has been raised and mentioned. For this study it was synthesized two kinds of HAp nanocrystals; one with the initial (Zn+Ca)/P ratio of 1.67 and second one with (Zn+Ca)/P ratio equal to 2.00, in order to compare the biocompatible properties and also doped with Zn for enhance biocompatible properties as well as also generate an antibacterial activity. It is suggested that the use of deposition techniques nanocrystals in the polymer substrate without the use of chemical reagents such as electrophoretic deposition promotes biocompatibility by the elimination of cytotoxicity. It is desired the prevention of bacterial infections (i.e., down-growth) by indwelling Zn: HAp nanocrystals just beneath the skin.

In "**Chapter 2**: *Wet Chemical Synthesis of Zinc-substituted Hydroxyapatite Nanocrystals*", It shows methodology for the synthesis of Zn-substituted HAp Nanocrystals with initial (Zn+Ca)/P ratio of 1.67 and with initial (Zn+Ca)/P ratio of 2.00 doped with the different concentrations of Zn (0, 2.5, 5.0. and 10 mol%) and present the characterization of these powders with XRD patterns, XRF spectra, FTIR patterns, Nitrogen physisorption and TEM observation. The principal difference between the ZnHAp nanocrystals with initial (Ca+Zn)/P ratio of 1.67 and with initial (Ca+Zn)/P ratio of 2.00 that is the content of carbonate ions, where the initial (Ca+Zn)/P =2.00 has more content of carbonate ions, results in the reduce of Zn concentration, so that the initial Ca/P ratio=1.67 relatively exhibits the wider range of Zn ion. The XRD results showed the effect of the initial ratio on the HAp structure when the HAp is doped with Zn/Ca+Zn= 0, 2.5, 0.5 and 10 mol%. It was observed that the crystallinity, the lattice parameters "*a*" and "*c*" and the crystalline size (d_{200} and d_{300}) decreased with the increasing Zn ion amount, making the crystals smaller. These results are consistent with those seen in TEM images. In the nitrogen adsorption, both types of HAp nanocrystals are materials with narrow pores and observed that the hysteresis loop gradually is opening a little more with the increasing Zn ion amount, indicating an increase in porosity, which is reflected in the increase in pore volume. Also, the S_{BET} increased with the addition of Zn ion.

In "**Chapter 3**: *Fabrication of Nanocrystalline Zinc-substituted Hydroxyapatite Films on Biomedical Polymers and Their Fibroblast Compatibility and Antibacterial Properties*" it is presented the deposition of the nanocrystalline Zn-substituted HAp nanocrystals on the conductive polymer substrate using electrophoretic deposition (EPD) technique. For both kind of HAp with the Zn/(Ca+Zn)=0, 2.5, 5 and 10 mol %, the optimum voltage condition

was 100V, where the surface of the film was completely covered by the Zn: HAp nanocrystals. The nanocrystalline Zn-substituted HAp films were characterized using Thin-Film-XRD and FTIR, for both kind of Zn: HAp nanocrystals. The XRD and FTIR spectra are similar between both nanocrystals. But, the nanocrystalline Zn-substituted HAp films with the initial HAp (Ca+Zn)/P ratio of 2.00 corresponding to the peak carbonate ions is more pronounced than for the nanocrystalline Zn-substituted HAp films with the initial (Ca+Zn)/P ratio of 2.00. Also, the deposited Zn: HAp nanocrystals on three different catheters was successfully achieved. Due to the catheters is composite, the surface of the catheter is conductive for that reason can occur the EPD of the Zn: HAp nanocrystals on the surface of the catheters Because it is desired to use this material as a covering material for biomedical applications, the dissolution test is important. After 10 day of immersion in DMEM the Zn:HAp nanocrystals ((Ca+Zn)/P ratio of 1.67 and (Ca+Zn)/P ratio of 2.0) are dissolved in the cell culture medium for 14 days and 10 days, respectively, indicating that this Zn:HAp nanocrystals are too long stable in the DMEM medium.

Nanocrystalline Zn-substituted HAp films were evaluated by *in vitro* assays with NIH3T3 fibroblast cells. In the fibroblast compatibility test all the nanocrystalline Zn-substituted HAp films presented higher bio- and cytocompatibility compared with the polymer substrate using as the reference PDMS, nevertheless the nanocrystalline Zn-substituted HAp films with the initial (Zn+Ca)/P ratio=2.00 showed better possibility of usage for tissue engineering scaffold because nanocrystalline Zn-substituted HAp films with the initial (Zn+Ca)/P ratio=2.00 presented higher bio- and cytocompatibility, more cell density and aspect ratio than nanocrystalline Zn-substituted HAp films with the initial (Zn+Ca)/P ratio=1.67. The nanocrystalline Zn-substituted HAp film with the initial

(Zn+Ca)/P ratio=2.00 and, in particular, Zn concentration of 5.0 mol% was the most biocompatible sample with the highest cell density amount. These results indicated that the property of the Zn: HAps deposited in the conductive polymer films affected the adhesion and spreading of the fibroblast cells, and the best conditions were Zn: HAp with initial Ca/P =2.0 and Zn/(Ca+Zn)=5 mol%.

For antibacterial activity, *E. coli* DH5α was used in the experimental procedure of the exposure and culture (fish culture) on the sample films; after 17 hours was the extraction of the bacteria from the sample films and the subsequent viable bacterial growth culture (second culture) and finally counting the viable *E. coli* DH5α colonies after 24h. In general, viable *E. coli* DH5α colonies could still be observed for all the nanocrystalline Zn-substituted HAp films. In the nanocrystalline Zn-substituted HAp films with the initial (Zn+Ca)/P of 1,67 and film nanocrystalline Zn-substituted HAp films with initial HAp initial (Zn+Ca)/P ratio of 2.00 with increasing concentration of Zn, a number of viable bacteria decreased. The lowest amount of viable bacteria was at the concentration of 10 mol%. However, the nanocrystalline Zn-substituted HAp films with initial HAp initial (Zn+Ca)/P ratio of 2.00 exhibits less number of viable *E. coli* DH5α colonies at the concentration of 10 mol% than nanocrystalline Zn-substituted HAp films with the initial (Zn+Ca)/P ratio of 1,67 at the same concentration. The lowest amount of viable *E. coli* DH5α colonies was with the nanocrystalline Zn-substituted HAp films with initial HAp initial (Zn+Ca)/P ratio of 2.0 containing 10.0 mol% of Zn. It was successfully demonstrated the antibacterial properties.

In conclusion, chemically precipitated Zn-substituted HAp (initial (Zn+Ca)/P ratio of 1.67 and initial (Zn+Ca)/ratio of 2.0 and containing 0, 2.5, 5.0 and 10.0 mol%) nanocrystals

were electrophoretically deposited on a conductive polymer substrate as a continuous coating without cracks. The nanocrystalline Zn: HAp coatings provides a bioactive surface on the polymer substrate for fibroblast ingrowth. The nanocrystalline Zn-substituted HAp films showed viable cell reduction of *E. coli* DH5α colonies. The reduction assay suggested that the nanocrystalline Zn-substituted HAp films were capable of inhibiting bacteria growth, nevertheless for completely prevent the bacterial infections it is necessary to provide more amount of Zn. Therefore, the films on biomedical polymer surfaces were summarized to provide good biocompatibility as well as antibacterial properties, suggesting useful catheter surface modification technique.

4.2 Future perspectives

(1) Study further the antibacterial properties of Zn: HAp nanocrystals deposited on the silicone rubber.

(2) The conductive film is a little rigid silicone film with titanium thin film for suppressing static electricity, that partially protrudes through the skin like this may, however, limit mobility and cause discomfort so it will be better to deposit the HAp in a soft silicone rubber film in order to be easier to adapt to the form of the body and don't cause discomfort.

(3) Zn interacts with bacteria´s membrane and thereby, activates antimicrobial property, should be investigated further.

(4) Because it is important to investigate the stability of the nanocrystalline Zn-substituted HAp films in the biological medium. It is important to make a more stable Zn: HAp nanocrystals in order to stay more time as a coating in biomedical implants.

(5) In order to completely prevent the bacteria infection, I would be necessary to increase the amount of Zn ion; however, the increased amount of Zn ion will break the HAp structures.

(6) Continue biological evaluations of Zn: HAp nanocrystals on the silicone rubber film not only via cell-culture studies but also an animal in order to really know how to react a living organism with the Zn: HAp nanocrystals on the silicone rubber film.

(7) Because the Zn: HAp had good compatibility could be studied, the other applications can have the Zn ion-doped calcium phosphate compounds like dental implant as well as a bone implant or metal coatings to improve the biocompatibility of implants.